TESIS DE LA UNIVERSIDAD DE ZARAGOZA

2019 101

Mariella Polino

Ion-exchange membranes for protein crystallization and protein crystals derivatization

Departamento

Ingeniería Química y Tecnologías del Medio Ambiente

Director/es

MALLADA VIANA, REYES
GOULAO CRESPO, JOAO PAULO
GARDENIERS, HAN

ISSN 2254-7606

Prensas de la Universidad Universidad Zaragoza

ISSN 2254-7606

Universidad Zaragoza
1542

Tesis Doctoral

ION-EXCHANGE MEMBRANES FOR PROTEIN CRYSTALLIZATION AND PROTEIN CRYSTALS DERIVATIZATION

Autor

Mariella Polino

Director/es

MALLADA VIANA, REYES
GOULAO CRESPO, JOAO PAULO
GARDENIERS, HAN

UNIVERSIDAD DE ZARAGOZA

Ingeniería Química y Tecnologías del Medio Ambiente

2019

Mariella Polino

Master of Science in Chemistry and Pharmaceutical Technologies

Ion-exchange membranes for protein crystallization and protein crystals' derivatization

Dissertation for obtaining the degree of

Doctor of Philosophy in

Membrane Engineering

Adviser: João Paulo Serejo Goulão Crespo, Full Professor, NOVA University of Lisbon

Co-advisers: Reyes Mallada, Associate Professor, University of Zaragoza

Han Gardeniers, Full Professor, University of Twente

March, 2019

Ion-exchange membranes for protein crystallization and protein crystals' derivatization

This document was created using the (pdf)LaTeX processor, based in the "novathesis" template[1], developed at the Dep. Informática of FCT-NOVA [2].
[1] https://github.com/joaomlourenco/novathesis [2] http://www.di.fct.unl.pt

To my Family.

Acknowledgements

Pursuing a PhD was for me, so far, the most amazing experience. It was the best way to challenge myself, learn and perform different things every day. I was blessed with the possibility to carry out my own research work in three different universities in three different countries and benefit from the support and advice of many supervisors. The help received from all of them was crucial for both my professional and personal development. Hence, I would like to dedicate here few lines of acknowledgements to each one of them.

First of all, I would like to express my sincere gratitude to Prof. João Crespo, for giving me the opportunity to carry out my PhD in his research group and for the guidance, the constant encouragement and support, especially in the last phase of the PhD.

I would like to profoundly thank Prof. Isabel Coelhoso, for her kindness, constant availability and for being an important reference point since my first day in the Faculdade de Ciências e Tecnologia, Universidade Nova de Lisboa. I also would like to sincerely acknowledge Dr. Carla Portugal for the scientific advices that enhanced the value and quality of my work.

I am deeply grateful to Prof. Reyes Mallada, for the constant motivation and the energy she transmitted to me, during the time I spent at the Instituto de Nanociencia de Aragón, Universidad de Zaragoza. I owe my gratitude also to Prof. María Pilar Pina for teaching me the importance of small details in doing a good job and also for the interest and excitement towards my work.

I would like to greatly acknowledge Prof. Han Gardeniers, for welcoming me in the Mesoscale Chemical Systems Group at University of Twente and for providing me the opportunity to learn about microfluidics. I am definitely grateful

to Dr. Hoon Sook Rho for the patience in teaching me about microfluidics and all the advices that helped me improve my work.

Apart from the supervisors, I feel other people too contributed to the development of my thesis and should be acknowledged here.

I would like to acknowledge all the members of Erasmus Mundus Doctorate in Membrane Engineering for the support during the program and the annual meetings.

At Nova University of Lisbon, I would like to express my gratitude to:

Prof. Maria João Romao for allowing me to collaborate with her research group. Prof. Ana Luisa de Carvalho and Dr. Ramesh Pandian for their constant availability and help during the crystallographic analysis. Dr. Lina Juknaité for the assistance during the process of structure resolution of my crystals. Joana Monte for being a reference point in the lab, and for helping me always with a smile. Dª Maria Jose and Dª Palmina for the kindness and help whenever I needed it. Nuno from the cafeteria for all the pasteis de nata and the jokes that turned my grumpy face into a smile during difficult days.

At the University of Zaragoza, I would like to acknowledge:

Nuria Navascues for the constant support in the lab. Marta Lafuente for helping me with the nanoimprint lithography equipment and the spotting machine. All the technicians from the Cleanroom and SEM for their kindness and patience during the trainings.

At the University of Twente, I extend my gratitude to:

Stephan for preparing my devices and for the patience in showing me all the processes in the cleanroom. Pino for his availability and constant help. Brigitte Boogaard and Susan for the assistance during bureaucratic issues.

Besides the desire to challenge myself with science, one of the main reasons that motivated me to join the EUDIME program was the concept of experiencing life in three different countries. The very first moment my brain processed the idea of pursuing this PhD, I could picture myself not just in the lab but also travelling, having international friends and speaking new languages.

After 4 years, I can say reality did not disappoint my expectations. I am

grateful for all the trips and experiences I had. But mostly, for all the amazing friends that supported me during the difficult moments of my journey and/or shared with me the good times.

I am grateful to my conference companion and desk neighbour Carla Martins, for the daily encouragements, the scientific and life related discussions and the amazing trips. I owe my gratitude also to Paloma, (the only “pigeon” I can ever befriend) for supporting and tolerating me during the most difficult months of my work. Many thanks to Giorgia, for bearing with me the emotions and the stress of writing a PhD thesis and the proposition for a healthy life.

I would like to thank Costa for all the talks at "the bar" with a *copo de vinho verde* or a bottle of super bock, and also Mani, Alex and Yen for always being there to take care of me and cheer me up! I definitely want to thank Inês and Rafael for all the funny moments in the office and outside and for improving my culture about Marvel movies.

I wish to thank Roberta, the most generous and kind person, for making me feel at home in Zaragoza and for sharing lots of hard-working moments with me. I am thankful to Thijs for being a good friend, for the road trip he planned for me just because I wanted to see the seals and for introducing me to Trap music. My gratitude goes also to Amaia, Yannick, Michela, Sho, Peter and Pieter, Yiyuan, Hanky and Brigitte Bruijns that made my days at UTwente better and funnier!

When I got my acceptance to this PhD, I had no idea that I was going to be part of a big family: the Eudime Family. My Eudimates were a crucial part of this experience and I cannot fail to acknowledge them:

I would like to thank Magda for the constant support and motivation, all the skype-calls and the beard jokes that only We can understand; Usman for taking care of me whenever I needed and for cheering me up during difficult moments; also my good friends Sergio Santoro, Nayan and Lakshmeesha for all the help, the jokes, the trips and the good time spent together.

I met many amazing friends also outside the university and I feel they also supported me during all these years. I am definitely grateful to my first Portuguese friend Alda, for welcoming me in Portugal, helping during my initial days here,

and for being an inspiring person to me.

I feel grateful to Sergio Casimiro for helping me when I reached Lisbon for the first time, Elisa for the funny and crazy moments we shared, Paulo and Catia, always kind and helpful, Nichin and Marie, for the veggy dinners on Thursday night and for teaching me amazing words like *Kudlapura* and *Yelito Kopito Platito*!

Many thanks to my old friend Cinzia *Uncol* for always being present in my life and being supportive despite the distance. I wish to acknowledge Bianca, my best roomie ever, for all the *Credence Clearwater Revival* sessions of house cleaning and the karaoke in the kitchen with *Abba*'s songs.

Lastly, but definitely not because of lesser importance, I express my deepest gratitude to my family who has always taken care of me and in particular my brothers Mario and Nico for all the advices and support and my parents, the first people who believed in me and never failed to show their encouragement during the challenges I undertook and their pride for my achievements.

Ever tried. Ever failed. No matter. Try Again.
Fail again. Fail better.
- Samuel Beckett -

Abstract

This PhD thesis is focused on the application of ion-exchange membranes for protein crystallization and protein crystals derivatization. The experimental work is divided in three parts. The first part of the work is focused on the understanding of the effect of topography on nucleation. Soft lithography is used to modify the surface topography of Nafion® membranes with target designs, avoiding changes of surface chemistry that might mask the effect of topography on nucleation. The imprinted membranes are characterized by Atomic Force Microscopy (AFM), Scanning Electron Microscopy (SEM) and contact angle and tested for the crystallization of Trypsin from Bovine Pancreas. Nucleation and crystals growth are followed over time by optical microscope. Experimental results are compared with theoretical calculations of the ratio of change of Gibbs free energy of heterogeneous to homogeneous nucleation. The second part of the work is focused on the development of a method for performing a gentle derivatization of protein crystals using ion-exchange membranes. Nafion® and Neosepta 01 were selected after an initial screening of several membranes, due to their ability of promoting nucleation. The kinetics of ion-transport for Br^-, $PtCl_4^{2-}$ and Hg^{2+} is evaluated and used for modelling the transport in the derivatization set-up. Stability of crystals derivatized by ion-exchange membranes over time is compared with the stability of crystals derivatized by the conventional soaking method. The crystals derivatized by the help of the ion-exchange membranes are analysed by synchrotron and protein structure resolved with the Isomorphous Replacement technique. The third part of the work involves the integration of the ion-exchange

membrane derivatization concept in a Polydimethylsiloxane (PDMS) microdevice. A microdevice composed of two compartments, one with channels and one with wells is designed and built by photolithography and soft-lithography. Bonding of the membrane to the PDMS parts is done by grafting. Transport modelling of water, NaCl and Hg^{2+} transport in the microdevice, crystallization experiments where supersaturation is achieved by osmosis and evaluation of the crystals' diffraction quality are performed.

Keywords: Crystallization, Derivatization, Protein, Ion-exchange membranes ...

Resumo

Nesta tese de doutoramento foi investigada a utilização de membranas de permuta iónica, para cristalização de proteínas e derivatização dos cristais de proteínas. O trabalho experimental está dividido em três partes. A primeira parte do trabalho está focada na compreensão do efeito da topografia no processo de nucleação. A *soft*-litografia é usada para modificar a topografia de superfície das membranas Nafion® com padrões específicos, evitando alterações da composição química de superfície que possam mascarar o efeito da topografia na nucleação. As membranas impressas são caracterizadas por Microscopia de Força Atómica (AFM), Microscopia Eletrónica de Varrimento (SEM) e ângulo de contacto e testadas para a cristalização de Tripsina de Pâncreas de Bovino. A nucleação e o crescimento dos cristais são controlados ao longo do tempo através de microscopia óptica. Os resultados experimentais são comparados com cálculos teóricos da razão de variação de energia livre de Gibbs de nucleação heterogénea e homogénea. A segunda parte do trabalho está focada no desenvolvimento de um método para realizar uma *soft*-derivatização de cristais de proteína usando membranas de permuta iónica. Nafion® e Neosepta 01 foram selecionadas após uma triagem inicial de várias membranas devido à sua capacidade de promover a nucleação. A cinética de transporte de iões Br^-, $PtCl_4^{2-}$ e Hg^{2+} foi avaliada e usada para modelar o transporte na célula de derivatização. A estabilidade dos cristais derivatizados com a membrana de permuta iónica ao longo do tempo foi comparada com os cristais derivados pelo método convencional de imersão. Os cristais obtidos com as membranas de permuta iónica foram analisados por sincrotrão e a estrutura proteica resolvida com a técnica de substituição isomórfica. A terceira parte do

trabalho envolveu a integração do conceito de derivatização da membrana de permuta iónica num microdispositivo de polidimetilsiloxano (PDMS). Um microdispositivo composto por dois compartimentos, um com canais e outro com poços, foi desenhado e construído por fotolitografia e *soft*-litografia. A ligação da membrana ao PDMS foi feita por *grafting*. Foi realizada a modelação do transporte de água, NaCl e Hg^{2+} no microdispositivo, bem como ensaios de cristalização onde a supersaturação foi obtida por osmose e a qualidade de difração dos cristais foi avaliada.

Palavras-chave: Cristallização, Derivatização, Proteínas, Membranas de permuta iónica ...

Resumen

Esta tesis doctoral se centra en la aplicación de membranas de intercambio iónico para la cristalización de proteínas y la derivatización de cristales de proteínas. El trabajo experimental se divide en tres partes. La primera parte del trabajo se centra en la comprensión del efecto de la topografía en la nucleación. La *soft*-litografía se utilizó para modificar la topografía superficial de las membranas Nafion® con diseños específicos, evitando así cambios en la química de la superficie que pueden enmascarar el efecto de la topografía en la nucleación. Las membranas impresas se caracterizaron por microscopia de fuerza atómica (AFM), microscopia electrónica de barrido (SEM) y ángulos de contacto, y se analizó la cristalización de tripsina de páncreas bovino. La nucleación y el crecimiento de los cristales se controlaron a lo largo del tiempo mediante el uso de microscopía óptica. Los resultados experimentales se compararon con los cálculos teóricos del ratio de la variación de la energía libre de Gibbs de nucleación heterogénea y homogénea. La segunda parte del trabajo se centró en una *soft*-derivatización de cristales de proteínas utilizando membranas de intercambio iónico. Nafion® y Neosepta 01 se seleccionaron entre varias membranas por su capacidad de facilitar la nucleación. La cinética del transporte de iones para Br^-, $PtCl_4^{2-}$ y Hg^{2+} se evaluó para modelar el transporte en la celda de derivatización. La estabilidad de los cristales derivatizados por membranas de intercambio iónico a lo largo del tiempo fue comparada con la estabilidad de los cristales derivatizados por el método convencional de inmersión. Los cristales derivatizados con las membranas de intercambio iónico se analizaron mediante sincrotrón y la estructura de la proteína se resolvió con la técnica de reemplazo isomorfo. La tercera parte del

trabajo consistió en la integración del concepto de derivatización con membranas de intercambio iónico en un microdispositivo de polidimetilsiloxano (PDMS). El microdispositivo se diseñó y construyó mediante las técnicas de fotolitografía y *soft*-lithography. La unión de la membrana al PDMS se realizó mediante *grafting*. Se realizaron la modelización del transporte de agua, NaCl y Hg^{2+} en el microdispositivo, los experimentos de cristalización donde la sobresaturación se conseguió mediante ósmosis, y la evaluación de la calidad de difracción de los cristales se realizó.

Palavras-llave: cristalizacion, derivatizacion, proteinas, membranas de intercambio ionico . . .

Abstract

Dit PhD proefschrift gaat over de applicatie van non-ion-wisselende membranen voor proteïne kristallisatie en proteïne kristal derivatisering. Het experimentele deel is onderverdeeld in drie delen. Het eerste deel van het onderzoek is gefocust op het begrijpen van het effect van oppervlakte topografie op nucleatie. Zachte lithografie wordt gebruikt om de oppervlaktetopografie van Nafion® membranen met specifieke ontwerpen te modificeren, terwijl veranderingen in de oppervlaktechemie van het membraan, die de effecten van de topografiemodificering zouden kunnen maskeren, worden vermeden. De gemodificeerde membranen worden gekarakteriseerd door middel van Atomic Force Microscopy (AFM), Scanning Electron Microscopy (SEM) en contacthoekmetingen. Ook worden ze getest op de kristallisatie van rundertrypsine. De experimentele resultaten worden vergeleken met theoretische berekeningen over de Gibbs vrije energie van heterogene tot homogene nucleatie. Het tweede deel van het onderzoek richt zich op de ontwikkeling van een methode voor zachte derivatisering van proteïne kristallen via het gebruik van ionuitwisselende membranen. Na een eerste screening van membranen zijn Nafion® en Neosepta 01 geselecteerd, omdat deze membranen nucleatie kunnen bevorderen. De kinetiek van iontransport voor Br^{-}, $PtCl_4^{2-}$ en Hg^{2+} wordt geëvalueerd en gebruikt voor het modelleren van het iontransport in de derivatie opstelling. De stabiliteit van de kristalderivatie door ionuitwisselende membranen over tijd is vergeleken met de stabiliteit van kristallen die zijn gederiveerd via de tradionele weekmethode. De eiwitstructuur van de met behulp van ionenuitwisselingsmembranen gederivatiseerde kristallen worden geanalyseerd door middel van synchrotron, waarna de vergaarde data verwerkt is met behulp van

de isomorfe vervangingstechniek. Het derde deel van het onderzoek bestaat uit de integratie van ionuitwisselingsmembranen in een concept apparaat bestaande uit polydimethylsiloxaan (PDMS). Dit apparaat bestaat uit twee compartimenten, een met kanalen en een met putjes, wordt ontworpen en gefabriceerd door middel van zachte lithografie en fotolithografie. Het hechten van het membraan aan de PDMS-delen gebeurt via enten. Ook worden het transport van water, NaCl en Hg^{2+} in het apparaat, de kristallisatie experimenten waarbij superverzadiging plaatsvind door middel van osmose en de evaluatie van de diffractie kwaliteit van de kristallen gemodelleerd.

Sleutelwoorden: kristallisatie, derivatisering, proteïne, ion-wisselende membranen ...

Contents

List of Figures

List of Tables

List of Acronyms

Abbreviations

AFM atomic force microscopy.

BPT bovine pancreatic trypsin.

BSA bovine serum albumin.

$CC_{1/2}$ Pearson's correlation coefficient.

CNI compact nano imprint.

DMF N,N-dimetilformammide.

CNT classic nucleation theory.

DSC differential scanning calorimetry.

F feeding compartment.

GA glutaraldehyde.

HEWL hen egg white lysozyme.

I reflection intensity.

IEM ion-exchange membrane.

MAC membrane-assisted crystallization.

MD membrane distillation.

MEMS micro electro-mechanic systems.

MIR multiple isomorphous replacement.

MR molecular replacement.

PDB protein data bank.

PDMS polydimethylsiloxane.

PEG polyethylene glycol.

PEGDE poly(ethylene glycol) diglycidyl ether.

pI isoelectric point.

PTFE Polytetrafluoroethylene.

PVA polyvinyl alcohol.

PVDF polyvinylidene difluoride.

R receiving compartment.

Ra average of absolute values of profile height deviations from the mean line.

R$-factor$ discrepancy between experimental data and the model.

R$_{free}$ discrepancy between experimental data and the model for 1000 random diffracted beams.

RH relative humidity.

R$_{meas}$ multiplicity-corrected version of R$_{merge}$.

R$_{merge}$ spread of multiple measurements of a given reflection.

RMS root-mean-square.

R$_{work}$ R$-factor$ for the larger "working" set of reflections.

SAD single-wavelength anomalous dispersion.

SAM self-assembled monolayer.

SCA static contact angle.

SEM scanning electron microscopy.

SLS Swiss light source.

TCDB 1,3,5-tris(10-carboxydecyloxy) benzene.

TFOCS tridecafluoro-1,1,2,2-tetrahydrooctyl-1-trichlorosilane.

VTES triethoxyvinylsilane.

Variables

A area $\left(m^2\right)$ or $\left(cm^2\right)$ or $\left(\mu m^2\right)$.

C concentration $\left(\frac{mol}{L}\right)$.

d specific mass $\left(\frac{g}{cm^3}\right)$.

D diffusion coefficient $\left(\frac{m^2}{s}\right)$.

f fraction.

G Gibbs free energy (J).

h depth (μm).

J molar flux $\left(\frac{mol}{m^2 s}\right)$.

K mass transfer coefficient $\left(\frac{m}{s}\right)$.

l thickness (μm).

M_w molecular weight $\left(\frac{g}{mol}\right)$.

n number of wells.

p vapour pressure (Pa).

Q volumetric flow rate $\left(\frac{mL}{h}\right)$.

R^* critical nucleation radius (m).

R gas constant $\left(\frac{m^3 Pa}{K mol}\right)$.

t time (s) or (min) or (h).

T temperature $(°C)$.

Tg glass transition temperature $(°C)$.

V volume of solution (μL) or (mL) or (m^3).

Greek symbols

γ interfacial energy between nucleus and liquid $\left(\frac{J}{m^2}\right)$.

μ chemical potential $\left(\frac{J}{mol}\right)$.

Ω molar volume $\left(\frac{m^3}{mol}\right)$.

ϕ ratio between Gibbs free energy variation of heterogeneous to homogeneous nucleation.

σ estimated error.

Γ ratio between actual and projected surface.

θ contact angle $(°)$.

Subscripts

0 initial.

c critical.

cb Cassie-Baxter.

eq equilibrium.

Het heterogeneous nucleation.

Hom homogeneous nucleation.

i compound i.

N nucleus.

NL nucleus-liquid.

NS nucleus-substrate.

rep repetition unit.

SL substrate-liquid.

tri triangle.

w water.

wz Wenzel.

Y Young.

Chapter 1

Introduction: motivation and thesis outiline

1.1 Motivation

Proteins are biological macromolecules able to carry out several important functions in the human body: they can act as enzymes, transporters, messengers, structural components, provide energy and so on. Therefore, understanding the three-dimensional structure of protein molecules represents an important step for the investigation of metabolic pathways involved in physiological and pathological processes and for the design of more selective drugs [1]. So far, the main technique used for protein structure resolution is X-ray crystallography: when a monochromatic beam of x-rays shoots a crystal, the interaction of the waves with the electrons of the matter produces a light scattering in different directions. The scattered waves can be collected by a film sensitive to x-rays where a diffraction pattern (dispersed black spots) is generated. Each spot of the diffraction pattern is the result of all the interactions between the initial wave and the matter. The intensity and the scattering angle of the waves are strictly related to the orientation of the molecules in the space, in respect to the x-ray beam. Hence, from the analysis of the diffraction pattern, the electron density map of the unit molecule can be

recovered and finally the molecular structure can be resolved. Bearing in mind the importance of molecules' orientation in the data collection, it becomes clear that molecules in a powder or in a solution with a random orientation lighted with x-rays will not give a diffraction pattern useful for structure determination. Instead, using a repeating organized unit (a crystal) it is possible to generate constructive interferences between the waves that will amplify the signal generated by a single molecule. At this point we can understand how crucial it is for this technique to obtain well-diffracting crystals.

The process of formation of protein crystals is called protein crystallization. Protein crystallization is an event unlikely to occur and only specific conditions may lead to the formation of crystals. Hence, being able to induce nucleation is the first important milestone to achieve in order to obtain well-diffracting crystals. Playing with the types of additives and concentration, temperature, pH, among others helps to find out a range of conditions where crystallization is more likely to occur [2]. Trial-and-error is therefore the most used strategy when a protein has to be crystallized, and finding a way to explore uncommon conditions, investigating the effect of new techniques or materials and developing methods to increase the control of the protein crystallization process is important to amplify the chances of success.

Membrane technology contributed so far to protein crystallization by controlling the solvent removal rate with hydrophobic porous membranes and using the membrane surface as an heterogeneous nucleation promoter, by adjusting their chemistry and topography[3, 4]. In the last years, several studies are pointing out how the chemical interactions can be enhanced by a suitable topography. Indeed, topographical features may affect surfaces' wettability and create physical obstacles for protein molecules creating local supersaturation spikes [5–8]. Different approaches have been used to create surfaces with different topography (functionalization [9], coatings [10], oxidation treatments [11] and so on). However, the topographical change was, in these cases, always promoted as a consequence of a chemical treatment; therefore, it was always difficult to distinguish whether the effects of these surfaces on nucleation were due to the chemistry or to the

topography of the surfaces.

Considering this situation, the first part of this thesis is dedicated to the understanding of the effect of pure topographical differences on the nucleation process. To do so, membranes were modified by soft lithographic techniques to imprint specific topographies. The advantages of such techniques, besides the affordability and ease of use, are the possibility to design the target topography and minimise changes in the surface chemistry of the material. Several geometries were designed, and the crystallization results obtained with the imprinted membranes were compared based on theoretical calculations of the ϕ values, which correspond to the ratio between heterogeneous and homogeneous Gibbs free energy variation of nucleation, using a model that takes into consideration the topographical features.

In some situations, despite all efforts and attempts, when the crystals obtained diffract poorly, or in some other cases such as for completely unknown protein molecules, routine diffraction analysis (Molecular Replacement Techniques) are not able to solve the structure. It becomes essential, in these cases, the introduction of heavy atoms into the crystal (derivatization), in order to facilitate the resolution process by means of Isomorphous Replacement Techniques [12–16]. The crystals derivatization is effective and useful only when the introduction of the heavy atoms occurs without changing the orientation of macromolecules in the space group of the native crystal (isomorphism)[12]. To diffuse those species into the protein crystals and keep the crystalline lattice isomorphous, the native preformed crystals are soaked in a solution containing low concentrations of these compounds, so they can diffuse into the solvent channels of the crystals. The main problems of this procedure are related with the sensitivity of the crystals to abrupt environmental changes. To perform soaking, crystals have to be harvested, removed from their native environment and brought in contact with a solution with a different composition from the growing buffer. All these steps may easily damage the crystals. For this reason, soaking has to be performed in several stages involving the use of several solutions with an increasing concentration of the halide or metal ion to be incorporated[12],being therefore time consuming

and involving laborious procedures.

Hence, the second part of this PhD thesis is devoted to the development of a new membrane-based derivatization method able to overcome the most common problems faced by crystallographers in derivatizing protein crystals. Ion-exchange membranes were chosen for this work because they have suitable characteristics for performing derivatization: they are semipermeable barriers, where fixed charged groups are attached to a hydrophobic backbone (usually made of polystyrene)[17]. The hydrophobic backbone guarantees that the protein solution remains on the top of the membrane, and it is not absorbed by the support. At the same time, the presence of charged groups allows the selective transport of the desirable ions across the membrane. Furthermore, controlling protein and derivatization solutions concentration it is possible to have a controlled diffusion avoiding abrupt changes of the environment, preserving and/or improving diffraction quality of the crystals.

Developing a system where the operator can control the processes involved in x-ray crystallography brings numerous advantages: mostly, the possibility of exploring crystallization conditions with a rational that might bring improvements in the diffraction quality. However, prediction capabilities are still limited, and a screening of conditions is still very important. Besides the time and human work needed for screening conditions, the very limiting requirement is represented by the amount of protein available for performing experiments [18].

For this reason, the last part of this PhD thesis is focused on the design and development of a microfluidic device that can integrate ion-exchange membranes and guarantee a control of both crystallization and derivatization process with a low consumption of reagents.

1.2 Thesis outline

This thesis consists of six chapters. The content of the chapters is the following:

Chapter 1 Introduction: motivation and thesis outline. It describes the motivation and aim of the work and the PhD thesis outline.

Chapter 2 Membrane-assisted crystallization for structure elucidation by x-ray diffraction. It describes the current state of the art on which this thesis is based. The content of this chapter was submitted to Crystal Growth and Design

Chapter 3 Structured Nafion® membranes for protein crystallization. It describes the surface topography modification of ion-exchange membranes by nanoimprint lithography and their effect on protein crystallization compared with theoretical calculations.

Chapter 4 Ion-exchange-membranes for protein crystals derivatization. It describes the development of an ion-exchange membrane contactor to perform derivatization of protein crystals. The content of this chapter was published in Crystal Growth and Design, 2017, 17 (9),4563–4572.

Chapter 5 Ion-exchange membrane-integrated microdevice for protein crystallization and protein crystals derivatization. It describes the design and development of a microdevice integrating an ion-exchange membrane to be used for protein crystallization and protein crystals derivatization.

Chapter 6 Outlook and future work. It describes the general conclusions of this Ph.D. thesis and suggestions for future work.

References

[1] R. Giegé. "A historical perspective on protein crystallization from 1840 to the present day." In: *FEBS Journal* 280.24 (2013), pp. 6456–6497. DOI: 10.1111/febs.12580.

[2] J. Newman. "A review of techniques for maximizing diffraction from a protein crystal in stilla." In: *Acta Crystallographica Section D: Biological Crystallography* 62.1 (2006), pp. 27–31. DOI: 10.1107/S0907444905032130.

[3] G. Di Profio, A. Caridi, R. Caliandro, A. Guagliardi, E. Curcio, and E. Drioli. "Fine dosage of antisolvent in the crystallization of L-histidine: Effect on polymorphism." In: *Crystal Growth and Design* 10.1 (2010), pp. 449–455. DOI: 10.1021/cg901038g.

[4] E. Curcio, G. Di, and E. Drioli. "Microporous Hydrophobic Membranes for Crystallization of Biomolecules." In: *Chemical Engineering Transactions* 47.2 (2016), pp. 421–426. DOI: 10.3303/CET1647071.

[5] A. S. Ghatak and A. Ghatak. "Precipitantless Crystallization of Protein Molecules Induced by High Surface Potential." In: *Crystal Growth & Design* 16 (2016), pp. 5323–5329. DOI: 10.1021/acs.cgd.6b00833.

[6] A. S. Ghatak, G. Rawal, and A. Ghatak. "Precipitant-Free Crystallization of Protein Molecules Induced by Incision on Substrate." In: *Crystals* 7.8 (2017), p. 245. DOI: 10.3390/cryst7080245.

[7] U. V. Shah, N. H. Jahn, S. Huang, Z. Yang, D. R. Williams, and J. Y. Heng. "Crystallisation via novel 3D nanotemplates as a tool for protein purification and bio-separation." In: *Journal of Crystal Growth* 469 (2017), pp. 42–47. DOI: 10.1016/j.jcrysgro.2016.09.029.

[8] U. V. Shah, D. R. Williams, and J. Y. Heng. "Selective crystallization of proteins using engineered nanonucleants." In: *Crystal Growth and Design* 12.3 (2012), pp. 1362–1369. DOI: 10.1021/cg201443s.

[9] Y. X. Liu, X. J. Wang, J. Lu, and C. B. Ching. "Influence of the roughness, topography, and physicochemical properties of chemically modified surfaces on the heterogeneous nucleation of protein crystals." In: *Journal of Physical Chemistry B* 111.50 (2007), pp. 13971–13978. DOI: 10.1021/jp0741612.

[10] W. De Poel, J. A. W. Mu, J. A.A. W. Elemans, W. J. P. Van Enckevort, A. E. Rowan, and E. Vlieg. "Surfaces with Controllable Topography and Chemistry Used as a Template for Protein Crystallization." In: *Crystal Growth & Design* 18 (2018), pp. 763–769. DOI: 10.1021/acs.cgd.7b01174.

[11] H. Hou, B. Wang, S.-Y. Hu, M.-Y. Wang, J. Feng, P.-P. Xie, and D.-C. Yin. "An investigation on the effect of surface roughness of crystallization plate on protein crystallization." In: *Journal of Crystal Growth* 468.October 2016 (2017), pp. 290–294. DOI: 10.1016/j.jcrysgro.2016.10.007.

[12] A. C. W. Pike, E. F. Garman, T. Krojer, F. von Delft, and E. P. Carpenter. "An overview of heavy-atom derivatization of protein crystals." In: *Acta crystallographica. Section D, Structural biology* 72.Pt 3 (2016), pp. 303–318. DOI: 10.1107/S2059798316000401.

[13] G. L. Taylor. "Introduction to phasing." In: *Acta Crystallographica Section D: Biological Crystallography* 66.4 (2010), pp. 325–338. DOI: 10.1107/S0907444910006694.

[14] M. Dauter and Z. Dauter. "Phase determination using halide ions." In: *Methods in molecular biology (Clifton, N.J.)* 364.9 (2007), pp. 149–158. DOI: 10.1385/1-59745-266-1:149.

[15] J. P. Morth, T. L. M. Sørensen, and P. Nissen. "Membrane's eleven: Heavy-atom derivatives of membrane-protein crystals." In: *Acta Crystallographica Section D: Biological Crystallography* 62.8 (2006), pp. 877–882. DOI: 10.1107/S0907444906023547.

[16] C. Giacovazzo, M. Ladisa, and D. Siliqi. "The approach of the joint probability distribution functions: the SIR-MIR, SAD-MAD and SIRAS-MIRAS, cases." In: *Zeitschrift für Kristallographie - Crystalline Materials* 217.12 (2002), pp. 703–709. DOI: 10.1524/zkri.217.12.703.20660.

[17] T. Xu. "Ion exchange membranes: State of their development and perspective." In: *Journal of Membrane Science* 263.1-2 (2005), pp. 1–29. DOI: 10.1016/j.memsci.2005.05.002.

[18] L. Li and R. F. Ismagilov. "Protein Crystallization Using Microfluidic Technologies Based on Valves, Droplets, and SlipChip." In: *Annu. Rev. Biophys* 39 (2010), pp. 139–58. DOI: 10.1146/annurev.biophys.050708.133630.

Chapter 2

Membrane-Assisted Protein Crystallization for Structure Elucidation by X-ray Diffraction

Submitted as: Mariella Polino, Carla A.M. Portugal, Gianluca Di Profio, Isabel M.R. Coelhoso, João G. Crespo, Membrane-assisted Protein Crystallization for Structure Elucidation by X-ray Diffraction, 2019, Crystal Growth & Design*

Summary

Protein crystallization is the key event for applying x-ray crystallography and discover how the molecules are spatially organized. However, even though the general concept of reaching a supersaturated state for promoting nucleation represents a must, no general method was found yet to guarantee crystallization for all types of protein. Hence, a continuous search and development of methods for crystallization keeps being important. In the last years, membrane technology succeeded in improving the control of the crystallization process of protein molecules to be used for structure resolution purposes. This article revises new and old aspects of the topic: the membrane-assisted crystallization principle,

the heterogeneous nucleation phenomena, the ligand-diffusion control and the protective effect of hydrogel-composite membranes. Furthermore, it aims to persuade about the benefits of using microfabrication technology in order to promote further advancements of this field.

2.1 Introduction

Protein crystallization is the limiting step for elucidating the tri-dimensional structure of protein molecules by X-ray diffraction analysis. There are numerous parameters that can affect the final diffraction resolution and the steps required to obtain well-diffracting crystals: the supersaturation rate, types of additives and concentration, temperature, pH, protein-surface interactions and crystals modifications, among others [1–3]. Moreover, the complex nature of proteins makes difficult the prediction of the adequate conditions for promoting nucleation and obtaining well-diffracting crystals [4]. Therefore, there is not a unique technique that ensures that crystallization will occur for any type of protein. For this reason seeking new methods to generate supersaturation and control all parameters involved in crystals growth is crucial[5]. The most common methods studied for achieving superaturation are: the batch method (protein and precipitant solution are mixed under oil reaching the supersaturation state immediately), vapour diffusion (protein and precipitant are mixed and placed in a closed system, part of the solvent in the protein mix migrates towards a stripping solution determining a slow increase of protein concentration), liquid-liquid diffusion (protein and precipitant slowly mix by diffusion inside a capillary creating a gradient of concentrations) [1].

Among all the investigated methods, the concept of membrane-assisted crystallization (MAC) was developed almost 20 years ago and research has been pursued to fully understand how membranes contribute to a fine control of crystallization of both inorganic and macro molecules [6–9]. Membranes were firstly used to control the evaporation rate of the process, but in the last years many advances

have been accomplished by studying surface-protein interactions [10, 11], by improving crystals stability during post-crystallization treatments and the effect on crystals diffraction quality [1]. On this matter, hydrogel-composite membranes, by combining the transport properties of a microporous hydrophobic membrane with the ability of the gel for promoting specific polymer-solute interactions and protection of the crystals from environmental stress, contributed to a high improvement of the crystals' diffraction quality [12, 13].

Membrane technology has also become more efficient in the last years by the coupling with microfabrication techniques. The small volumes, the laminar flow and the low-cost fabrication processes of micro-devices brought several benefits to the most common membrane processes[14, 15]. However, few studies are available yet regarding the use of micro-technology for improving membranes' properties and processes for protein crystallization.

This review is focused on the development of membrane-assisted crystallization processes of protein molecules for x-ray diffraction purposes, addressing the conventional and new aspects of the topic, namely the concept of crystallization assisted by membranes, the heterogeneous nucleation process, the post-crystallization treatments and enlighten the advantages that microfabrication techniques might bring to this field.

2.2 Membranes for protein crystallization

The term membrane crystallizer appeared for the first time in 2001, when Curcio et al. [7] applied the concept of membrane distillation (MD) to the crystallization of sodium chloride. It did not take long for extending the idea of using membranes to control the nucleation and growth rate of small inorganic molecules to the crystallization of proteins. Indeed, in 2002, Lysozyme molecules were successfully crystallized in a membrane contactor [16]. Since membrane crystallization was born as an extension of the concept of MD, it was initially associated with hydrophobic micro-porous membranes with the role of a mere separation wall rather than a selective barrier. Two solutions with different water activity due to

different solute concentration or temperature tend to equilibrate themselves in the vapour phase, through the membrane pores. However, the role of a membrane crystallizer in controlling nucleation and growth was also promptly associated with the heterogeneous effect that different types of surfaces are likely to induce [17].

The topography and the chemistry of the membrane materials showed to have a relevant role in crystallization. Indeed, nucleation, which is the first necessary step for protein crystallization, is also affected by the interactions between protein molecules and external surfaces. Other attempts were done for protein crystallization by using membranes to generate supersaturation. An example is the work of Todd et al. [18] in 1991, where a reverse osmosis membrane was used to control supersaturation of a Lysozyme solution. The driving force, in this case, was the difference between the hydrostatic and osmotic pressure that determined the diffusion of water from the protein to the stripping solution through a non-porous membrane. Latter, membranes were also used to control protein-ligand interactions and diffusion of specific ligands to the protein solution [19, 20].

Also, new composite materials combined with hydrogels, were tested for the control of crystallization kinetics and the preservation of protein bioactivity. Therefore, several different roles can be outlined for membranes in the crystallization of macromolecules:

i Separation barrier, for the fine control of solvent (usually water) removal rate;

ii Heterogeneous support, modulating protein-surface interactions and, ultimately, drive protein-protein aggregation;

iii Selective barrier, controlling the selective diffusion of components from/to the protein solution;

iv Protective environment for protein conformation/bioactivity against osmotic shock when combined with hydrogels.

2.3 Principle of Membrane-Assisted Protein crystallization

Protein crystallization is the process of formation of protein crystals. Protein crystals form when the molecules are able to organize themselves in an ordered lattice maintained by different types of protein-protein interactions (hydrogen bonding, ionic interactions, hydrophobic interactions, etc).

The crystallization process starts when an under-saturated solution reaches the unstable supersaturated state (the amount of solute in solution is higher than the solubility limit). The supersaturated state is conventionally achieved by solvent removal to the vapour phase (vapour diffusion techniques) [3–5] and by the use of additives that can increase the protein concentration (for this reason called precipitants) with different mechanisms: salts such as $(NH_4)_2SO_4$ or NaCl interact with water molecules decreasing their availability for the solvation of the protein and also create protein-ion interactions affecting the morphology and diffraction quality; organic solvents such as ethanol reduce the polarization of the medium promoting attraction between the protein molecules; polymers such as polyethylene glycol force protein molecules in a restricted space favouring their interaction [3].

As the solvent is removed, both protein and precipitant concentration increase until reaching the supersaturated zone, where nucleation can finally start. As protein concentration in solution decreases because of nuclei formation the system can reach the metastable zone where nucleation stops and only crystal growth occurs (Figure 2.1).

In membrane-assisted crystallization (MAC), the supersaturated state can be achieved by taking advantage of the structure, morphology and transport properties of microporous hydrophobic membranes that control solvent migration and promote nucleation (Figure 2.2).

The water repellent character of the membrane prevents water in the liquid phase to enter the pores and, therefore, water transport occurs only in vapour

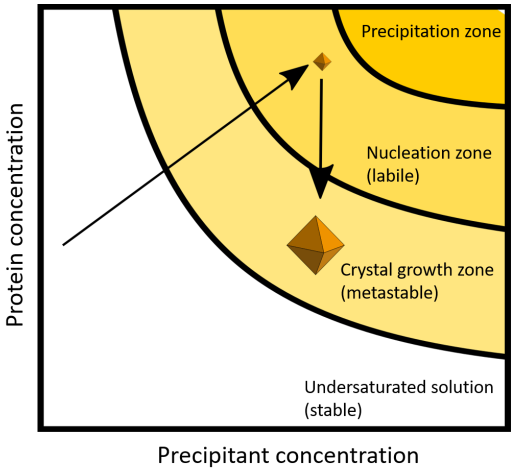

Figure 2.1: Solubility diagram. Four zones can be identified: under-saturated zone where no nucleation or crystal growth can occur, a supersaturated metastable zone where only crystal growth can occur but no nucleation, a supersaturated labile zone where both nucleation and crystal growth can occur, a precipitation zone.

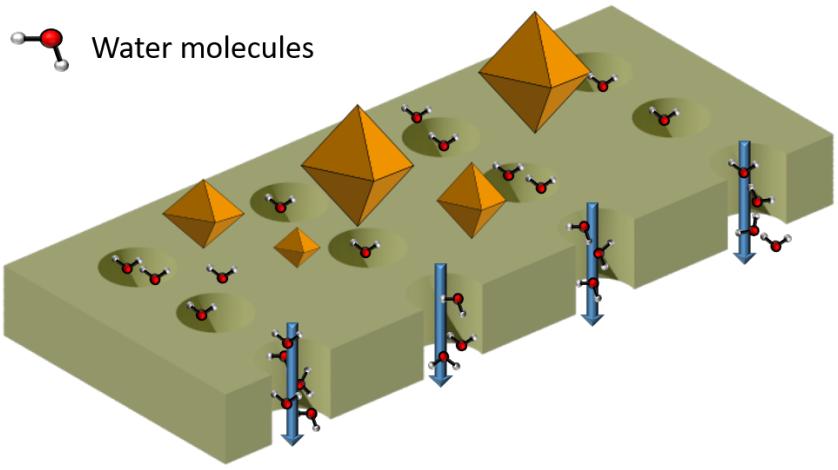

Figure 2.2: Membrane-assisted crystallization principle. Protein and stripping solution are on different sides of the membrane. The volatile solvent is removed from the protein solution in vapour phase, supersaturation is reached and crystals formation occurs.

phase [21, 22]. The transport of solvent across hydrophobic microporous membranes is driven by a difference in partial pressure across the two sides of the membrane. The driving force can be generated by a temperature gradient, concentration gradient or the addition of an anti-solvent [22]. However, in order to avoid thermal degradation, concentration differences are mostly used for protein crystallization. The MAC process is normally performed in membrane contactors. The membrane separates two compartments and both solutions (protein and stripping) are in contact with the membrane. The flux (J_i) of solvent i can be calculated according to Dusty Gas Model Theory:

$$J_i = -\frac{D}{RT}\Delta p_i \tag{2.1}$$

where D is the diffusion coefficient inside the pores, R is the gas constant, T is the temperature, Δp_i is the difference in vapour pressure generated across the two sides of the membrane [23, 24].

Tuning membrane morphological characteristics such as porosity, pore size and thickness consents to control the transmembrane flux and consequently the crystallization process. More in detail, increased porosity and pore size and lower thickness determine higher area for transport and faster transmembrane flux leading to a faster achievement of the supersaturated state and consequently higher nucleation rate [29]. The fine control of the surface area for evaporation allows to obtain a sharp size distribution of the crystals compared to crystals grown using conventional methods [30]. The crystals' size is also affected by the transmembrane flux. Indeed, a lower transmembrane flux induces a slower nucleation rate, promoting the growth of crystals with larger size. Moreover, ionic strength and water activity also strongly affect the process. Nucleation rate increases with the ionic strength. Indeed, even though the increased precipitant concentration leads to a lower transmembrane flux due to a lower water activity of the solution, at the same time it decreases the solubility of the protein, promoting supersaturation at lower protein concentration [29]. Furthermore, under conventional conditions of protein, precipitant and stripping concentration, a decrease of the induction time for nucleation occurs when the crystallization takes place at the surface of

a hydrophobic microporous membrane such as Polypropilene, probably due to non-specific protein-surface interactions that facilitate the formation of nuclei at lower concentrations [17].

Different membrane configurations can be used:

- Hollow fibres: the stripping solution flows inside the fibre and the protein solution flows outside;
- Flat membranes: they separate the environment in two compartments, one for the stripping and the other for the protein solution.

Furthermore, the membrane crystallizer may have different set-up configurations (Figure 2.3):

- Static mode: the two solutions are contacted by the membrane until equilibrium is achieved and crystals are obtained [16, 25]
- Dynamic mode: the solutions are pumped in counter-current; the supersaturated protein solution is collected in a separate vessel, where nucleation occurs [16, 25].

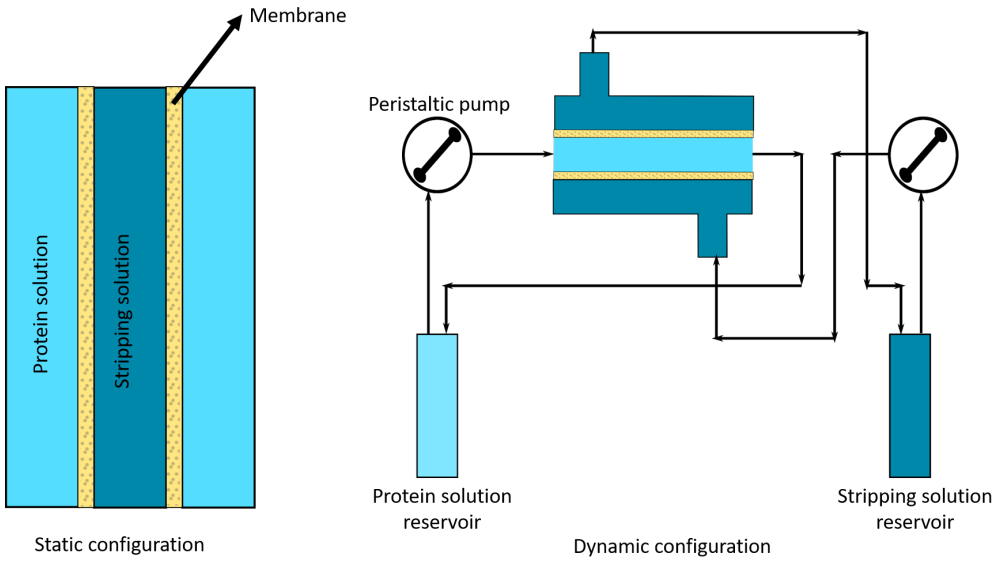

Figure 2.3: Set-up configurations for membrane-assisted protein crystallization

The crystallization process is also affected by the configuration set-up: In a static configuration the solvent removal rate, hence the rate of achievement of

the supersaturated state, depends on the transport area available at the surface (porosity in the case of hydrophobic micro-porous membranes)[16]. By combining the transport area available, the driving force, the effect of the precipitant and protein-surface interactions it is possible to control the kinetics of crystals growth [17, 20].

In a dynamic configuration, additionally to supersaturation due to membrane transport properties and protein-surface interactions, an increased control is achieved by adjusting the flowrates of the stripping and protein solutions. Over time, the transmembrane flux tends to drop due to progressive (or gradual) equilibrium between the protein and stripping solutions. Water activity is reinstated due to the constant refresh of solution during the process, hence, higher flow rates reinstate the driving force more quickly promoting a faster solvent evaporation and higher nucleation rate. Furthermore, an increase of convection forces acting on the protein molecules occurs. The convective flux imposes the molecules a certain orientation and increases their concentration in the solid-liquid interface enhancing crystal's growth, towards a single direction [8, 26, 27]. It was observed from diffraction analysis that this behaviour resulted in a change in the unit cell (smallest repeating unit with the symmetry of the crystal structure) dimensions (a,b and c). Indeed, Trypsin crystals grown in a dynamic configuration exhibited an increased value for a and b and a decreased value for c, compared to the ones grown in static configuration. The diffraction resolution of crystals grown in both static and dynamic configuration was excellent: Trypsin crystals diffracted at 1.9 Å in static configuration and 2.0 Å in dynamic configuration, demonstrating that the convection generated by the flux towards a single direction does not have a negative effect on the diffraction quality of the crystals.

In summary, controlling supersaturation with membranes offers a great number of advantages: besides the control due to type and concentration of additives and protein, it allows to control the evaporation area (and hence the rate of solvent removal), leading to a higher reproducibility of the results and a fine control of the crystals' size and nucleation rate. Additionally, the possibility to tune the

flow velocity allows to further increase supersaturation at later stages of the process and to control morphology, guaranteeing a comparable diffraction quality with crystals obtained with conventional crystallization techniques.

2.4 Effect of the properties of membrane surface on protein crystallization

Growing crystals of inorganic molecules from the interaction with mineral substrates by epitaxial nucleation led McPherson [28] in 1988 to the idea that the same concept might be applied also for macromolecules. Since then, several studies have been conducted to investigate and understand the effect of protein-surface interactions on nucleation and crystal growth. During membrane-assisted crystallization, a protein solution is in contact with the membrane surface, therefore, membranes may also act as heterogeneous nucleants. The main effects in terms of chemistry, topography and epitaxy have been summarized here

2.4.1 Charged surfaces

Proteins are molecules containing several ionisable groups, therefore, their total electric charge and electric charge distribution varies according to the pH of the solution. Electrically charged amino-acids can easily form ionic interactions or repulsions with electrically charged surfaces, motivating the development of improved protein crystallization processes based on a suitable control of protein-surface ionic interactions. Different protein crystallization studies have been conducted using electrically charged films. In 2001 Fermani et al. [29], carried out crystallization experiments of Concanavalin A and Lysozyme on positively charged surfaces. Concanavalin A (negatively charged at experimental pH) interacted with charged substrates promoting nucleation at a lower induction time and for a lower protein concentration than conventional hanging drop experiments. However, no effect was found for Lysozyme (positively charged at experimental pH). Also, in 2008 Tosi et al. [30] tested positively and negatively charged

polystyrene on proteins (Insulin and Ribonuclease A) with different net charges. They explained protein crystallization according to two different mechanisms depending on the relationship between the type of charge at the surface and the protein molecules:

- surface-induced crystallization: repulsion between protein molecules and the surface occurs, therefore protein concentrates in a thin layer above the surface determining crystallization at lower protein concentrations;
- surface-controlled crystallization: attraction forces occur between the protein and surface determining the accumulation of a thin layer of protein on the top of the surface promoting nucleation at lower protein concentrations and also decreasing the induction time.

Hence, although with a different mechanism, both cases (same or opposite charge between protein molecules and surface) might lead to the attainment of crystals at lower protein concentration, which is advantageous because it allows to obtain crystals in the metastable region, where the moderate supersaturation determines a slow crystals growth and higher chance of obtaining well-diffractive crystals.

Recently, Ghatak et *al.* [31, 32]tested protein crystallization on patterned and electric charged films. PDMS films with charges, surface wrinkles and a combination of the two were tested in Lysozyme crystallization. When charges and wrinkles acted together, Lysozyme crystals were obtained without the need of precipitants. In fact, according to Ghatak, electric charge combined with topographical features led to the creation of a surface potential by the orientation of the hydrogen bonds of water molecules that helps the self-organization of the protein molecules. Successful crystallization without precipitant was obtained for single proteins and for mixtures of proteins. The crystals obtained without precipitant were analysed by X-rays diffraction showing unit cell dimensions very close to the reference crystals with precipitant. Therefore, these types of surfaces might be used for screening crystallization conditions without precipitant, simplifying the search of the optimal combination of ingredients.

2.4.2 Porous and rough surfaces

Since 2001, Chayen and co-workers have been demonstrating the effectiveness of using silicon porous materials with a pore size within the range of the protein molecular dimension to induce nucleation of several proteins such as Lysozyme, Trypsin, Thaumatin, Catalase and Phicobiliprotein. The hypothesis about the mechanism of porous surfaces nucleation induction is the entrapment of protein molecules inside the narrow space of the pores that accumulate over time increasing the local concentration [33–35]. The confinement effect was also supported by the formation of submicron protein crystals within square shaped pores with dimensions from 100 to 1000 nanometers [36]. Therefore, the use of porous surfaces might promote local accumulation of protein molecules, for a wide range of pore-sizes. Indeed, Chayen assumed that a surface with a wide pore-size distribution might increase the possibilities of finding the adequate pore dimension for promoting nucleation [37]. On the contrary, the work of Shah, defined a preferential size of pores for inducing crystallization related to the size of the gyration radius of the protein [38]. Later on, Shah demonstrated that the pore size effect could be enhanced by the appropriate surface chemistry. Indeed, substrates with different pore size (from 3 to 12 nm diameter) and functional groups (-OH, -CH_3, -NH_3, etc.) were applied for the crystallization of Lysozyme, Concanavalin A, Thaumatin, Catalase and Human Serum Albumin. The hypothesis for the enhanced nucleation was a combined effect where the small pores promoted the entrapment and restricted mobility of the protein molecules with consequent nuclei formation, whereas the functional groups helped the stabilization of the nuclei by interacting with a specific crystal face [39]. Hydrophobic microporous membranes were also used for tuning the interactions between protein molecules and ligands, such as ions, in order to improve diffraction resolution of the crystals. Crystallization of lysozyme on the top of polypropylene membranes in the presence of $CuCl_2$ allowed the formation of protein crystals with a different space group compared to the crystallization of lysozyme in the presence of $CuCl_2$ without membrane, suggesting that membrane-protein interactions might also drive

crystal polymorphism [20]. Functionalization of PVDF membranes with sulfonammide groups induced the formation of additional protein-surface interactions that in turn, induced protein orientation and agglomeration. This resulted in faster nucleation and higher number of crystals compared to the ones obtained with conventional PVDF [40]. Curcio et al. [41] developed a mathematical model to correlate the free energy nucleation ratio and the porosity of a material, in which the conventional free energy of nucleation ratio takes into account also the geometry of the pores in the interaction with the surface. The porosity of the membrane has also impact on the solvent removal rate of the crystallization process, providing a fine control on the nucleation rate and on the size of the crystals. For this reason, porous polypropylene membranes coated with hydrogel were used to combine the control provided by membrane-assisted nucleation (control of solvent-removal rate and faster nucleation rate) with the advantages of crystallization in gel, such as mechanical stability, size increase, no convection and reproducibility. Highly stable and well-diffracting crystals of Lysozyme and Concanavalin A were obtained on the composite membranes compared to the precipitate on conventional plates and plain polypropylene, thanks to the action of the gel. Indeed, in this case even though the hydrogel material was found incorporated in the crystals determining larger size and higher mosaicity (higher internal disorder), spot statistic parameters such as $I/(I)$ (average ratio of reflections intensity to its estimated error), R$-factor$ and R_{free} (parameters describing how well the resolved structure fits the experimental data, R$-factor$ is calculated for all the diffracted beams, instead R_{free} is calculated for a 1000 random diffracted beams [42]), improved significantly compared to crystals grown in conventional hanging drop plat [12]. Also rough surfaces were investigated. Liu et al. [43] developed a model in 2007, to include roughness effect in the calculation of Gibbs free energy variation of heterogeneous to homogeneous nucleation. They assumed a rough surface to be formed by uniform cones, including the cones geometry in the model. They validated their model by forming different topographies on glass slides using different types of oxidation treatment. Later on, in 2010 Curcio et al. [10] produced a simulation of nucleation on rough surfaces.

A recent work on the investigation of the effect of roughness on nucleation was performed by Salehi et al. [44]. They tuned hydrogel composite membranes with different concentrations of iron oxide nanoparticles determining several degrees of roughness. The increased nanoparticles concentration in Poly(vinyl alcohol) (PVA) hydrogel, crosslinked with poly(ethylene glycol) diglycidyl ether (PEGDE) or glutaraldehyde (GA), determined higher probability and density of nucleation. The effect was more pronounced for the gel crosslinked with PEGDE due to the higher number of interactive groups that created more interaction sites with protein molecules. The type of crosslinker and the presence of nanoparticles had both a result in the diffraction quality of the crystals. PVA crosslinked with PEGDE has a high flexibility due to the long chain of the crosslinker, hence during the growth of the crystals it can reassemble adapting its position to the growing crystals. Instead, PVA crosslinked with GA that has a high mechanical stability, cannot be misplaced by the strength of crystal that is obliged to incorporate the gel fibers in the crystalline lattice to continue growing. The gel incorporation determines a higher crystals' growth rate and crystals size but with a higher internal disorder (higher mosaicity) and distortion of the unit cells dimensions. This effect is more evident with higher concentration of iron oxide nanoparticles. Instead, no influence on the mosaicity, R_{merge}(diffraction quality) and R_{es} (quantity) was found for crystals grown in a more flexible gel. The general idea about roughness is that, also in this case, as for the pores, the obstacles formed by the irregularity of the surfaces determines cavities where local accumulation of protein molecules occurs with the consequent formation of local supersaturation spikes. According to the developed models and most of the experiments performed, an increasing roughness is directly related with an increased nucleation activity. Furthermore, the recent work of Hou et al. [45] hypothesized the possibility that an ideal roughness size might exists. Indeed, cavities that are smaller than the protein size may not promote any protein accumulation due to size exclusion effects, and cavities much larger than a protein molecule size might be just perceived as flat surfaces. Therefore, cavities that accommodate few protein molecules might be the actual promoters of nucleation. Even though the choice of the most fruitful

topographical features size and shape is not obvious yet, it is possible to state that crystallization on surfaces with hillocks or pores might be advantageous for achieving supersaturation at lower protein concentrations due to the ability of accumulating protein molecules in tight spaces. In addition, combining the spatial confinement with adequate chemical interactions between protein molecules and the surface, an enhancement of the topographical effect might be achieved.

2.4.3 Epitaxial surfaces

Epitaxy (the growth of a crystalline material on the top of another material with a similar crystalline structure) was the first mechanism discovered for the induction of nucleation [28]. Ordered materials such as Mica, Self-Assembled Monolayers and Graphene have been investigated for the crystallization of several proteins. Mica surfaces were used to crystallize Trichosanthin protein. By X-rays analysis it was found the same crystalline structure on the substrate and on the crystal, confirming the epitaxial effect [46]. SAM (Self-assembled monolayers) with several different alkyl groups were used to enhance the crystallization of several proteins (Lysozyme, α-Lactoglobulin, Hemoglobin, Thaumatin, Catalase). The highly organized structure of SAM promoted the organization of protein molecules into well-ordered crystals and reduced the formation of precipitate [47]. Later, in 2013, SAMs were modified with methyl, sulfidryl and amino groups and several proteins were tested (Lysozyme, Subtilisin A type VII, Thaumatin, Ribonuclease A type I, Ribonuclease A type XII, α-chymotrypsinogen A type II, Proteinase K, Catalase, Concanavalin A type VI, Glucose Isomerase, Cellulase). The modified SAMs increased the number of crystals compared to non-modified SAMs because of the increased surface of interaction between the protein solution and the substrate. Furthermore, methyl groups were found to be more effective than sulfidryl and amino groups. In fact, sulfidryl and amino groups, although may create hydrogen-bond interactions with proteins, they can also create the same type of interaction with water molecules determining a competition. The methyl group, instead, can only create Van der Waals interactions with the proteins [48]. Furthermore, the ordered structure of Graphene and Graphene Oxide improved

the crystallization of model proteins such as Alcohol Dehydrogenase, Catalase, Trypsin and Lysozyme by inhibiting the nucleation rate of amorphous precipitate. Graphene was found incorporated in the structure of the proteins, however it did not affect the resolution [49]. Hence, creating surfaces with a crystalline structure close to the one of protein crystals might enhance the probability of inducing crystallization by controlling the spatial organization of the molecules.

2.5 Effect of protein nature

The studies developed so far on protein crystallization have shown that the effect of surface properties on the crystallization of different proteins cannot be explained by a single general correlation. Indeed, the same surface might induce different effects depending on the type of protein. An example of this is the work of De Poel [50], where Insulin, Lysozyme, Talin and Bovine Serum Albumin crystallization was investigated on the top of mica surfaces functionalized with 1,3,5-tris(10-carboxydecyloxy) benzene (TCDB), obtaining different degrees of hydrophilicity/hydrophobicity and roughness. From this study, each protein showed a different behaviour and the formation of the different protein crystals seemed to have been affected in different extent from the different surface characteristics. For instance, Insulin crystallization occurs preferentially at surfaces with higher topographical features. In this case, the surface roughness seems to have higher influence on the crystallization of Insulin than surface chemistry. In contrast, surface chemistry seems to exert a higher control than topography on the nucleation step, in the formation of Lysozyme and Talin crystals, whereas no significant variations are registered on the BSA crystallization carried out at different surfaces. Protein molecules are a combination of aminoacids, with different side chains. The final folded molecule is characterized by a specific surface charge and hydrophilicity or hydrophobicity level, therefore, the type of interaction that each protein may establish with an external substrate and with other protein molecules is related with the protein itself and also with the environmental conditions, especially the pH that may change the charge of the molecules

and surfaces. Indeed, environmental pH will change the protein surface charge depending on the isoelectric point (pI) of the protein: at lower pH than pI the molecule will be positively charged, instead a negative charge will be exhibited when the environmental pH is higher than the pI. The total charge of the molecule will affect its solubility: two uncharged molecules will have a higher tendency to establish interaction between them than two charged molecules carrying the same charge. Hence, nucleating a neutral protein might be easier than nucleating a charged one: Lysozyme crystallization (pI 10.5 – 11.2) occurs with a lower induction time at pH 8.5 than at pH 4.5 [24]. A change in morphology was also evident when performing crystallization at different pH values. Increasing the pH of the Lysozyme crystallization environment, the probability of obtaining orthorhombic over tetragonal crystals increases [48, 51]. Hydrogel composite membranes were also recently used to tune protein crystallization by using pH and temperature sensitive monomers. Indeed, changing the buffer pH and/or the temperature, a variation in the swelling properties, ion-adsorption and the determination of supersaturation occurred leading to Lysozyme crystals with different shapes, from rod-like to flower-shaped [52]. In sum, when working on the development of surfaces or conditions for inducing protein crystallization, the type of protein has always to be considered, and modulating conditions (surface, buffer, precipitant, pH, and so on) might give better results if done directly on real case studies.

2.6 Membranes and gels for post-crystallization modifications

The limiting step in protein crystallography is always the attainment of well-diffracting crystals. Diffraction quality is related to the packing of the molecules in the crystals. The more the molecules are well organized the higher are the chances to elucidate the structure of the protein. Directly controlling the molecular organization is not possible, however, improvements can be obtained by controlling several parameters of the process. Indeed, beside controlling the pH of the solution, the additives' type and concentration that affect the charge of the

molecules and the type of interactions between them, the kinetics of nucleation and crystals growth and also lowering convection to a minimum might make the difference: indeed, a slower process and less perturbations might give time to the molecules to better organize in the lattice and avoid also the incorporation of impurities [53].

Once crystals are obtained, they always have to endure post-crystallization treatments before undergoing x-ray diffraction, such as cryoprotection (soaking the crystals in glycerol, in order to protect the crystal from the formation of ice-rings during the flash-cooling process with liquid nitrogen flux), or crosslinking (incorporation of glutaraldehyde in the crystals to promote reaction with lysine and improve stability of the crystals during cryoprotection). Sometimes, in spite of all efforts to control crystal packing, poor diffraction quality crystals are obtained and they have to undergo derivatization (soaking of the crystal in a solution containing a ligand to be incorporated in the crystal, in order to facilitate resolution or to study ligand-protein interaction), or other types of modifications, such as dehydration (by solvent evaporation) or annealing (thaw/freeze cycle that might promote reorganization of the molecules) [1, 2, 54].

However, crystals are highly fragile and they are in equilibrium with the surrounding environment. Therefore, performing post-crystallization treatments, implies several drawbacks and problems, namely the breaking of the vapour diffusion equilibrium and the risk of wreckage due to handling and/or brusque change of the environment. Recently, membranes and hydrogel media have been used also to control post-crystallization treatments such as cryoprotection and the derivatization of the crystals with heavy atoms. The gel was found to be a good surrounding environment for slower ligands' diffusion compared to solutions hence avoiding the shock of immersing the bare crystal directly in the osmotic solution [55]. As previously referred, in some cases, crystals grown in gel can incorporate the gel fibers in the crystalline lattice [44] determining a higher mosaicity and distortion of the unit cell [56] however, the presence of the gel

inside the crystal structure has the advantage of improving the mechanical stability and determining a higher resistance to osmotic shock when soaking in concentrated solutions of heavy atoms or organic solvents [13]. Also, ion-exchange membranes have been used to control the diffusion of heavy metals and halides in ionic form in Lysozyme crystals. The crystals were grown by vapour diffusion in an ion-exchange membrane contactor. On one side the protein solution was placed, relative humidity was controlled and supersaturation was generated by removal of water (Figure2.4A). Once crystallization occurred, and crystals were in equilibrium with the environmental relative humidity (Figure 2.4B), the bottom compartment was filled with the derivatizing solution (Figure 2.4C). The ion-exchange membrane regulated the diffusion of the ions to the protein solution and then diffused into the crystal. The regulated diffusion performed by the membrane allowed to avoid any damage due to abrupt changes of the environment, breaking of the vapour diffusion equilibrium and handling of the crystals. Diffraction analysis showed how unit cell parameters did not differ significantly from the PDB (Protein Data Bank, online archive gathering the 3D structure of macromolecules that were resolved so far https://www.rcsb.org/) model maintaining isomorphism allowing to resolve the tridimensional structure of the protein by isomorphous replacement technique. Therefore, the use of membranes and hydrogels resulted to be of significant impact also in performing post-crystallization treatments. The controlled diffusion of molecules performed by selective membranes and hydrogels and the higher mechanical resistance provided by the incorporation of hydrogel fibres in the crystalline lattice contributed both to the improvement/maintenance of the diffraction quality of the crystals.

2.7 Membrane-assisted protein crystallization and microfabrication technologies

The unpredictable nature and behaviour of proteins make protein crystallization a trial-and-error science. When the structure of an unknown protein has to be unravelled, several combinations of compounds and compositions have to be

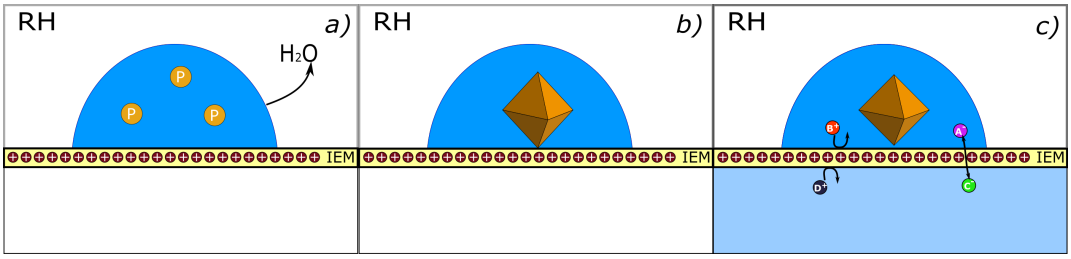

Figure 2.4: Membrane-assisted crystallization with a ion-exchange membrane. a) Supersaturation is generated by controlling relative humidity b) Crystals are formed and in equilibrium with the environment c) Derivatization of the crystals by ion-diffusion

tested in order to find out (when possible) the right recipe for good-diffracting crystals. Therefore, the limitations in protein crystallization (apart from the difficulties due to the protein structure itself) are the availability of a high amount of reagents and time required to perform extensive screenings. Microfluidics science and technology had a high impact in the last years in protein crystallography, developing creative designs (valve based, droplet based [57, 58], slip chip [59] or centrifugal design [60]) for minimizing the consumption of reagents and, at the same time, maximizing the number of conditions screened [61, 62]. Investigations about protein phase change behaviour [63], crystallization kinetics [64, 65], mixing effect [66] have been also performed in microfluidic devices. In addition, efforts are being made for developing x-ray transparent materials in order to perform in-situ x-ray analysis and avoid the manipulation of crystals [67, 68].

The main characteristic of microfluidics is the ability of manipulating very small volumes of fluids. They are used in several fields, from analytical techniques, to bioreactors, or electro-mechanic systems (MEMS). Their small dimensions allow not only the possibility to have a low consumption of reagents but also to carry out processes under laminar flow conditions, process automation through a series of valves and pumps systems that can be integrated, and high throughput [69] at low fabrication costs. Few examples of membrane-based micro-devices are available for protein crystallization where the gas permeability of PDMS was exploited to control supersaturation. Indeed, controlling the thickness of PDMS layer and the surrounding relative humidity it was possible to control evaporation rate and the attainment of crystals with different dimensions [70, 71].

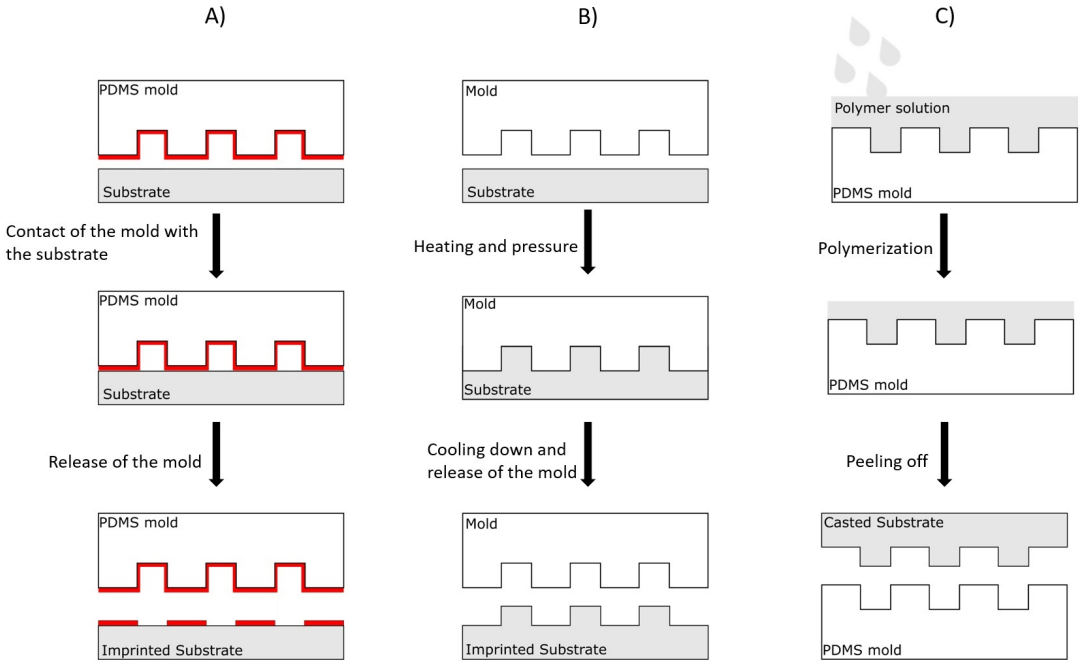

Figure 2.5: Soft lithographic techniques for surface patterning. A) Microcontact Printing; B) Embossing; C) Casting

The main material used for microfabrication is Polydimethylsiloxane (PDMS) which is optically transparent, non-toxic and inexpensive, when mixed with a crosslinking agent can be casted and shaped on microstructured moulds. Also, it has a high resolution in terms of size of the details that can be shaped in it. For this reason it is used for the fabrication of microfluidics devices or as a mould for the synthesis and modification of membrane materials by soft lithographic techniques [72, 73]. Indeed, soft lithography is a group of low-cost microfabrication techniques that make use of an elastomeric stamp (PDMS) for transferring a pattern to another substrate. The main soft lithography techniques (represented in Figure 2.5) for transferring a pattern are:

- Microcontact printing: the PDMS mould can be wet into an ink that will be released onto the surface by contact. During contact, the ink can form a self-assembled monolayer. It is used for patterning membranes for cell cultures [74, 75].

- Embossing: the substrate is softened with heat and by pressurized contact, the mold shape is transferred to the substrate. Several types of membranes

have been successfully molded with micro and nano structures such as PDMS [76], Nafion [77–80], Polypropilene [81] etc. Membrane patterning has been used for improving transport properties of membrane processes, such as microfiltration, ultrafiltration membranes [82], for reducing fouling [83], improving the flux, and control deposition [84].

- Casting: the PDMS mould can be used for casting a polymer solution that will take the the mould's shape after polymerization.

Patterning of a membrane material for protein crystallization purposes might allow the fabrication of tailored shaped or functionalized surfaces that may help in the investigation of heterogeneous nucleation effect. Furthermore, creating specific surface topographies by casting or embossing would avoid chemical modifications and a more reliable comparison between different structures for a deeper understanding of the strict topographical effect on nucleation. Creating chemical patterns by microcontact printing might induce localized interactions with protein molecules promoting supersaturation spikes.

2.8 Conclusions

Membrane-assisted protein crystallization technology has been developed in the last two decades and still advancements are being produced. In the last years, research work has been focused on the application of membranes for other processes involved in protein crystallography such as for efficient cryoprotection and derivatization. Several advantages can be highlighted by the use of membrane technology for crystallographic purposes. The tuning of membrane transport properties can achieve a fine control of the solvent removal rate and consequently of the generation of supersaturation. Furthermore, membranes can act as heterogeneous nucleants accelerating crystallization kinetics and favouring nucleation at lower protein concentration, and as protective environment for protein bioactivity. The use of membranes for post-crystallization treatments allows to improve or preserve the diffraction quality of the crystals by avoiding crystals manipulation

and sudden changes of the crystals environment, due to the diffusive transport of ligands and substances. Membrane-assisted crystallization and membrane-assisted post-crystallization treatment might be combined for developing a system able to control nucleation and crystal growth first and potentially perform post-crystallization modifications later. In this sense, membrane-assisted protein crystallization might find benefits from integration in a microfluidic device, also to improve throughput, and for automation of the processes. Microfabrication techniques might help to develop surfaces with well-defined characteristics for a more intensive screening of parameters (inherent to heterogeneous nucleation) allowing systematic studies of their impact on the different steps of protein crystallization (e.g. nucleation and crystal growth). Furthermore, most of these studies are conducted on model proteins. Attempts on real case studies should be performed in order to start thinking about membrane-assisted protein crystallization as a routine methodology for x-ray crystallography.

References

[1] B. Heras and J. L. Martin. "Post-crystallization treatments for improving diffraction quality of protein crystals." In: *Acta Crystallographica Section D: Biological Crystallography* 61.9 (2005), pp. 1173–1180. DOI: 10.1107/S0907444905019451.

[2] J. Newman. "A review of techniques for maximizing diffraction from a protein crystal in stilla." In: *Acta Crystallographica Section D: Biological Crystallography* 62.1 (2006), pp. 27–31. DOI: 10.1107/S0907444905032130.

[3] A. McPherson and J. A. Gavira. "Introduction to protein crystallization." In: *Acta Crystallographica Section F:Structural Biology Communications* 70.1 (2014), pp. 2–20. DOI: 10.1107/S2053230X13033141.

[4] R. Giegé. "A historical perspective on protein crystallization from 1840 to the present day." In: *FEBS Journal* 280.24 (2013), pp. 6456–6497. DOI: 10.1111/febs.12580.

[5] J. A. Gavira. "Current trends in protein crystallization." In: *Archives of Biochemistry and Biophysics* 602 (2016), pp. 3–11. DOI: 10.1016/j.abb.2015.12.010.

[6] G. Di Profio, E. Fontananova, E. Curcio, and E. Drioli. "From tailored supports to controlled nucleation: Exploring material chemistry, surface nanostructure, and wetting regime effects in heterogeneous nucleation of organic molecules." In: *Crystal Growth and Design* 12.7 (2012), pp. 3749–3757. DOI: 10.1021/cg3005568.

[7] E. Curcio, A. Criscuoli, and E. Drioli. "Membrane crystallizers." In: *Industrial and Engineering Chemistry Research* 40.12 (2001), pp. 2679–2684. DOI: 10.1021/ie000906d.

[8] G. Di Profio, E. Curcio, and E. Drioli. "Trypsin crystallization by membrane-based techniques." In: *Journal of Structural Biology* 150.1 (2005), pp. 41–49. DOI: 10.1016/j.jsb.2004.12.006.

[9] E. Drioli, E. Curcio, A. Criscuoli, and G. D. Di Profio. "Integrated system for recovery of CaCO3, NaCl and MgSO 4·7H2O from nanofiltration retentate." In: *Journal of Membrane Science* 239.1 (2004), pp. 27–38.

[10] E. Curcio, V. Curcio, G. D. Profio, E. Fontananova, and E. Drioli. "Energetics of Protein Nucleation on Rough Polymeric Surfaces." In: *Journal of Physical Chemistry B* 114 (2010), pp. 13650–13655.

[11] R.-B. Zhou, H.-L. Cao, C.-Y. Zhang, and D.-C. Yin. "A review on recent advances for nucleants and nucleation in protein crystallization." In: *CrystEngComm* 19.8 (2017), pp. 1143–1155. DOI: 10.1039/C6CE02562E.

[12] G. D. Profio, M. Polino, F. P. Nicoletta, B. D. Belviso, R. Caliandro, E. Fontananova, G. De Filpo, E. Curcio, and E. Drioli. "Tailored hydrogel membranes for efficient protein crystallization." In: *Advanced Functional Materials* 24.11 (2014), pp. 1582–1590. DOI: 10.1002/adfm.201302240.

[13] S. Sugiyama, M. Maruyama, G. Sazaki, M. Hirose, H. Adachi, K. Takano, S. Murakami, T. Inoue, Y. Mori, and H. Matsumura. "Growth of protein

crystals in hydrogels prevents osmotic shock." In: *Journal of the American Chemical Society* 134.13 (2012), pp. 5786–5789. DOI: 10.1021/ja301584y.

[14] X. Chen and J. Shen. "Review of membranes in microfluidics." In: *Journal of Chemical Technology and Biotechnology* 92.2 (2017), pp. 271–282. DOI: 10.1002/jctb.5105.

[15] J. De Jong, R. G. Lammertink, and M. Wessling. "Membranes and microfluidics: A review." In: *Lab on a Chip* 6.9 (2006), pp. 1125–1139. DOI: 10.1039/b603275c.

[16] E. Curcio, G. Di Profio, and E. Drioli. "Membrane crystallization of macromolecular solutions." In: *Desalination* 145.1-3 (2002), pp. 173–177. DOI: 10.1016/S0011-9164(02)00404-6.

[17] G. D. Di Profio, E. Curcio, A. Cassetta, D. Lamba, and E. Drioli. "Membrane crystallization of lysozyme: Kinetic aspects." In: *Journal of Crystal Growth* 257.3-4 (2003), pp. 359–369. DOI: 10.1016/S0022-0248(03)01462-3.

[18] P. Todd, S. K. Sikdar, C. Walker, and Z. R. Korszun. "Application of osmotic dewatering to the controlled crystallization of biological macromolecules and organic compounds." In: *Journal of Crystal Growth* 110.1-2 (1991), pp. 283–292. DOI: 10.1016/0022-0248(91)90897-E.

[19] M. Polino, A. Luísa Carvalho, L. Juknaite, C. A. M Portugal, I. M. Coelhoso, M. J. Romao, and J. G. Crespo. "Ion-Exchange Membranes for Stable Derivatization of Protein Crystals." In: *Crystal Growth & Design* 17 (2017), pp. 4563–4572. DOI: 10.1021/acs.cgd.7b00315.

[20] S. Simone, E. Curcio, G. Di, M. Ferraroni, and E. Drioli. "Polymeric hydrophobic membranes as a tool to control polymorphism and protein – ligand interactions." In: *Jornal of Membrane Science* 283 (2006), pp. 123–132. DOI: 10.1016/j.memsci.2006.06.028.

[21] G. Di Profio, E. Curcio, and E. Drioli. "Supersaturation control and heterogeneous nucleation in membrane crystallizers: Facts and perspectives." In: *Industrial and Engineering Chemistry Research* 49.23 (2010), pp. 11878–11889. DOI: 10.1021/ie100418z.

[22] E. Drioli, G. D. Profio, E. Curcio, W. S. W. Ho, and K Li. "Progress in membrane crystallization." In: *Current Opinion in Chemical Engineering* 1 (2012), pp. 178–182. DOI: 10.1016/j.coche.2012.03.005.

[23] E. Curcio, G. Di, and E. Drioli. "Microporous Hydrophobic Membranes for Crystallization of Biomolecules." In: *Chemical Engineering Transactions* 47.2 (2016), pp. 421–426. DOI: 10.3303/CET1647071.

[24] C. Y. Zhang, D. C. Yin, Q. Q. Lu, Y. Z. Guo, W. H. Guo, X. K. Wang, H. S. Li, H. M. Lu, and Y. J. Ye. "Cycling temperature strategy: A method to improve the efficiency of crystallization condition screening of proteins." In: *Crystal Growth and Design* 8.12 (2008), pp. 4227–4232. DOI: 10.1021/cg800689j.

[25] G. D. Profio, G. Perrone, E. Curcio, A. Cassetta, D. Lamba, and E. Drioli. "Preparation of Enzyme Crystals with Tunable Morphology in Membrane Crystallizers." In: *Ind Eng Chem Res* (2005), pp. 10005–10012. DOI: 10.1021/ie0508233.

[26] E. Curcio, G. Di, and E. Drioli. "A new membrane-based crystallization technique : tests on lysozyme." In: *Jornal of Crystal Growth* 247 (2003), pp. 166–176. DOI: 10.1016/S0022-0248(02)01794-3.

[27] E. Curcio, S. Simone, G. Di, E. Drioli, A. Cassetta, and D. Lamba. "Membrane crystallization of lysozyme under forced solution flow." In: *Jornal of Membrane Science* 257 (2005), pp. 134–143. DOI: 10.1016/j.memsci.2004.07.037.

[28] A. Mcpherson and P. Shlichta. "Heterogeneous and Epitaxial Nucleation of Protein Crystals on Mineral Surfaces." In: *Science* 239 (1988), pp. 385–387. DOI: 10.1126/science.239.4838.385.

[29] S. Fermani, G. Falini, M. Minnucci, and A. Ripamonti. In: *Journal of Crystal Growth* ().

[30] G. Tosi, S. Fermani, G. Falini, J. A. Gavira Gallardo, and J. M. Garcia Ruiz. "Crystallization of proteins on functionalized surfaces." In: *Acta Crystallographica Section D: Biological Crystallography* 64.10 (2008), pp. 1054–1061. DOI: 10.1107/S0907444908025079.

[31] A. S. Ghatak and A. Ghatak. "Precipitantless Crystallization of Protein Molecules Induced by High Surface Potential." In: *Crystal Growth & Design* 16 (2016), pp. 5323–5329. DOI: 10.1021/acs.cgd.6b00833.

[32] A. S. Ghatak, G. Rawal, and A. Ghatak. "Precipitant-Free Crystallization of Protein Molecules Induced by Incision on Substrate." In: *Crystals* 7.8 (2017), p. 245. DOI: 10.3390/cryst7080245.

[33] S. Khurshid, E. Saridakis, L. Govada, and N. E. Chayen. "Porous nucleating agents for protein crystallization." In: *Nature Protocols* 9.7 (2014), pp. 1621–1633. DOI: 10.1038/nprot.2014.109.

[34] C. N. Nanev, E. Saridakis, and N. E. Chayen. "Protein crystal nucleation in pores." In: *Scientific Reports* 7 (2017), pp. 35821–35829. DOI: 10.1038/srep35821.

[35] N. E. Chayen, E Saridakis, R El-Bahar, and Y Nemirovsky. "Porous silicon: an effective nucleation-inducing material for protein crystallization." In: *Journal of Molecular Biology* 312.4 (2001), pp. 591–595. DOI: 10.1006/jmbi.2001.4995.

[36] U. Salazar-Kuri, J. O. Estevez, E. E. Antunez, B. S. Martinez-Aguila, J. B. Warren, B. Andi, M. L. Cerniglia, V. Stojanoff, and V. Agarwal. "Nucleation of sub-micrometer protein crystals in square-shaped macroporous silicon structures." In: *Crystal Growth and Design* 15.6 (2015), pp. 2801–2808. DOI: 10.1021/acs.cgd.5b00243.

[37] N. E. Chayen, E. Saridakis, and R. P. Sear. "Experiment and theory for heterogeneous nucleation of protein crystals in a porous medium." In: *Proceedings of the National Academy of Sciences of the United States of America* 103 (2006), pp. 597–601. DOI: 10.1073/pnas.0504860102.

[38] U. V. Shah, D. R. Williams, and J. Y. Heng. "Selective crystallization of proteins using engineered nanonucleants." In: *Crystal Growth and Design* 12.3 (2012), pp. 1362–1369. DOI: 10.1021/cg201443s.

[39] U. V. Shah, M. C. Allenby, D. R. Williams, and J. Y. Y. Heng. "Crystallization of proteins at ultralow supersaturations using novel three-dimensional nanotemplates." In: *Crystal Growth and Design* 12.4 (2012), pp. 1772–1777. DOI: 10.1021/cg201190c.

[40] A. Gugliuzza, C Aceto, and E. Drioli. "Interactive functional poly (vinylidene fluoride) membranes with modulated lysozyme affinity : a promising class of new interfaces for contactor crystallizers." In: *Polym Int* 58 (2009), pp. 1452–1464. DOI: 10.1002/pi.2681.

[41] E. Curcio, E. Fontananova, G. D. Profio, and E. Drioli. "Influence of the Structural Properties of Poly(vinylidene fluoride) Membranes on the Heterogeneous Nucleation Rate of Protein Crystals." In: *Journal of Physical Chemistry B* 4.1 (2006), pp. 12438–12445. DOI: 10.1021/jp061531y.

[42] A. Wlodawer, W. Minor, Z. Dauter, and M. Jaskolski. "Protein crystallography for non-crystallographers, or how to get the best (but not more) from published macromolecular structures." In: *FEBS Journal* 275.1 (2015), pp. 1–21. DOI: 10.1111/j.1742-4658.2007.06178.x.Protein.

[43] Y. X. Liu, X. J. Wang, J. Lu, and C. B. Ching. "Influence of the roughness, topography, and physicochemical properties of chemically modified surfaces on the heterogeneous nucleation of protein crystals." In: *Journal of Physical Chemistry B* 111.50 (2007), pp. 13971–13978. DOI: 10.1021/jp0741612.

[44] S. M. Salehi, A. C. Manjua, B. D. Belviso, C. A. M. Portugal, I. M. Coelhoso, V. Mirabelli, E. Fontananova, R. Caliandro, Joa, G Crespo, E. Curcio, and G. D. Profio. "Hydrogel Composite Membranes Incorporating Iron Oxide Nanoparticles as Topographical Designers for Controlled Heteronucleation of Proteins." In: *Crystal Growth & Design* 18.6 (2018), pp. 3317–3327. DOI: 10.1021/acs.cgd.7b01760.

[45] H. Hou, B. Wang, S.-Y. Hu, M.-Y. Wang, J. Feng, P.-P. Xie, and D.-C. Yin. "An investigation on the effect of surface roughness of crystallization plate on protein crystallization." In: *Journal of Crystal Growth* 468.October 2016 (2017), pp. 290–294. DOI: 10.1016/j.jcrysgro.2016.10.007.

[46] L. H. Sun, C. Y. Xu, F. Yu, S. X. Tao, J. Li, H. Zhou, S. Huang, L. Tang, J. Hu, and J. H. He. "Epitaxial growth of trichosanthin protein crystals on mica surface." In: *Crystal Growth and Design* 10.6 (2010), pp. 2766–2769. DOI: 10.1021/cg100274m.

[47] T. Pham, D. Lai, D. Ji, W. Tuntiwechapikul, J. M. Friedman, and T. R. Lee. "Well-ordered self-assembled monolayer surfaces can be used to enhance the growth of protein crystals." In: *Colloids and Surfaces B: Biointerfaces* 34.3 (2004), pp. 191–196. DOI: 10.1016/j.colsurfb.2004.01.003.

[48] C.-y. Zhang, H.-f. Shen, Q.-j. Wang, Y.-z. Guo, and J. He. "An Investigation of the Effects of Self-Assembled Monolayers on Protein Crystallisation." In: *International Journal of Molecular Sciences* 14 (2013), pp. 12329–12345. DOI: 10.3390/ijms140612329.

[49] B. S. Gully, J. Zou, G. Cadby, D. M. Passon, K. S. Iyer, and C. S. Bond. "Colloidal graphenes as heterogeneous additives to enhance protein crystal yield." In: *Nanoscale* 4 (2012), pp. 5321–5324. DOI: 10.1039/c2nr31150j.

[50] W. De Poel, J. A. W. Mu, J. A.A. W. Elemans, W. J. P. Van Enckevort, A. E. Rowan, and E. Vlieg. "Surfaces with Controllable Topography and Chemistry Used as a Template for Protein Crystallization." In: *Crystal Growth & Design* 18 (2018), pp. 763–769. DOI: 10.1021/acs.cgd.7b01174.

[51] C. Longuet, A. Yamada, Y. Chen, D. Baigl, and J. Fattaccioli. "Spatially-controlled protein crystallization in microfluidic chambers." In: *Journal of Crystal Growth* 386 (2014), pp. 179–182. DOI: 10.1016/j.jcrysgro.2013.10.011.

[52] L. Wang, G. He, X. Ruan, and D. Zhang. "Tailored Robust Hydrogel Composite Membranes for Continuous Protein Crystallization with Ultrahigh Morphology Selectivity." In: *ACS Applied Materials & Interfaces* 10.31 (2018), pp. 26653–26661. DOI: 10.1021/acsami.8b08381.

[53] A. Adawy, E. Rebuffet, S. To Rnroth-Horsefield, W. J. De Grip, W. J. P. Van Enckevort, and E. Vlieg. "High Resolution Protein Crystals Using

an Efficient Convection-Free Geometry." In: 13 (2013), pp. 775–781. DOI: 10.1021/cg301497t.

[54] A. C. W. Pike, E. F. Garman, T. Krojer, F. von Delft, and E. P. Carpenter. "An overview of heavy-atom derivatization of protein crystals." In: *Acta crystallographica. Section D, Structural biology* 72.Pt 3 (2016), pp. 303–318. DOI: 10.1107/S2059798316000401.

[55] M. Sugahara. "A technique for high-throughput protein crystallization in ionically cross-linked polysaccharide gel beads for x-ray diffraction experiments." In: *PLoS ONE* 9.4 (2014), pp. 1–8. DOI: 10.1371/journal.pone.0095017.

[56] O Vidal, M. Robert, B Arnoux, and B Capelle. "Crystalline quality of lysozyme crystals grown in agarose and silica gels studied by X-ray diffraction techniques." In: *Journal of Crystal Growth* 196.2-4 (1999), pp. 559–571. DOI: 10.1016/S0022-0248(98)00917-8.

[57] Y. R. Liang, L. N. Zhu, J. Gao, H. X. Zhao, Y. Zhu, S. Ye, and Q. Fang. "3D-Printed High-Density Droplet Array Chip for Miniaturized Protein Crystallization Screening under Vapor Diffusion Mode." In: *ACS Applied Materials and Interfaces* 9.13 (2017), pp. 11837–11845. DOI: 10.1021/acsami.6b15933.

[58] H. Yamaguchi, M. Maeki, K. Yamashita, H. Nakamura, M. Miyazaki, and H. Maeda. "Controlling one protein crystal growth by droplet-based microfluidic system." In: *Journal of Biochemistry* 153.4 (2013), pp. 339–346. DOI: 10.1093/jb/mvt001.

[59] W. Du, L. Li, K. P. Nichols, and R. F. Ismagilov. "SlipChip." In: *Lab on a Chip* 9.16 (2009), p. 2286. DOI: 10.1039/b908978k.

[60] L. Wang, K. Sun, X. Hu, G. Li, Q. Jin, and J. Zhao. "A centrifugal microfluidic device for screening protein crystallization conditions by vapor diffusion." In: *Sensors and Actuators B: Chemical* 219 (2015), pp. 105–111. DOI: 10.1016/J.SNB.2015.04.105.

[61] L. Li and R. F. Ismagilov. "Protein Crystallization Using Microfluidic Technologies Based on Valves, Droplets, and SlipChip." In: *Annu. Rev. Biophys* 39 (2010), pp. 139–58. DOI: 10.1146/annurev.biophys.050708.133630.

[62] B. Zheng, C. J. Gerdts, and R. F. Ismagilov. "Using nanoliter plugs in microfluidics to facilitate and understand protein crystallization." In: *Current Opinion in Structural Biology* 15.5 (2005), pp. 548–555. DOI: 10.1016/j.sbi.2005.08.009.

[63] J. Ferreira, F. Castro, F. Rocha, and S. Kuhn. "Protein crystallization in a droplet-based microfluidic device: Hydrodynamic analysis and study of the phase behaviour." In: *Chemical Engineering Science* 191 (2018), pp. 232–244. DOI: 10.1016/j.ces.2018.06.066.

[64] P. C. Hansen. "Introduction and Motivation." In: *Discrete Inverse Problems: Insight and Algorithms* (2010), pp. 1–4. DOI: http://dx.doi.org/10.1137/1.9780898718836.

[65] S. V. Akella, A. Mowitz, M. Heymann, S. Fraden, and M. A. Fisher. "Emulsion-Based Technique To Measure Protein Crystal Nucleation Rates of Lysozyme." In: *Crystal Growth & Design* 14 (2014), pp. 4487–4509. DOI: 10.1021/cg500562r.

[66] D. L. Chen, C. J. Gerdts, and R. F. Ismagilov. "Using Microfluidics to Observe the Effect of Mixing on Nucleation of Protein Crystals." In: *Journal of the American Chemical Society* 127 (2018), pp. 9672–9673. DOI: 10.1021/ja052279v.

[67] C. J. J. Gerard, G. Ferry, L. M. Vuillard, J. A. Boutin, L. M. G. Chavas, T. Huet, N. Ferte, and R. Grossier. "Crystallization via tubing microfluidics permits both in situ and ex situ X-ray diffraction research communications." In: *Acta Crystallographica F* 73 (2017), pp. 574–578. DOI: 10.1107/S2053230X17013826.

[68] M. Heymann, A. Opthalage, J. L. Wierman, S. Akella, D. M. E. Szebenyi, S. M. Gruner, and S. Fraden. "Room-temperature serial crystallography

using a kinetically optimized microfluidic device for protein crystallization and on-chip X-ray diffraction." In: *IUCrJ* 1 (2014). DOI: 10.1107/S2052252514016960.

[69] G. M. Whitesides. "The origins and the future of microfluidics." In: *Nature* 442.7101 (2006), pp. 368–373. DOI: 10.1038/nature05058.

[70] Y. Yu, X. Wang, D. Oberthür, A. Meyer, M. Perbandt, L. Duan, and Q. Kang. "Design and application of a microfluidic device for protein crystallization using an evaporation-based crystallization technique." In: *Journal of Applied Crystallography* 45.1 (2012), pp. 53–60. DOI: 10.1107/S0021889811048047.

[71] B. Zheng, L. S. Roach, and R. F. Ismagilov. "Screening of protein crystallization conditions on a microfluidic chip using nanoliter-size droplets." In: *Journal of the American Chemical Society* 125.37 (2003), pp. 11170–11171. DOI: 10.1021/ja037166v.

[72] D. Qin, Y. Xia, and G. M. Whitesides. "Soft lithography for micro- and nanoscale patterning." In: *Nature Protocols* 5.3 (2010), pp. 491–502. DOI: 10.1038/nprot.2009.234.

[73] A. Pimpin and W. Srituravanich. "Review on Micro- and Nanolithography Techniques and their Applications." In: *Engineering Journal* 16.1 (2012), pp. 37–55. DOI: 10.4186/ej.2012.16.1.37.

[74] F. Evenou, J.-M. D. Meglio, B. Ladoux, and P. Hersen. "Micro-patterned porous substrates for cell-based assays †." In: *Lab on a Chip* 12 (2012), pp. 1717–1722. DOI: 10.1039/c2lc20696j.

[75] P. Gao, A. Hunter, S. Benavides, M. J. Summe, F. Gao, and W. A. Phillip. "Template Synthesis of Nanostructured Polymeric Membranes by Inkjet Printing." In: *ACS Applied Materials & Interfaces* 8.5 (2016), pp. 3386–3395. DOI: 10.1021/acsami.5b11360.

[76] T. Köpplmayr, L. Häusler, I. Bergmair, B. Farshchian, S. M. Hurst, J. Lee, and S. Park. "3D molding of hierarchical micro- and nanostructures." In: *Journal of Micromechanics and Microengineering* 21 (2011), pp. 1–8. DOI: 10.1088/0960-1317/21/3/035016.

[77] Y.-h. Cho, J. Woo, O.-h. Kim, J. Young, N. Jung, K. Shin, H. Choi, H. Choe, Y.-h. Cho, and Y.-e. Sung. "High performance direct methanol fuel cells with micro / nano-patterned polymer electrolyte membrane." In: *Journal of Membrane Science* 467 (2014), pp. 36–40. DOI: 10.1016/j.memsci.2014.03.069.

[78] M. H. Yildirim, J Braake, H. C. Aran, D. F. Stamatialis, and M Wessling. "Micro-patterned Nafion membranes for direct methanol fuel cell applications." In: *Journal of Membrane Science* 349 (2010), pp. 231–236. DOI: 10.1016/j.memsci.2009.11.050.

[79] A Omosebi and R. S. Besser. "Electron Beam Assisted Patterning and Dry Etching of Nafion Membranes." In: *Journal of Electrochemical Society* 158.10 (2011), pp. D603–D610. DOI: 10.1149/1.3615938.

[80] S Cuynet, A Caillard, T Lecas, N Semmar, J Bigarr, and P. Brault. "Membrane patterned by pulsed laser micromachining for proton exchange membrane fuel cell with sputtered ultra-low catalyst loadings." In: *Journal of Power Sources* 298 (2015), pp. 299–308. DOI: 10.1016/j.jpowsour.2015.08.019.

[81] M. Lafuente, E. Martínez, I. Pellejero, M. del Carmen Artal, and M. del Pilar Pina. "Wettability control on microstructured polypropylene surfaces by means of O2 plasma." In: *Plasma Processes and Polymers* 14.8 (2017), pp. 1–6. DOI: 10.1002/ppap.201700019.

[82] J. Hutfles, W. Chapman, and J. Pellegrino. "Roll-to-roll nanoimprint lithography of ultrafiltration membrane." In: *Journal of Applied Polymer Science* 135.11 (2018), pp. 1–12. DOI: 10.1002/app.45993.

[83] O. Heinz, M. Aghajani, A. R. Greenberg, and Y. Ding. "Surface-patterning of polymeric membranes: fabrication and performance." In: *Current Opinion in Chemical Engineering* 20 (2018), pp. 1–12. DOI: 10.1016/j.coche.2018.01.008.

[84] S. H. Maruf, L. Wang, A. R. Greenberg, J. Pellegrino, and Y. Ding. "Use of nanoimprinted surface patterns to mitigate colloidal deposition on ultrafiltration membranes." In: *Journal of Membrane Science* 428 (2012), pp. 598–607. DOI: 10.1016/j.memsci.2012.10.059.

CHAPTER 3

STRUCTURED NAFION® MEMBRANES FOR PROTEIN CRYSTALLIZATION

3.1 Summary

In this work Nafion® membranes were modified by soft lithografic techniques in order to create different topographies minimizing the chemical changes of the surface. The patterned membranes were tested for the crystallization of Trypsin from Bovine Pancreas. From the analysis of the induction time, nucleation and growth rate an enhanced nucleation activity resulted for all the patterned membranes compared to the flat one. Different mechanisms of nucleation were hypothesised depending on the size of the topographical feature and the chemistry of the membrane. Experimental results were also compared with theoretical calculations of the ratio between Gibbs free energy variation of heterogeneous and homogeneous nucleation.

3.2 Introduction

X-ray crystallography is the main technique used for resolving the tri-dimensional structure of proteins. The main limitation of X-rays analysis is the attainment

of well-diffracting crystals[1, 2]. The key event for obtaining protein crystals suitable for x-ray diffraction is nucleation. Nucleation is a phase change, occurring in supersaturated solutions that reinstate equilibrium by clustering protein molecules in small solid nuclei. This leads to the formation of an interface between the solid nuclei and the solution creating the need for overcoming an activation energy for the process to occur. In other words, nucleation only becomes effective when the nuclei reach a critical size[3, 4]. It is well known that the interaction of the target solution with external substrates alters the Gibbs free energy of the nucleation process promoting or inhibiting nucleation (heterogeneous nucleation)[5]. Heterogeneous nucleation for protein crystals was first reported in 1988, by McPherson, growing protein crystals onto minerals with a similar crystalline lattice (epitaxy) [6]. From there on, several surfaces were investigated for nucleation and several chemical interactions between protein molecules and the surfaces were hypothesized: ionic interactions, hydrogen bonding and hydrophobic interactions [7–11]. Furthermore, an always increasing number of studies are pointing out how combining chemical interactions with a suitable surface topography might enhance the probability of nucleation. For instance, Shah et al. [12–15] noticed that the increased nucleation due to protein accumulation in pores was enhanced by functionalizing the surfaces with specific chemical moieties (such as –OH, -NH_3 or CH_3). They hypothesised a further stabilization of the nuclei formed in the pores by physical entrapment of the protein molecules induced by the presence of the functional groups [12, 13]. Also the work of Ghatak et al. [16, 17], showed how combining a wrinkled PDMS surface with an oxidation treatment it was possible to obtain protein crystals without the help of precipitant. For this reason, recent efforts were directed towards studying the topography and roughness effect on nucleation, developing surfaces with similar chemistry and different topography. In spite of all efforts, the creation of different topographies was, so far, always associated with changes in the surface chemistry or composition. Liu et al. created different roughness values by the functionalization of glass slides with different monomers [18]. A more recent study, tried

to change the surface structure of Muscovite Mica by depositing layers of 1,3,5-tris(10-carboxydecyloxy) benzene (TCDB). The size of the features was correlated with the amount of TCDB deposited [19]. Topography effects were also investigated by modifying the surface of conventional protein crystallization plates with various types of oxidation treatments in order to generate different degrees of roughness [20].

During the last twenty years membranes have been used to control solvent transport, and also as heterogeneous nucleation promoters. Indeed, porosity of the materials resulted to be useful in controlling the evaporation rate of the solvent and at the same time creating sites for protein accumulation [21]. Microporous membranes were also covered with gel, in order to improve protein diffraction quality exploiting the convection-free environment of the gel [22]. Recently, the chemical and topographical features of hydrogel composite membranes were tuned by incorporating different amounts of iron oxide nanoparticles [23]. Therefore, creating materials with a tunable topography trying to minimize the changes in chemical composition of the surface seems to be a priority, but no method was found yet just to compare the topographies without any change in the surface chemistry. Thanks to soft lithography, it is possible today to design tailored geometries at different scales and transfer them to different surfaces minimizing surface chemistry changes. Soft lithography includes a set of techniques that make use of an elastomeric stamp, namely a PDMS stamp, to transfer a micro/nano structure onto a substrate. These techniques are cleanroom free and low-cost, which makes micro and nano-fabrication affordable for a wide range of applications. They rely on the fabrication of a silicon master mould that can be used to fabricate PDMS replicas by casting. The PDMS replicas can be then used for several times for thermal nanoimprint lithography or microtransfer moulding [24]. Thermal nanoimprint lithography is a powerful and inexpensive technique for reproducing large patterns onto thermoplastic materials [25–27]. It takes advantage of the ability of materials to become soft and suffer deformation at temperatures higher than their glass transition temperature (Tg) and reinstate their stiffness at temperatures below the Tg. The PDMS mould can also be used for casting a

polymer solution to conform the material directly within the mould shape.
This work takes advantage of soft lithographic techniques to create micro and nano features and a mixture of both periodically distributed on the top of a Nafion® membrane for the crystallization of Trypsin from Bovine Pancreas and understanding the effect of topography on nucleation. Nafion® membranes were chosen for this work due to their suitability for crystallization and their ability for controlling the diffusion of heavy metals obtaining a gentle derivatization of protein crystals [28]. Hence, optimizing a membrane surface suitable for a gentle derivatization, besides a more controlled nucleation, would allow for creating a support suitable for all steps required for protein X-ray resolution. The crystallization performance (induction time, nucleation and growth rate) is evaluated to demonstrate the benefits of the patterns on the membranes' surface and understand the effect of topography on nucleation. Finally, the model developed by Liu et al. [18] was adapted to the designed geometries to simulate the experimental results, in order to settle the guidelines for future development.

3.3 Materials and Methods

3.3.1 Fabrication of patterned Nafion® membranes

Different topographies, with micro and or nano features, were created on the surface of Nafion® membranes. Two types of Nafion® membranes were used: commercially available Nafion® 117 (Equivalent Weight 1100 g/eq and 178 μm thickness) purchased from Sigma Aldrich; and Nafion® NR50 (1100 g/eq Equivalent Weight) purchased from Ion-Power in the form of beads. Both polymers have the same chemical composition and the same ion-exchange capacity, however the different membrane preparation method produces a different behaviour in terms of water uptake (24% for Nafion® 117 and 15% for Nafion® NR50 solution in DMF casted), and different conductivity and resistance [29]. The fabrication process is based on the thermal nanoimprint lithography and the microtransfer moulding techniques. Both methods take advantage of the contact of the substrate with a

mould for transferring the designed structure. The designed structure was transferred to Nafion® 117 by thermal nanoimprint lithography using a silicon mould to obtain microscale surface patterning and a mould made of Silicon covered with BARC (AZ BARLi II 200, MicroChem.) and then with a gold layer [30] to obtain a surface patterning in the nanoscale range. The same microscale patterning was transferred to a Nafion® NR50 membrane by casting the polymer solution onto a PDMS mould.

3.3.2 Fabrication of the moulds

Three different moulds were prepared. A nano-mould (displayed in Figure 3.1A) made of Silicon covered with BARC (AZ BARLi II 200, MicroChem.) and a gold layer was produced by displacement Talbot lithography [30]. The pillars have a diameter of 110.7 ± 2 nm, a height of 115.4 ± 0.5 nm and a pitch of 250 nm. A Poly(dimethylsiloxane) (PDMS) (purchased by Sylgard 184 Dow Corning, Midland, MI) micromould (shown in Figure 3.1B) with triangle prisma shaped pillars with 160 μm side and 110 μm height was produced by casting uncured PDMS solution (10:1 ratio) onto a silicon master mould fabricated by photolithography [31]. Finally, a silicon mould with the same shape and dimensions of the PDMS micromould was produced by photolithography (details on the photolithography process are reported in the Appendix A.

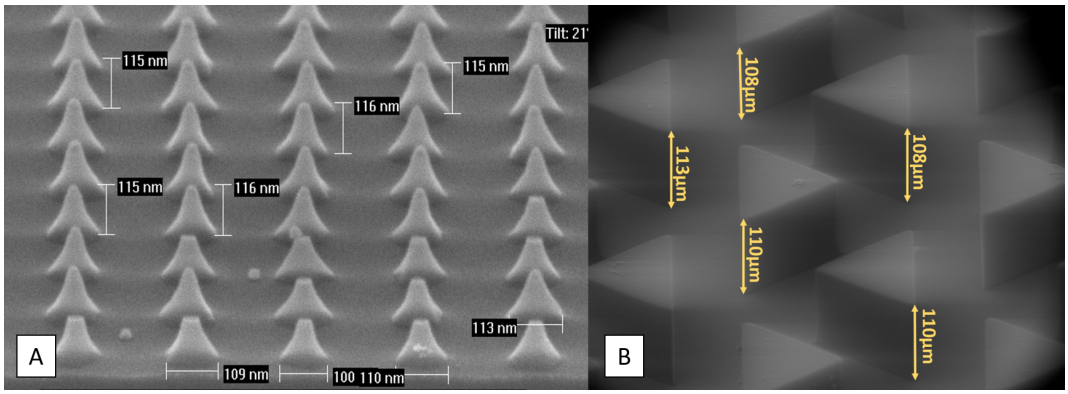

Figure 3.1: SEM images of a) Nano-mould ; b) PDMS micro-mould

3.3.3 Patterning of the membranes

The patterning of the membranes was made with two different techniques according to the different types of Nafion®. Nafion® 117 was patterned using a Compact NanoImprint (CNI) v.2.0 from NILT company. The Nafion® 117 and the mould (Silicon mould for the microstructure and BARC mould for the nanostructure) were contacted on the top of a ceramic heating plate. The chamber was closed and a program was set in order to firstly rise the temperature to 135 °C (20 °C above the Tg of Nafion®, which was measured by Differential Scanning Calorimetry and reported in the Supporting Information) to soften the membrane, then a pressure of 6 bar was applied for 6 minutes to improve the contact between the mould and Nafion® 117. Finally, the temperature was lowered to 60 °C (to freeze the structure of the mould in the substrate) and pressure released (see schematics in Figure 3.2A). Nafion® beads NR50 were, instead, dissolved in N,N-Dimethylformamide (DMF) purchased from Acros, at 240 °C for 24 hours in autoclave, at a concentration of 0.030 g/mL. The Nafion® solution was casted onto the mould (PDMS microstructured mould or a petri dish for flat membranes) and left on a hot plate at 90 °C until complete evaporation of the solvent (see schematics in Figure 3.2B and 3.2C). Controlling the amount of polymer used for casting allows to tune the thickness of the membrane and, when the thickness of the membrane is less than the height of the pillars (110 ±2 μm), a membrane with straight pores connecting both sides is obtained (See Figure 3.2C). In order to facilitate the release of the membrane, before Nafion® solution casting, the PDMS mold was treated with Tridecafluoro-1,1,2,2-tetrahydrooctyl-1-trichlorosilane (TFOCS, from Sigma Aldrich). Few drops of TFOCS were left evaporating and deposited as a thin layer onto the PDMS mould to make it more hydrophobic [24] . Membranes were washed in boiling water in order to remove traces of DMF solvent. Finally combining the micro structured membrane with holes and the nano imprinted membrane, a hierarchical structure with the nanowells inside the microwells has been fabricated (Figure 3.2C). All the fabricated membrane with the fabrication technique, topographical feature type, thickness, contact angle and roughness are reported in Table 3.1.

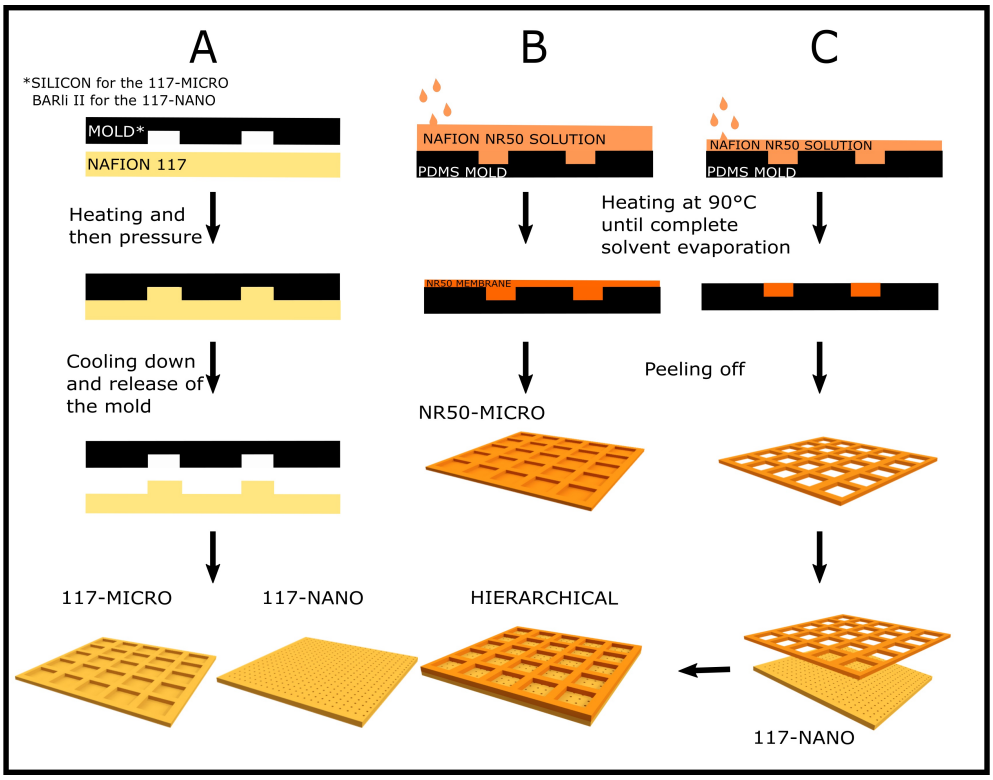

Figure 3.2: Fabrication Processes. A) Thermal Nanoimprinting lithography: the silicon mould has been produced by photolithography. B) A PDMS mould produced by casting of PDMS onto a Silicon mould can be used for casting of the polymer solution. C) Controlling the volume of polymer solution a membrane with micropores was obtained and combined with the Nano structured membrane to create a hierarchical surface

3.3.4 Characterization of Moulds and Membranes

In order to verify the successfulness of the fabrication processes, and measure the size of the features, moulds and membranes were characterized by AFM (Multimode 8 from Veeco/Bruker), SEM (Inspect F50, FEI) and optical microscopy (Nikon Eclipse ci). Samples for SEM were sputtered either with Au/Pd or carbon. AFM images were processed by Gwyddion software [32], SEM and optical microscopy images were processed by Image J [33]. In order to track chemical changes that may occur during the imprinting process FTIR spectra of the membranes were recorded.

3.3.5 Crystallization solutions

Trypsin from Bovine Pancreas (BPT), purchased from Panreac, was dissolved in 25 mM Hepes buffer (pH 7.5), with 10 mM $CaCl_2$ and 10 mg/mL Benzamidine (in order to inhibit the protease activity). The BPT concentration in this solution was 40 mg/mL. The precipitant solution was composed of 0.2 M $(NH_4)_2SO_4$ (purchased from Panreac), 20% PEG 8K (purchased from Sigma-Aldrich), and 0.1M Cacodylate (purchased from Sigma Aldrich) pH 6.5. The final protein concentration, after mixing up the protein and precipitant concentration was 20 mg/mL.

3.3.6 Crystallization experiments

The structured membranes were tested for the crystallization of Trypsin from Bovine Pancreas. The experiments were performed in the vapour diffusion mode [1] inside 24-wells plates from Qiagen, in sitting mode. The crystallization set-up is displayed in Figure 3.3. Briefly, an equal amount (5 μL) of protein and precipitant solution was mixed on the top of the membrane and left equilibrating with 500 μL of stripping solution with the same composition of the precipitant. The difference in water activity between the crystallization solution and the stripping solution determined solvent migration from the protein solution to the stripping solution, increasing protein concentration until reaching supersaturation and promote nucleation. Each condition was replicated 5 times. Data over time, on nucleation and crystal growth, were obtained by monitoring the crystals with an optical microscope (Nikon Eclipse ci) equipped with a camera and pictures were processed with the ImageJ software [33].

3.3.7 Contact Angle

The wetting properties of the topographies fabricated were studied based on the static contact angle (SCA) measurements. These were evaluated by the sessile drop method in a contact angle goniometer (CAM 100, KSV Instruments Ltd., Finland). The solution used for the measurement was the same solution used for the crystallization experiments, hence: 20 mg/mL Trypsin from Bovine Pancreas,

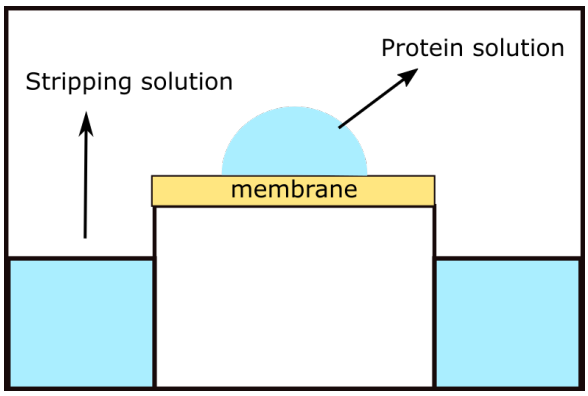

Figure 3.3: Crystallization set-up. The membrane was laid out onto a plastic bridge surrounded by the stripping solution. The protein solution was placed on the top of the membrane's patterned surface and left equilibrating with the stripping solution.

12.5 mM Hepes buffer (pH 7.5), with 5 mM $CaCl_2$ and 5mg/mL Benzamidine, 0.1 M $(NH_4)_2SO_4$ (purchased from Panreac), 10% PEG 8K, 0.05 M of Cacodylate pH 6.5. Each measurement was repeated 5 times. The drop volume used for the measurement was 9 μL.

3.4 Results and Discussion

3.4.1 Characterization of the imprinted topographies on Nafion® membranes

The imprinting and casting processes were assessed by AFM, SEM and optical microscopy analysis of the patterned surfaces. The nanostructured membrane (Figure 3.4A) has wells with 110 nm diameter and a repeating unit of 230 nm x 230 nm. The membranes with the micro structure have a side of the triangle of 164m and a repeating unit of 187 μm x 355 μm (Figure 3.4B).

The roughness parameters, Ra (that represents the average of absolute values of profile height deviations from the mean line) and Rms (that represents the root mean square average of the profile height deviations from mean line) were determined by processing the AFM images of the surfaces with patterning (Figure 3.5) using the software Gwyddion [32] . As shown in figure 3.6B, in the case of 117-Nano the line for determining the roughness was drawn across the hillocks,

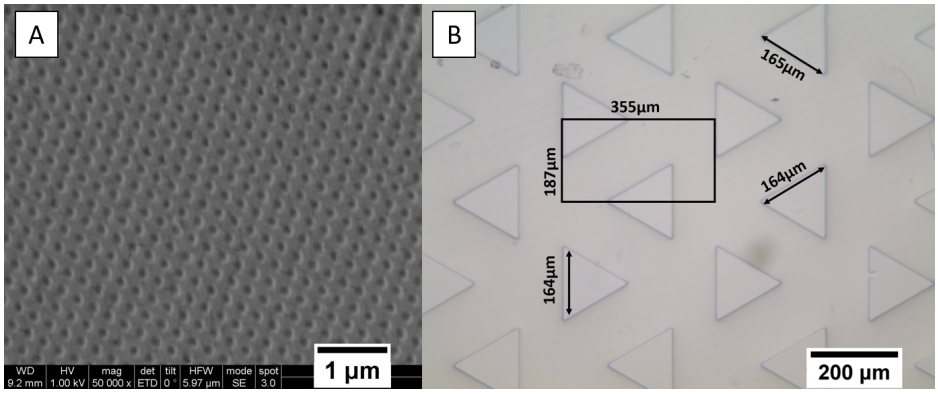

Figure 3.4: A) SEM image of 117-Nano B) Optical microscope image of 117-Micro, with side dimensions

instead in the case of the 117-Micro and NR50-Micro the AFM measurement was done on the top of the surface and not inside the wells.

Table 3.1: Membranes characterization: type of features, thickness, contact angle and roughness. (*Roughness of the Hierarchical membrane: these values were calculated by weighted average between Nafion® 117-Nano and Nafion® NR50-Micro)

Type of Membrane	Type of features	Thickness (μm)	Contact Angle (°)	Ra (nm)	Rms (nm)
117-Flat	No	178	64.7±2.9	1.0±0.2	3.1±3.4
117-Nano	Nano wells	178	63.2±2.4	14.9±4.9	16.8±7.2
117-Micro	Micro wells	178	48.1±4.2	4.0±0.4	6.4±1.1
NR50-Flat	No	90	77.7±4.4	22.2±6.0	38.5±21.9
NR50-Micro	Micro wells	90	100±4	2.8±0.4	3.8±0.6
Hierarchical (117+ NR50)	Micro wells with inside nanowells	268	87.3±1.6	4.52*	5.07*

As it is possible to see from the results reported in Table 3.1, even though, 117-Flat and 117-Micro have different topographies at a microscopic level, they have a comparable roughness at nanoscopic scale. This is due to the fact that the area of analysis is smaller than the microstructure features (see figure 3.6A).

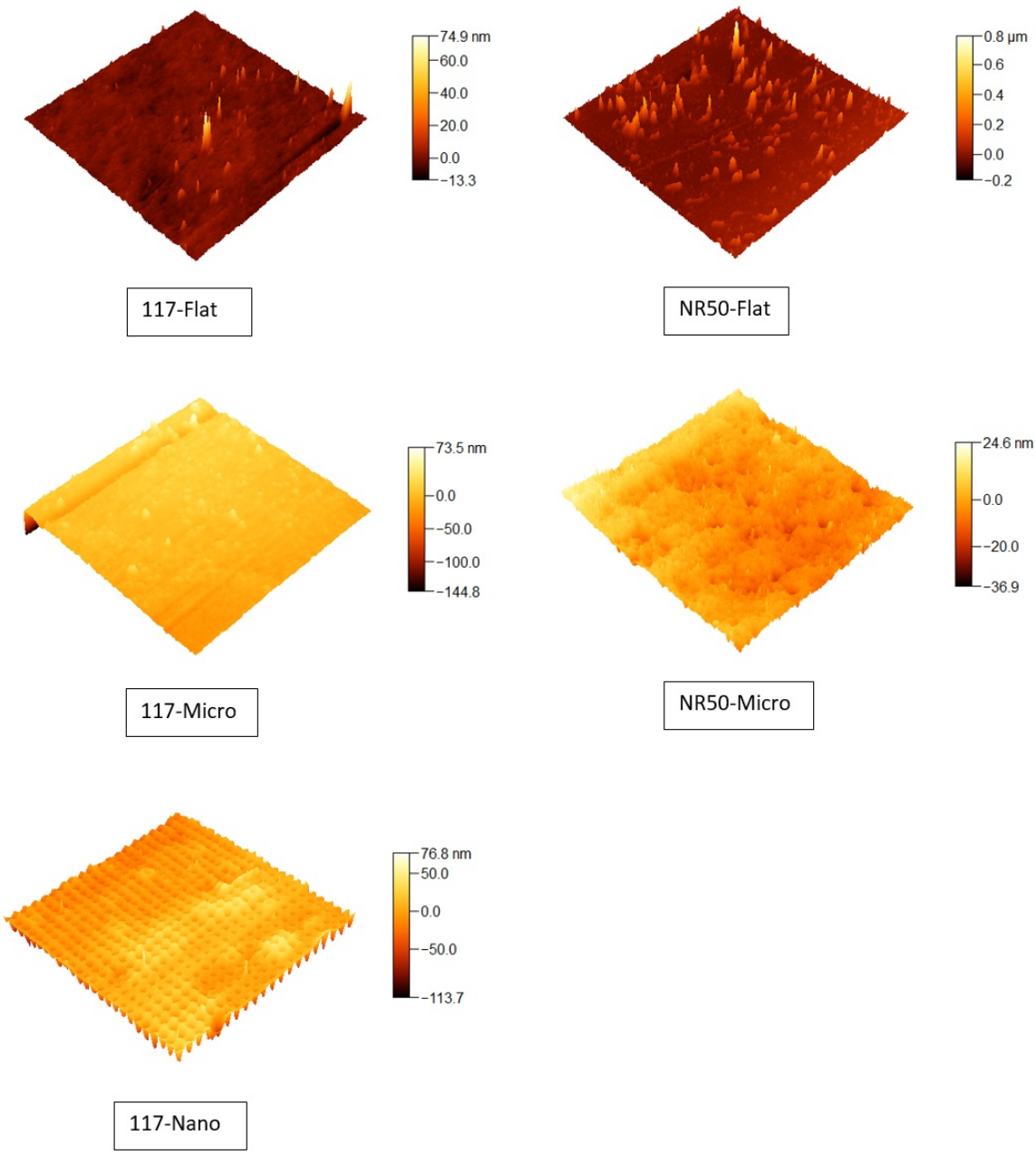

Figure 3.5: AFM images. The scanned area was 5 μm X 5 μm for all the membranes except for the NR50-Flat that was 25 μm X 25 μm. The measurement of the micro structure surface has been done on the top of the surface, not inside the wells. In the case of the 117-Nano, the roughness measurement has been done crossing the hills.

On the contrary, the nanostructure imprinted on 117-Nano increases the value of roughness compared to that of 117-Flat, due to the crossing of the wells during image processing. NR50-Flat has a higher roughness compared to NR50-Micro probably due to defects of the petri dish used for the casting. NR50-Micro has a roughness comparable to 117-Micro. The hierarchical membrane has a hybrid surface: the area inside the wells is made of 117-Nano, instead the superficial area is made of NR50-Micro (see Figure 3.6C), therefore the roughness has been calculated by a weighted average taking into account the percentage of surface area of each type of membrane (more details about the calculations are reported in the Appendix A).

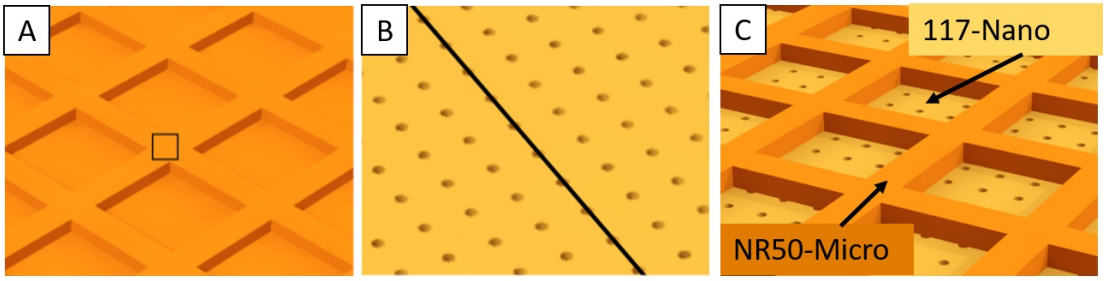

Figure 3.6: A) Schematics of membrane with micro-pattern (117-Micro). The AFM analysis has been performed on the top of the surface (black square in A)) and not inside the wells; B) Schematics of the 117-Nano. The measurement of the roughness has been done crossing the nano. C) Schematics of Hierarchical membrane. The roughness has been calculated has weighted average between the NR50-Micro and 117-Nano

Previous investigations related to the thermal behaviour of Nafion® membranes have shown that treatment of Nafion® membranes with high temperature may induce changes in the crystallinity of the material leading to a lower water uptake and conductivity [34, 35]. However, according to the literature, the conditions at which nanoimprinting is performed in this work (T = 135 °C) induce a minimum change in the water content (2%) and in the conductivity (3.75%) and no changes in the crystallinity of the material [34]. In order to confirm that no significant changes occur in the chemistry of the material, FTIR spectra were recorded of the 117-Flat and 117-Nano.

The FTIR spectra is represented in Figure 3.7. The peak at 3451 is slightly more intense in the case of the 117-Flat membrane. This peak can be related to

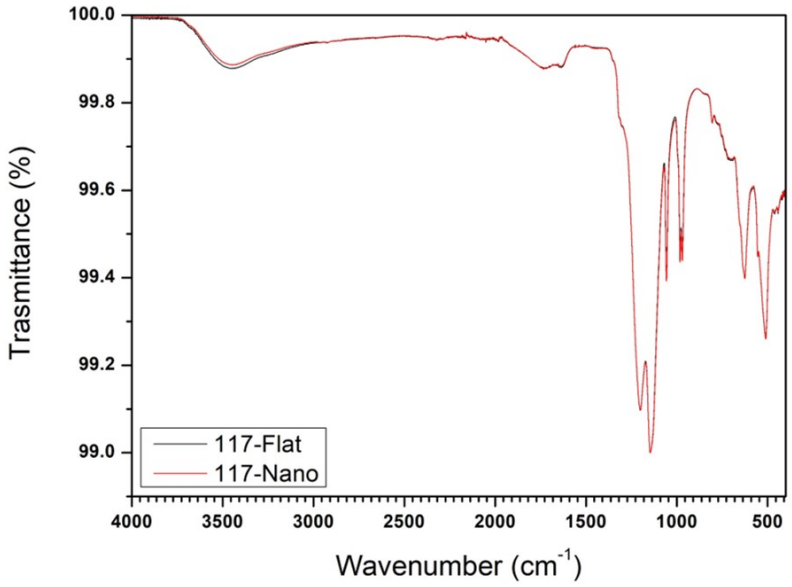

Figure 3.7: FTIR spectra of 117-Flat and 117-Nano

the stretching of –OH group, hence, as expected, with the water content of the two membranes. However, for the rest, the two spectra are perfectly overlapping. This indicates that no significant chemical changes occur after the thermal treatment due to the imprinting process.

3.4.2 Influence of surface patterning on the wetting properties

The determination of the contact angles allowed the establishment of the membrane wettability. Measurements were performed by using the same protein solution as the one used for the crystallization experiments. The results are reported in Figure 3.8. First of all, it is possible to notice a difference in wettability between the 117-Flat and NR50-flat. Both membranes contain the same monomer, and they have the same ion-exchange capacity (0.9 meq/g) [29]. However, they present different water uptake values (24% for Nafion® 117 and 15% for Nafion® NR50 [29]) and, consequently, proton conductivity. According to the literature, the water uptake depends on the organization of the molecular chains in the membranes, which in turn is a result of the preparation method.

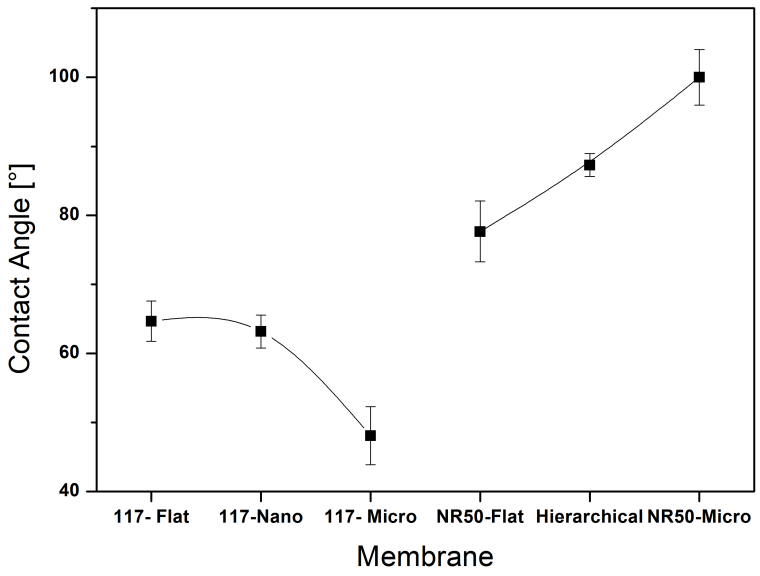

Figure 3.8: Contact angle values measured for the patterned membranes with Trypsin protein solution

These types of membranes contain hydrophobic (Teflon backbones) and hydrophilic regions (sulfonated groups). From investigations of the internal structure of Nafion® it is known that the hydrophobic region is a continuous semi-cristalline area, meanwhile the hydrophilic region is organized in clusters that can incorporate water and allow for ions/protons and water transport. Hence, the water uptake is directly related to the size of these clusters [36]. Nafion® 117 is a commercial membrane prepared by extrusion; instead, the Nafion® NR50 polymer was dissolved in DMF and later the membrane was formed by solvent evaporation. Due to the higher affinity of DMF for the Teflon backbone than for the sulfonated groups, the Nafion® chains in DMF assume a coiled-like shape where the sulfonated groups are buried inside, in order to minimize the contact with the solvent. This organization leads to a random distribution of the hydrophobic and hydrophilic regions that prevents the formation of large clusters. Also, in the final membrane, due to this organization, there is a low clustering of the sulfonated groups that reduces the water uptake when in contact with water [29]. Therefore, the different clusters' organization and water uptake cause the different wettability of Nafion® 117 and Nafion® NR50. From the results reported

in Figure 3.8 it is also possible to notice that, as expected, there is a change in wettability of the patterned membranes compared to the flat ones of the same type. This change in wettability can be explained by two different models: If the liquid is able to follow the pattern shape and fill all the cavities generated by the topography, the apparent contact angle can be predicted by using the Wenzel's equation [37]:

$$\Gamma cos\theta_Y = cos\theta \tag{3.1}$$

Where Γ represents the ratio between the actual surface area and the projected surface area and θ_Y represents the Young's contact angle (contact angle for an ideal flat surface). If the liquid is not able to fill all the cavities of a surface, or when the surface is not homogeneous, the Cassie-Baxter equation (equation 3.2) should instead be applied, where the contact angle of the different phases is considered and weighted by the relative fraction area [37]:

$$cos\theta = f_{solid} cos\theta_Y - f_{air} \tag{3.2}$$

Where f_{solid} is the fraction area of the top surface of the membrane, θ_Y is the Young contact angle of the membrane and f_{air} is the fraction area of the wells. In order to predict which of the two models applies to the patterned membranes it is possible to calculate the critical contact angle (θ_c) as follows:

$$cos\theta_c = -\frac{(1 - f_{solid})}{\Gamma - f_{solid}} \tag{3.3}$$

For $\theta_Y < \theta_c$ the Wenzel state is energetically more favourable. However, a metastable Cassie-Baxter state can occur. For $\theta_Y > \theta_c$ only the Cassie-Baxter state is possible [38]. Comparisons between the Critical and Young contact angle are reported in Table 3.2.

According to these results, all membranes have a $\theta_Y < \theta_c$. This means that the Wenzel state is favourable compared to the Cassie-Baxter state. However, a metastable Cassie-Baxter state can be still possible. Calculations of the theoretical contact angle for all the patterned membranes have been done both with the Wenzel and Cassie Baxter model and compared with the experimental results, in

Table 3.2: Comparison between Young (θ_Y) and Critical contact angle (θ_c)

Membrane	θ_Y (°)	θ_c (°)
117-Nano	63	109
117-Micro	48	101
NR50-Micro	100	101
Hierarchical	87	102

order to understand the behaviour of the protein solution during the contact with the membranes. The results from these calculations are shown in Table 3.3.

It is possible to notice that the experimental results of the contact angle of patterned 117 membranes are well predicted by the Wenzel model. Instead, in the case of the NR50, the experimental results are closer to the Cassie-Baxter model. Looking at the comparison between experimental contact angle and Wenzel and Cassie-Baxter predictions, it looks like 117 membranes follow the Wenzel model, instead the NR50 membranes might be in a metastable Cassie-Baxter state.

Table 3.3: Comparison between experimental contact angle (θ_{exp}) and theoretical contact angle calculated by Wenzel equation (θ_w) (3.1) and by Cassie Baxter equation (θ_{cb}) (3.2)

Membrane	θ_{exp} (°)	θ_{wz}(°)	θ_{cb} (°)
117-Flat	64.7±2.9		
117-Nano	63±2.4	54	80
117-Micro	48±4.2	42	80
NR50-Flat	77±4.4		
NR50-Micro	100±4	69	90
Hierarchical	87±4.6	70	75

3.4.3 Impact of surface patterning on protein crystallization

The Nafion® membranes with topographical patterning, both 117 and NR50 types, were tested for the crystallization of Trypsin from Bovine Pancreas. The crystallization and precipitant solutions were mixed on the top of the membranes and left equilibrating with the stripping solution in a closed system. The experiments were performed in adapted crystallization well plates and followed over time by optical microscopy. Results of nucleation and growth rate are reported in Figure 3.9 and Figure 3.10.

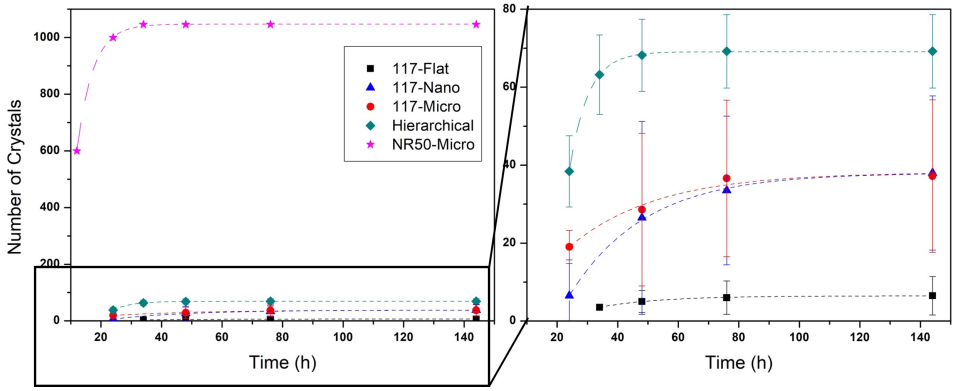

Figure 3.9: Number of crystals observed versus time. On the left side it is shown the evolution of the number of crystals as a function of time for all the patterned membranes. On the right side a magnification of the down area of the graph is displayed

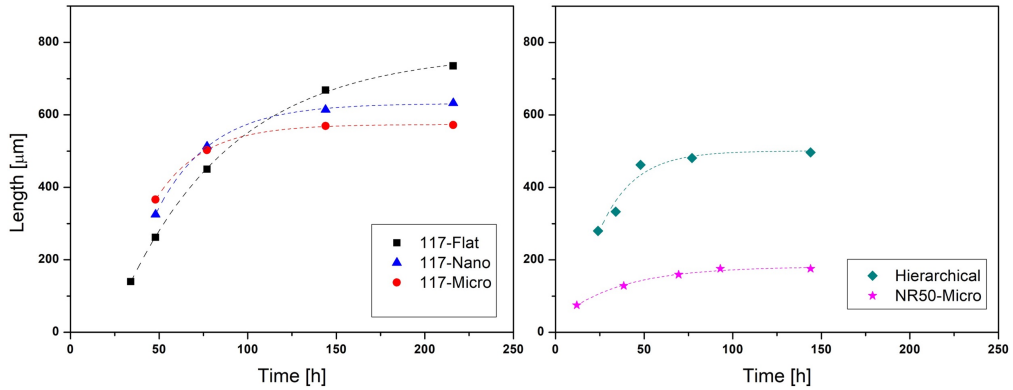

Figure 3.10: Length of crystals over time

From the data shown in Figures 3.9 and 3.10, crystallization parameters such as induction time, nucleation and growth rate were calculated. The induction time reported in Table 3.4 was extrapolated from the intersection point of the

Table 3.4: Estimated values of induction time, nucleation rate and growth rate for the different membranes

Membrane	Induction Time (h)	Nucleation rate (nuclei/h)	Growth rate (μm/h)
117-Flat	18.17	0.32±0.04	12.27±0.43
117-Nano	19.28	1.51±0.20	20.38±1.24
117-Micro	4.01	1.31±0.61	21.38±0.79
NR50-Micro	7.51	198.52±7.96	12.95±0.43
Hierarchical	19.04	11.30±0.39	25.85±13.90

curves in Figure 3.9 with the axis of time, whereas nucleation rate and growth rate, also reported in Table 3.4, were calculated as the first derivative at the time axis intersection of the curves in Figures 3.9 and 3.10, respectively. As expected, from both nucleation rate and crystal growth rate it can be concluded that all structured membranes produce a higher number of crystals compared to the original flat membrane because topographical features induce changes in the number of nucleation points on the surface. Comparing the curves in Figures 3.9 and 3.10 it is also evident, as expected, that membranes that lead to the formation of higher number of crystals also generate crystals with smaller dimensions.

In the case of 117 Nafion® membranes for both 117-Micro and 117-Nano there is a significant increase of the number of crystals and crystals growth rate compared to 117-Flat. However, when looking at the induction time, 117-Nano does not show any improvement compared to 117-Flat, whereas 117-Micro displays a significant lower time. This fact may be explained by the different scale of the geometry of the two membranes. Indeed, 117-Nano has wells in a nano size range that have a minimal effect on the contact angle, however, they affect the roughness of the material and create narrow sites where protein molecules can accumulate. In fact, the probability for a molecule to enter a narrow space (up to 1000 nm) is the same as on a flat surface, however, due to the Brownian motion in all directions, escaping from a narrow space may result much more difficult determining physical entrapment and local accumulation. When this event occurs over time, the concentration of molecules inside the well increases, determining nucleation

in the pores and formation of extra nucleation sites (see Figure 3.11) [39].

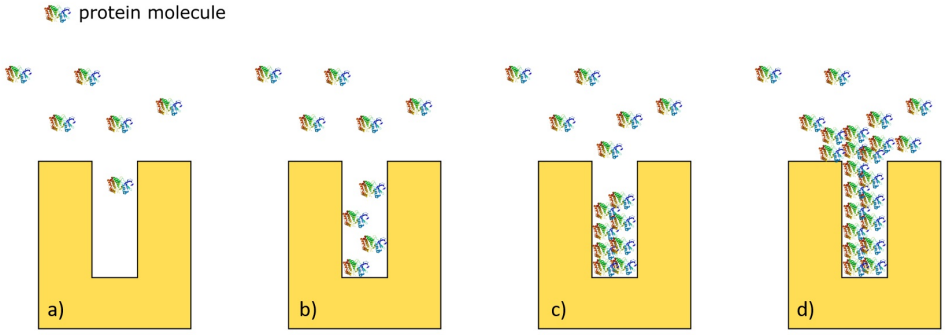

Figure 3.11: Proposed nucleation mechanism in a narrow cavity. a) The probability of a protein molecule of entering in a narrow cavity is the same as on the top of the surface; b) the narrow cavity determines entrapment of the protein molecules that will consequently accumulate over time; c) the increased concentration inside the pore promotes nucleation; d) the top surface of a cavity filled with a nucleus becomes a nucleation point for crystal growth outside the pore.

In the case of the 117-Micro membrane, the topographical features are much larger, therefore they cannot determine physical entrapment of protein molecules. Furthermore, the micro-features have a significant effect on the contact angle, the area of interaction between the solution and substrate is increased ($\Gamma = 1.74$) and, consequently, the number of potential nucleation sites available for the same volume of solution increases. For both membranes, i.e. 117-Nano and 117-Micro, an increase in the nucleation sites number occurs, however, while in the case of 117-Micro this occurs immediately, due to the spreading of the solution on the surface and the higher ratio between actual and projected area, in the case of 117-Nano some time is required for accumulation of protein molecules inside the nano wells. Regarding the NR50-Micro membrane, even though the microstructure is the same as the 117-Micro, the two membranes lead to completely different outputs. Indeed, even though the induction time is comparable (just slightly higher for NR50-Micro), the nucleation rate and final the number of crystals is much higher in this case. Protein adsorption due to the presence of the micro-features might be enhanced by the distinctive hydrophobic character of the NR50 surface, motility of the molecules might be reduced and a high number of nuclei rapidly formed. Due to the formation of this high number of nuclei in a short

time, a lower amount of protein is available in the solution determining a slower growth rate compared to the hydrophilic membranes. The hierarchical membrane (which is a hybrid membrane of NR50-Micro and 117-Nano) has an intermediate behaviour between the 117-nano and the NR50-Micro membranes.

3.4.4 Modelling the Gibbs free energy of heterogeneous nucleation for the membranes with designed patterns

The free energy variation for heterogeneous nucleation (ΔG_{Het}) is defined as [40]:

$$\Delta G_{Het} = \phi \Delta G_{Hom} \tag{3.4}$$

Where ϕ is the ratio of Gibbs free energy variation of heterogeneous to homogeneous nucleation and ΔG_{Hom} is the Gibbs' free energy variation for homogeneous nucleation. According to literature [18], for an ideally flat surface (without any patterning), ϕ is defined as:

$$\phi = \frac{(2 - 3cos\theta_Y + 3cos\theta_Y)^3}{4} \tag{3.5}$$

Therefore, the main parameter affecting heterogeneous nucleation is the Young's contact angle θ_Y between the forming nucleus (assumed to be spherical) and the substrate that defines the area of interaction between the nucleus and the surface. In fact, surfaces with lower contact angles lead to lower values of ϕ (ratio of Gibbs free energy variation of heterogeneous to homogeneous nucleation) according to Equation 3.5. In order to include the effect of surface topography in the calculations, Liu et al. [18] developed a model for calculating the ratio of Gibbs free energy variation of heterogeneous to homogeneous nucleation for a rough surface, assuming the surface to be composed by uniform cones and a Wenzel's wetting state.

In this work the model developed by Liu et. al was adapted to the geometry of the topography of the patterned membranes and theoretical values correlated with experimental results. On the top of the substrate, a nucleus with a hypothetical

round shape of radius R contacting the substrate with an apparent contact angle θ is considered (Figure 3.12). Details on the derivation of the equations are reported in the Appendix A.

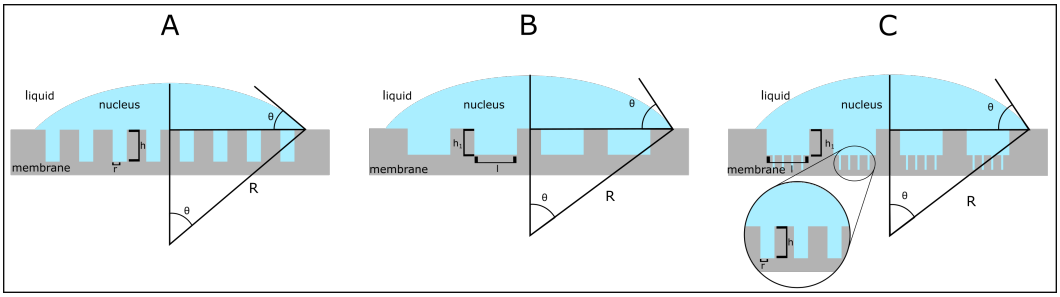

Figure 3.12: Diagram of the geometry parameters of a surface with cylindrical wells

For the 117-Nano membrane the equation used was the following

$$\phi_{117-Nano} = \frac{\Delta G_{het117-Nano}}{\Delta G_{Hom}} = \frac{1}{4}\frac{[2(1-cos\theta)-cos\theta sin^2\theta]^3}{[(1-cos\theta)^2(2+cos\theta)+3n\alpha^2\beta]^2} \tag{3.6}$$

Where $\alpha = r/R$, $\beta = h/R$, r is the radius of the wells, n is the number of wells under the drop area, θ is the apparent contact angle of the protein solution with the surface (Figure 3.12 A).

In the case of 117-Micro and NR50-Micro the same model (replacing the geometric parameters of a cylinder with the ones of a triangular prism) was applied, for a Wenzel surface, resulting in the following equation:

$$\phi_{Micro} = \frac{1}{4}\frac{\pi^2[2(1-cos\theta)-cos\theta sin^2\theta]^3}{[\pi(1-cos\theta)^2(2+cos\theta)+\frac{3}{2}\sqrt{3}n_1\alpha_1^2\beta_1]^2} \tag{3.7}$$

Where $\alpha_1 = l/R$, $\beta_1 = h_1/R$, l is the side of the triangle base of the prisma well, h_1 is the depth, n_1 is the number of wells under the nucleus area θ is the apparent contact angle of nucleus with the surface (Figure 3.12 B).

For the Hierarchical membrane (Triangular prism wells with cylindrical wells inside), both geometries of the cylinder and prisma were included in the model, resulting:

$$\phi_{Hierarchical} = \frac{1}{4}\frac{\pi^2[2(1-cos\theta)-cos\theta sin^2\theta]^2}{[\pi(1-cos\theta)^2](2+cos\theta)+\frac{3}{2}\sqrt{3}n_1\alpha_1^2\beta_1+3n\alpha^2\beta]^2} \tag{3.8}$$

Where $\alpha = r/R$, $\beta = h/R$ $\alpha_1 = l/R$, $\beta_1 = h_1/R$, r is the radius of the nanowells, h is their depth, l is the side of the triangle base of the prisma wells and h_1 is their depth, n is the number of nanowells inside a microwell, n_1 is the number of wells under the nucleus area, θ is the apparent contact angle of the nucleus with the surface(Figure 3.12 C).

From Equations 3.5, 3.6, 3.7, 3.8 it was possible to calculate the ϕ (ratio of the Gibbs free energy of heterogeneous nucleation to homogeneous nucleation) for each membrane and compare the obtained values with crystallization results.

Table 3.5: Ratio of the Gibbs free energy variation of heterogeneous nucleation to homogeneous nucleation

Membrane	ϕ
117-Flat	0.19
117-Nano	0.18
117-Micro	0.07
NR50-Micro	0.52
Hierarchical	0.45

According to the results of these calculations, reported in Table 3.5, for 117 Nafion® membranes, the topographical features induce a reduction in the ratio of the Gibbs free energy variation of heterogeneous nucleation to homogeneous nucleation (ϕ). This decrease is much higher for the 117-Micro compared to 117-Nano. However, the experimental results are not in total agreement with the theoretical calculations. According to the heterogeneous nucleation theory, surfaces with lower contact angles, hence with high degree of hydrophilicity, favour nucleation of proteins. Indeed, a lower contact angle means a wider spreading of the solution on the top of the surface increasing the contact area for the same volume of solution, and thus the probability of nuclei formation. Furthermore, considering the Wenzel behaviour when the roughness on a certain surface is increased, the character of the surface is enhanced: a hydrophilic surface will turn into a more hydrophilic surface and a hydrophobic surface will increase hydrophobicity. All of this explains what is happening in the case of 117-Micro membrane. In

fact, even though the nanoscale roughness value is comparable to the 117-Flat membrane, the presence of the micro structure determines a significant decrease of the contact angle that results in higher contact area between protein solution and membrane, which leads to a higher number of crystals compared to 117-Flat. Since the model is accounting essentially for the area of interaction between the protein solution and the membrane, and the fact that this area is enhanced by the presence of quite large topographical features, the effect of the 117-Micro is well predicted by the theoretical calculations for heterogeneous nucleation. However, in the case of 117-Nano where, due to the scarce contribution of nanofeatures to the actual surface area, the change in contact angle is more modest and, therefore, the theoretical calculations give a ϕ value comparable to the 117-Flat. Indeed, the phenomenon of protein accumulation in the restricted well space illustrated in Figure 11, which is more pronounced in nano cavities, is not accounted for by the model. The higher value of ϕ for NR50 and Hierarchical membrane compared to 117-Flat can be attributed to their hydrophobic character. Indeed, according to this model, the hydrophobic character reduces the nucleation effect due to a lesser area of interaction between the solution and the surface, leading to the idea that hydrophilic membranes are better nucleating surfaces than the hydrophobic ones. This seems to be the case when comparing 117-Micro and NR50-Micro, which have exactly the same geometry, although with a different character. However, the experimental results show the opposite trend: a significantly higher number of crystals is obtained for NR50-Micro than for 117-Micro. We attribute this behaviour to the more predominant role of the surface chemistry. In fact, even though the chemical composition of Nafion 117 and Nafion® NR50 is the same, the two membranes have a different polymer chains organization that leads to different surface chemistry. In the NR50 membrane the hydrophilic groups are buried inside, enhancing the outside hydrophobic character of the membrane. The higher superficial hydrophobicity may promote stronger protein-surface interactions and consequently higher degree of nucleation. Furthermore, the model developed by Liu et al. is based on the assumption that the liquid phase is following the Wenzel behaviour on the surface topography and, as previously reported

(Table 3.3), metastable Cassie-Baxter state may occur in the case of NR50 membranes.

3.4.5 Guidelines for designing membrane topographies for improved nucleation and crystallization

Nucleation is a probability event, hence different conditions lead to different chances of obtaining crystals. Enhancing the probability for this phenomenon to occur is extremely important for increasing the possibility of obtaining well-diffracting crystals, especially in the case of protein molecules difficult to nucleate. Designing of specific surface topography membranes demonstrated to have an impact on the crystallization process. However, predicting which type of surface topography may promote a more effective nucleation is not obvious and simple. Taking into account the results of this work, we would like to draw guidelines for designing surfaces suitable for nucleation:

- Small features, in the nano size range lead to higher nucleation due to the creation of extra nucleation sites by physical entrapment. Hence, they might be useful for implementing nucleation on surfaces with a surface chemistry that does not favour nucleation;
- Larger features on highly hydrophilic surfaces induce an increase in the wettability and consequently in the surface/volume ratio enhancing the effect of the chemistry of the material. Hence, they can be useful to amplify the nucleation on surfaces with properties that favour the nucleation process;
- Larger features on hydrophobic surfaces may lead to higher protein-surface interactions with a much stronger effect on nucleation compared to hydrophilic surfaces carrying the same features

Hence, depending on the chemistry of the surface and the effect of this surface on nucleation it is possible to decide the best strategy for introducing small or large features, or both, in order to control the number of nuclei and the size of the crystals. Theoretical calculations based on the model developed by Liu et al.

help in predicting the effect of a defined geometry on nucleation rate, however, this model presents some obvious limitations. The model relies on the Wenzel equation and the surface/volume ratio (described by the contact angle) is considered the main controlling factor for protein nucleation on the membrane surface. This applies only for hydrophilic surfaces with a high Γ (ratio between actual and projected area). In the case of small surface features, which do not have a strong effect on the contact angle, or more hydrophobic surfaces where the solution does not follow the Wenzel behaviour, other phenomena such as physical entrapment and chemical interactions might occur playing a significant role, that are not taken into consideration by the Liu et al. model. Therefore, a different theoretical approach including the fluid dynamics of the protein solution contacting specific nano cavities and protein-surface interactions should be accounted for a model closer to reality and with a higher prediction capacity.

3.5 Conclusions

Controlling heterogeneous nucleation by surface topography can be regarded as a very effective way to handle the complex process of protein crystallization. So far, modifications of the surface topography were always associated with chemical modifications, making difficult a comparison with a flat surface. What emerged from previous investigations was that an incremented nucleation activity could be observed for surfaces with increased roughness. In this work, Nafion® membranes were processed with soft lithographic techniques in order to create periodic surface topographies with different sizes (micro, nano and a combination of both) minimizing the surface chemistry changes in order to study the specific effect of topography on the nucleation process. The results obtained showed, as expected, an increased nucleation activity for all the patterned membranes. The increased nucleation was comparable in the case of nano and micro structures made of the same type of Nafion®. However, different nucleation rates were reported that might be an indication that different nucleation mechanisms might occur, depending on the size of the topographical features. It was also shown that the

same topography might result in a different output for membranes with the same overall chemical composition but with different surface chemistry. Experimental results were compared with theoretical calculations of the ratio of the Gibbs free energy variation of heterogeneous nucleation to homogeneous nucleation (ϕ) from the model developed by Liu et al. adapted to the designed geometries. Some discrepancies were observed between the theoretical calculations from the Liu at al. model and the experimental results. This model is based on the Wenzel's equation, which is not applicable to all situations and is unable to account for important phenomena that affect nucleation, such as the local accumulation of protein in a restricted space and protein-surface interactions.

References

[1] J. A. Gavira. "Current trends in protein crystallization." In: *Archives of Biochemistry and Biophysics* 602 (2016), pp. 3–11. DOI: 10.1016/j.abb.2015.12.010.

[2] R. Giegé. "A historical perspective on protein crystallization from 1840 to the present day." In: *FEBS Journal* 280.24 (2013), pp. 6456–6497. DOI: 10.1111/febs.12580.

[3] J. M. Garcia. "Nucleation of protein crystals." In: 142 (2003), pp. 22–31. DOI: 10.1016/S1047-8477(03)00035-2.

[4] P. G. Vekilov. "Nucleation of protein crystals." In: *Progress in Crystal Growth and Characterization of Materials* 62.2 (2016), pp. 136–154. DOI: 10.1016/J.PCRYSGROW.2016.04.007.

[5] R.-B. Zhou, H.-L. Cao, C.-Y. Zhang, and D.-C. Yin. "A review on recent advances for nucleants and nucleation in protein crystallization." In: *CrystEngComm* 19.8 (2017), pp. 1143–1155. DOI: 10.1039/C6CE02562E.

[6] A. Mcpherson and P. Shlichta. "Heterogeneous and Epitaxial Nucleation of Protein Crystals on Mineral Surfaces." In: *Science* 239 (1988), pp. 385–387. DOI: 10.1126/science.239.4838.385.

[7] A. Gugliuzza, C Aceto, and E. Drioli. "Interactive functional poly (vinylidene fluoride) membranes with modulated lysozyme affinity : a promising class of new interfaces for contactor crystallizers." In: *Polym Int* 58 (2009), pp. 1452–1464. DOI: 10.1002/pi.2681.

[8] C.-y. Zhang, H.-f. Shen, Q.-j. Wang, Y.-z. Guo, and J. He. "An Investigation of the Effects of Self-Assembled Monolayers on Protein Crystallisation." In: *International Journal of Molecular Sciences* 14 (2013), pp. 12329–12345. DOI: 10.3390/ijms140612329.

[9] D. S. Tsekova, D. R. Williams Nn, and J. Y. Y. Heng. "Effect of surface chemistry of novel templates on crystallization of proteins." In: *Chemical Engineering Science* 77 (2012), pp. 201–206. DOI: 10.1016/j.ces.2012.01.049.

[10] T. Pham, D. Lai, D. Ji, W. Tuntiwechapikul, J. M. Friedman, and T. R. Lee. "Well-ordered self-assembled monolayer surfaces can be used to enhance the growth of protein crystals." In: *Colloids and Surfaces B: Biointerfaces* 34.3 (2004), pp. 191–196. DOI: 10.1016/j.colsurfb.2004.01.003.

[11] E. Curcio, E. Fontananova, G. D. Profio, and E. Drioli. "Influence of the Structural Properties of Poly(vinylidene fluoride) Membranes on the Heterogeneous Nucleation Rate of Protein Crystals." In: *Journal of Physical Chemistry B* 4.1 (2006), pp. 12438–12445. DOI: 10.1021/jp061531y.

[12] U. V. Shah, D. R. Williams, and J. Y. Heng. "Selective crystallization of proteins using engineered nanonucleants." In: *Crystal Growth and Design* 12.3 (2012), pp. 1362–1369. DOI: 10.1021/cg201443s.

[13] U. V. Shah, M. C. Allenby, D. R. Williams, and J. Y. Y. Heng. "Crystallization of proteins at ultralow supersaturations using novel three-dimensional nanotemplates." In: *Crystal Growth and Design* 12.4 (2012), pp. 1772–1777. DOI: 10.1021/cg201190c.

[14] U. V. Shah, C. Amberg, Y. Diao, Z. Yang, and J. Y. Heng. "Heterogeneous nucleants for crystallogenesis and bioseparation." In: 8 (2015), pp. 69–75. DOI: 10.1016/j.coche.2015.03.002.

[15] U. V. Shah, N. H. Jahn, S. Huang, Z. Yang, D. R. Williams, and J. Y. Heng. "Crystallisation via novel 3D nanotemplates as a tool for protein purification and bio-separation." In: *Journal of Crystal Growth* 469 (2017), pp. 42–47. DOI: 10.1016/j.jcrysgro.2016.09.029.

[16] A. S. Ghatak and A. Ghatak. "Precipitantless Crystallization of Protein Molecules Induced by High Surface Potential." In: *Crystal Growth & Design* 16 (2016), pp. 5323–5329. DOI: 10.1021/acs.cgd.6b00833.

[17] A. S. Ghatak, G. Rawal, and A. Ghatak. "Precipitant-Free Crystallization of Protein Molecules Induced by Incision on Substrate." In: *Crystals* 7.8 (2017), p. 245. DOI: 10.3390/cryst7080245.

[18] Y. X. Liu, X. J. Wang, J. Lu, and C. B. Ching. "Influence of the roughness, topography, and physicochemical properties of chemically modified surfaces on the heterogeneous nucleation of protein crystals." In: *Journal of Physical Chemistry B* 111.50 (2007), pp. 13971–13978. DOI: 10.1021/jp0741612.

[19] W. De Poel, J. A. W. Mu, J. A.A. W. Elemans, W. J. P. Van Enckevort, A. E. Rowan, and E. Vlieg. "Surfaces with Controllable Topography and Chemistry Used as a Template for Protein Crystallization." In: *Crystal Growth & Design* 18 (2018), pp. 763–769. DOI: 10.1021/acs.cgd.7b01174.

[20] H. Hou, B. Wang, S.-Y. Hu, M.-Y. Wang, J. Feng, P.-P. Xie, and D.-C. Yin. "An investigation on the effect of surface roughness of crystallization plate on protein crystallization." In: *Journal of Crystal Growth* 468.October 2016 (2017), pp. 290–294. DOI: 10.1016/j.jcrysgro.2016.10.007.

[21] E. Drioli, G. D. Profio, E. Curcio, W. S. W. Ho, and K Li. "Progress in membrane crystallization." In: *Current Opinion in Chemical Engineering* 1 (2012), pp. 178–182. DOI: 10.1016/j.coche.2012.03.005.

[22] G. D. Profio, M. Polino, F. P. Nicoletta, B. D. Belviso, R. Caliandro, E. Fontananova, G. De Filpo, E. Curcio, and E. Drioli. "Tailored hydrogel membranes for efficient protein crystallization." In: *Advanced Functional Materials* 24.11 (2014), pp. 1582–1590. DOI: 10.1002/adfm.201302240.

[23] S. M. Salehi, A. C. Manjua, B. D. Belviso, C. A. M. Portugal, I. M. Coelhoso, V. Mirabelli, E. Fontananova, R. Caliandro, Joa, G Crespo, E. Curcio, and G. D. Profio. "Hydrogel Composite Membranes Incorporating Iron Oxide Nanoparticles as Topographical Designers for Controlled Heteronucleation of Proteins." In: *Crystal Growth & Design* 18.6 (2018), pp. 3317–3327. DOI: 10.1021/acs.cgd.7b01760.

[24] D. Qin, Y. Xia, and G. M. Whitesides. "Soft lithography for micro- and nanoscale patterning." In: *Nature Protocols* 5.3 (2010), pp. 491–502. DOI: 10.1038/nprot.2009.234.

[25] T. Glinsner and G. Kreindl. "Nanoimprint Lithography." In: *Lithography* 24 (2010), pp. 495–516.

[26] A. Fernandez, J. Medina, C. Benkel, M. Guttmann, B. Bilenberg, L. H. Thamdrup, T. Nielsen, C. M. Sotomayor Torres, and N. Kehagias. "Residual layer-free Reverse Nanoimprint Lithography on silicon and metal-coated substrates." In: *Microelectronic Engineering* 141 (2015), pp. 56–61. DOI: 10.1016/j.mee.2014.11.025.

[27] B. Radha, S. H. Lim, M. S. M. Saifullah, and G. U. Kulkarni. "Metal hierarchical patterning by direct nanoimprint lithography." In: *Scientific Reports* 3.1 (2013), p. 1078. DOI: 10.1038/srep01078.

[28] M. Polino, A. Luísa Carvalho, L. Juknaite, C. A. M Portugal, I. M. Coelhoso, M. J. Romao, and J. G. Crespo. "Ion-Exchange Membranes for Stable Derivatization of Protein Crystals." In: *Crystal Growth & Design* 17 (2017), pp. 4563–4572. DOI: 10.1021/acs.cgd.7b00315.

[29] C.-H. Ma, T. L. Yu, H.-L. Lin, Y.-T. Huang, Y.-L. Chen, U.-S. Jeng, Y.-H. Lai, and Y.-S. Sun. "Morphology and properties of Nafion membranes prepared by solution casting." In: *Polymer* 50 (2009), pp. 1764–1777. DOI: 10.1016/j.polymer.2009.01.060.

[30] H. Le-the, E. Berenschot, R. M. Tiggelaar, N. R. Tas, A. V. D. Berg, and J. C. T. Eijkel. "Shrinkage Control of Photoresist for Large-Area Fabrication

of Sub-30 nm Periodic Nanocolumns." In: *Advanced Materials Technologies* (2017). DOI: 10.1002/admt.201600238.

[31] A. Pimpin and W. Srituravanich. "Review on Micro- and Nanolithography Techniques and their Applications." In: *Engineering Journal* 16.1 (2012), pp. 37–55. DOI: 10.4186/ej.2012.16.1.37.

[32] P. K. David Neˇ cas. "Gwyddion : an open-source software for SPM data analysis." In: *Central Euopean Journal of Physics* 10.1 (2012), pp. 181–188. DOI: 10.2478/s11534-011-0096-2.

[33] C. A. Schneider, W. S. Rasband, and K. W. Eliceiri. "NIH Image to ImageJ: 25 years of image analysis." In: *Nature Methods* 9.7 (2012), pp. 671–675. DOI: 10.1038/nmeth.2089.

[34] H.-y. Jung and J. Won. "Role of the glass transition temperature of Nafion 117 membrane in the preparation of the membrane electrode assembly in a direct methanol fuel cell (DMFC)." In: *International Journal of Hydrogen Energy* 37.17 (2012), pp. 12580–12585. DOI: 10.1016/j.ijhydene.2012.05.121.

[35] S. H. de Almeida and Y. Kawano. "Thermal Behavior of Nafion Membrane." In: *Journal of Thermal Analysis and Calorimetry* 58 (1999), pp. 569–577. DOI: 10.1023/A:1010196226309.

[36] K. A. Mauritz and R. B. Moore. "State of Understanding of Nafion." In: *Chem. Rev.* 104 (2004), pp. 4535–4585. DOI: 10.1021/cr0207123.

[37] E. Celia, T. Darmanin, E. T. D. Givenchy, S. Amigoni, and F. Guittard. "Recent advances in designing superhydrophobic surfaces." In: *Journal of Colloid and Interface Science* 402 (2013), pp. 1–18. DOI: 10.1016/j.jcis.2013.03.041.

[38] P. Esa, R. Tiina, S. Mika, and A. P. Tapani. "Superhydrophobic Polyolefin Surfaces: Controlled Micro- and Nanostructures." In: *Langmuir* 23.13 (2007), pp. 7263–7268.

[39] C. N. Nanev, E. Saridakis, and N. E. Chayen. "Protein crystal nucleation in pores." In: *Scientific Reports* 7 (2017), pp. 35821–35829. DOI: 10.1038/srep35821.

[40] T. E. Paxton, A. Sambanis, and R. W. Rousseau. "Influence of vessel surfaces on the nucleation of protein crystals." In: *Langmuir* 17.10 (2001), pp. 3076–3079. DOI: 10.1021/la0015841.

Chapter 4

Ion-Exchange Membranes for Stable Derivatization of Protein Crystals

Published as: Mariella Polino, Ana Luısa Carvalho, Lina Juknaite, Carla A. M. Portugal, Isabel M. Coelhoso, Maria João Romão, and João G. Crespo, Ion-Exchange Membranes for Stable Derivatization of Protein Crystals, Cryst. Growth Des., 2017, 17 (9), pp 4563–4572*

4.1 Summary

Ion-exchange membranes were applied in this work to diffuse ions and heavy atoms inside protein crystals in order to gently perform their derivatization. The ion-exchange process rate for three different ions, bromide (Br^-), platinum (Pt^+ through $PtCl_4^{2-}$), and mercury (Hg^{2+}), was evaluated, allowing to determine the concentration of these ions in the crystal solution over time and to evaluate their effect on the crystals. Nafion® and Neosepta AXE01, cation and anion exchange-membranes, respectively, were used for transport of cations and anions to hen egg white lysozyme (HEWL) crystals, selected as model protein. X-ray diffraction analysis of the crystals confirmed the attainment of the derivatives and allowed the *ab initio* building of the bromide derivative model. Derivatization experiments

were also conducted by the conventional method, directly soaking the crystals in the heavy atom solution. It was possible to conclude that the controlled diffusion, regulated by the membrane, increases the crystal's stability, avoiding handling procedures (*in-situ* derivatization) and maintaining a safer environment near the crystals without disturbing the vapor diffusion equilibrium.

4.2 Introduction

Protein crystal derivatization is a modification process required by the multiple isomorphous replacement (MIR) method to solve the unknown structure of macromolecules using single crystal X-ray crystallography [1–4]. Protein crystal derivatization consists of introducing in the crystal heavy atoms like Pt and Hg [4, 5] or halide ions like Br^- and I^- [4, 6–8] without changing the packing of macromolecules in the space group of the native crystal (isomorphism)[9]. In order to diffuse those species into the protein crystals and keep the crystalline lattice isomorphous,[10] the native preformed crystals are soaked in a solution containing low concentrations of these compounds, so they can slowly diffuse into the solvent channels of the crystals [11, 12]. The main problem of this procedure is that the crystals are sensitive to environmental changes, and if they are directly brought in contact with a solution with a different composition from the growing buffer, the crystals very often crack and get damaged. For this reason, soaking has to be performed in several steps involving the use of several solutions with an increasing concentration of the halide or metal ion to be incorporated.

In this work, we propose the use of ion-exchange membranes to gently transport ions by diffusion within the protein drop, avoiding the problems of handling and environmental shock, and the several steps needed to perform this operation in a safer way for the crystals. The use of membranes has been reported in the literature to control supersaturation [13], heterogeneous nucleation rate [13–18], and the formation of polymorphs[19, 20]. However, membranes have not been used before to derivatize protein crystals. Even though ion-exchange membranes, to the best of our knowledge, have never been used to crystallize

macromolecules (Nafion® [20] and chitosan [21] were used only for the crystallization of small molecules such as glycine or acetaminophen), they seem to have the ideal properties to achieve protein crystallization and derivatization. Ion-exchange membranes are semipermeable barriers, where fixed charged groups are attached to a hydrophobic backbone (usually made of polystyrene). The presence of charged groups will facilitate the transport of ions with opposite charge and reject those ones carrying the same charge as the groups attached to the membrane (Donnan exclusion)[22–26]. The hydrophobic backbone guarantees that the protein solution remains on the top of the membrane, and it is not completely adsorbed by the support. At the same time, the presence of charged groups allows the transport of ions across the membrane. In the case of protein crystallization, pH is a key factor with impact on molecule aggregation. Due to the diversity of chemical groups present in the protein amino acids, the total charge of the protein will change, as well as the distribution of charge within the protein molecules, which impacts on the stability of the molecule itself [27]. This determines if the protein molecules will be able to pack together in a well-ordered network (forming a crystal) or if they will just amorphously precipitate when the concentration increases[28–30]. Once the crystals are formed, in order to avoid damages or dissolutions, pH, osmotic pressure, and temperature[31] must be kept stable. Taking into account these considerations, the membrane system for crystal derivatization was designed to prevent the transport of small ions (H^+ and OH^- that could even slightly change the pH) and the leak of water due to a difference in osmotic pressure from the crystal derivatization compartment [32–34]. Figure 4.1 shows the system configuration with an anion exchange membrane separating two compartments. The receiving compartment (**R**) is the crystal growth environment, containing the buffer at a defined pH, the precipitant, and the protein. The feed compartment (**F**), instead, contains a solution of the same composition in terms of buffer type, concentration, and pH, and the same total molar concentration as compartment **R**, just replacing a precise amount of precipitant salt with the salt intended to be used for derivatization. In this way, the "derivatization" anion of

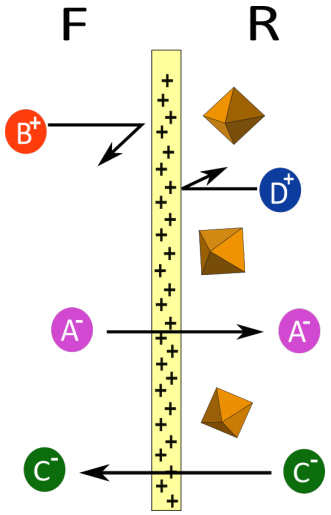

Figure 4.1: Anion exchange membrane to gently exchange the anion A^- in compartment F with the anion C^- in the protein drop. A^- is not initially present in compartment R, so it will diffuse, leading C^- to compartment F. The buffer has the same pH concentration in both compartments. Salt AB is at the same concentration of salt CD. F is the feeding compartment and R is the receiving compartment.

compartment **F** will diffuse into compartment R driving the anion in compartment **R** to compartment **F**. Since the pH is the same in both compartments, there will not be any leakage of H^+ OH^- ions, and since the osmotic pressure is also the same (the contribution of the protein and crystals is negligible), no osmosis will occur and osmotic shock will be prevented. The process is expected to be completely controlled because the only driving force is the difference in species concentration across the membrane. The ionic diffusive transport is what is needed to give the crystals time to adapt to the different ions. Therefore, it is possible to take advantage of the transport properties of ion-exchange membranes to improve the process of derivatization of protein crystals. This concept was implemented for crystals of hen egg white lysozyme (HEWL), as model protein, and using bromide (Br^-), platinum (Pt through $PtCl_4^{2-}$, and mercury (Hg^{2+})as derivatization agents. Conventional crystallization conditions [35–37] were used to obtain HEWL crystals on the top of an anion and a cation exchange membrane. The use of an anion or cation exchange membrane for the derivatization process depends on the charge of the ions used. Therefore, a cation exchange membrane was used for crystal derivatization, when Hg^{2+} was present in the feed solution, and an

anion exchange membrane was used for crystal derivatization with $PtCl_4^{2-}$ and Br^-. The kinetics of diffusion of each ion across the membrane may be previously calculated in order to estimate the time of diffusion into the protein solution and predict when the ion-exchange process will be completed. The advantage of crystal derivatization by the ion-exchange process is here evaluated by comparing the quality of the derivatized protein crystals to the ones obtained by conventional soaking, using X-ray diffraction analysis. In a preliminary analysis, indexing of diffraction intensities was sufficient to confirm that crystal isomorphism was maintained. In a more detailed analysis, by collecting complete diffraction data at the appropriate X-ray absorption wavelength, it was also possible to identify the heavy atoms in the calculated anomalous difference electron density maps. Furthermore, in the case of HEWL crystals derivatized with bromide, it was possible to achieve *ab-initio* structure solution by experimental Br-SAD phasing.

4.3 Materials and Methods

4.3.1 Materials

Hen egg white lysozyme (HEWL) purchased from Sigma-Aldrich was used for the crystallization experiments. The protein was solubilized in a 0.1 M $Na(CH_3COO)$ buffer (purchased from Scharlau), pH 4.6, and experiments were carried out with a protein concentration of 25 mg/mL. NaCl (purchased from Applichem Panreac) was added to the protein solution with a final concentration of 0.3 M and used as hypertonic solution to control relative humidity with a concentration of 0.6 M. For crystal derivatization, NaBr (purchased from Applichem Panreac) was solubilized in the protein buffer at a concentration of 0.6 M, while K_2PtCl_4 or $Hg(CH_3COO)_2$ was solubilized in 0.1 M $Na(CH_3COO)$ buffer, pH 4.6 at 5 mM and 10 mM, respectively, together with 0.6 M NaCl and used as solutions for the different derivatization procedures: conventional and within the ion-exchange membrane cell. The design of a membrane based system able to assist consecutive protein crystallization and derivatization processes requires the selection of membranes with ideal transport properties allowing for a suitable diffusion of

the derivatizing ions while offering the surface chemistry and topography characteristics needed to promote nucleation. In this regard, it was important to screen several membranes in conventional vapor diffusion plates in order to select the ones allowing nucleation[14–18, 20, 38, 39]. Neosepta Axe 01 (purchased from Tokuyama Soda) and Nafion® (purchased from Sigma-Aldrich) allowed the attainment of crystals (12 hours) under conventional conditions of protein protein and precipitant concentration. Therefore, they were selected to support protein crystallization and derivatization processes. Neosepta Axe 01, an anion exchange membrane, was used to transport Br^- and $PtCl_4^{2-}$, while Nafion®, a cation exchange membrane, was used to diffuse Hg^{2+} to the protein crystals solution.

4.3.2 Contact Angle Measurements

The contact angles of Nafion® and Neosepta AXE01 were measured by the sessile drop method in a contact angle goniometer (CAM 100, KSV Instruments Ltd., Finland). The solution used for the measurement was 25 mg/mL HEWL and 0.3 M NaCl in 0.1 M $Na(CH_3COO)$, pH 4.6. Each measurement has been repeated five times

4.3.3 Operating Procedure for Crystallization and Derivatization Processes in the Ion-Exchange Membrane Cell

The setup used for crystal derivatization is shown in Figure 4.2. Experiments of crystallization and crystal derivatization in the ionexchange membrane cell were performed using the membrane Neosepta Axe01 to derivatize HEWL crystals with Br^- and Pt^{2+} (through $PtCl_4^{2-}$) that diffuse as anions, and Nafion® to derivatize HEWL crystals with $Hg(CH_3COO)_2$ that diffuse as cations of Hg^{2+}.

In Figure 4.2, the membrane was placed in the middle of the cell, generating two compartments: an upper compartment (receiving compartment) for the protein solution connected to a hypertonic solution to control the air relative humidity and a bottom compartment (feeding compartment) filled with a heavy

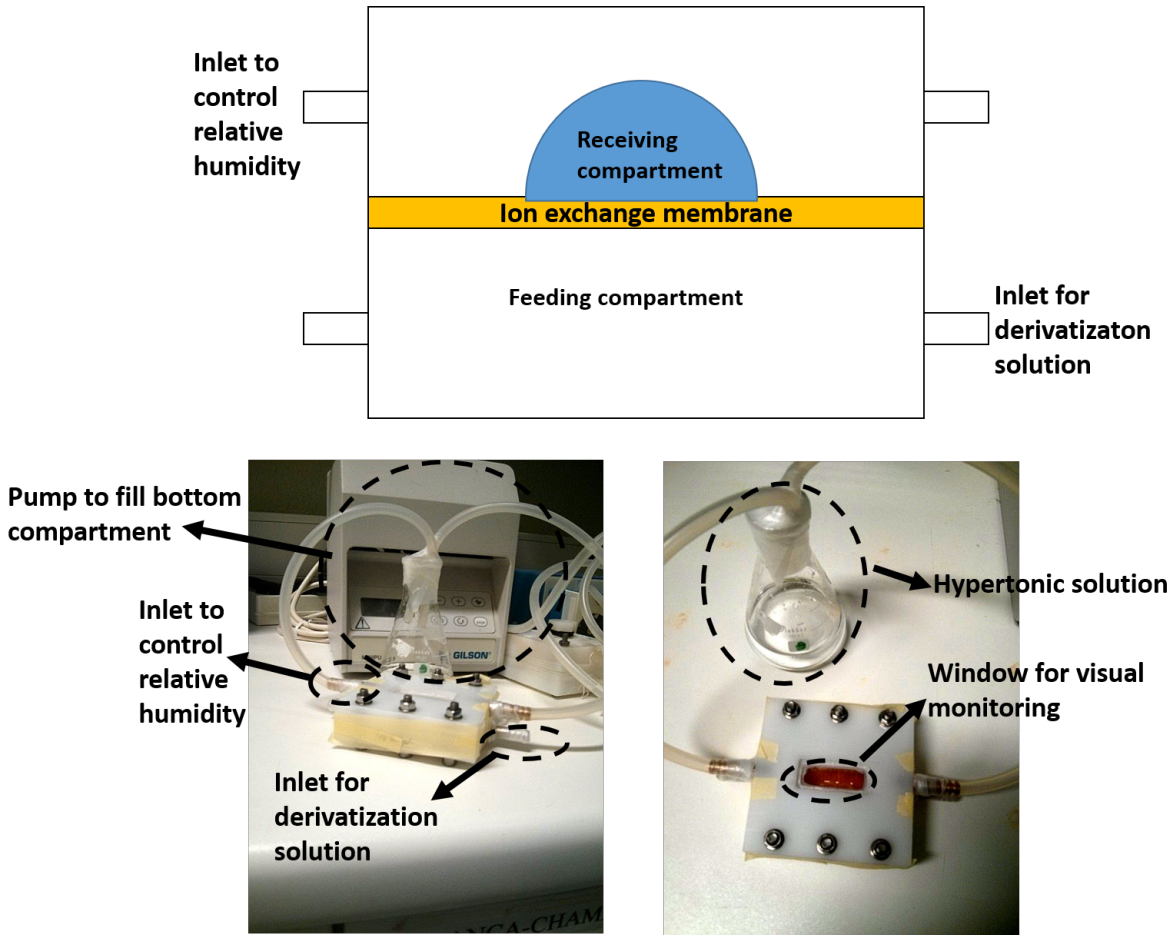

Figure 4.2: Schematic representation and picture of the cell. The feeding compartment is the compartment for heavy atom/halide solution. The receiving compartment is the protein solution. The cell was built by the company IrmaSolda. Details can be provided upon request to the author

atomhalide solution using a peristaltic pump (Minipulse, Gilson) (recirculation was not applied in these experiments). In the receiving compartment, 5 μL of protein solution was placed at the membrane surface and then mixed with the same volume of precipitant solution. The cell was sealed, and the relative humidity (RH) was allowed to reach the equilibrium by connecting the receiving compartment with the hypertonic solution (Figure 4.3a). Due to the difference in water activity between the protein and the reservoir solution, supersaturation was reached [28, 30]. The nucleation process was checked under the microscope until crystals appeared (Figure 4.3b). Only at this point the feeding compartment was filled with a solution containing the halide ion or the heavy atom (feeding solution) (Figure 4.3c) and left to equilibrate with the drop containing the protein

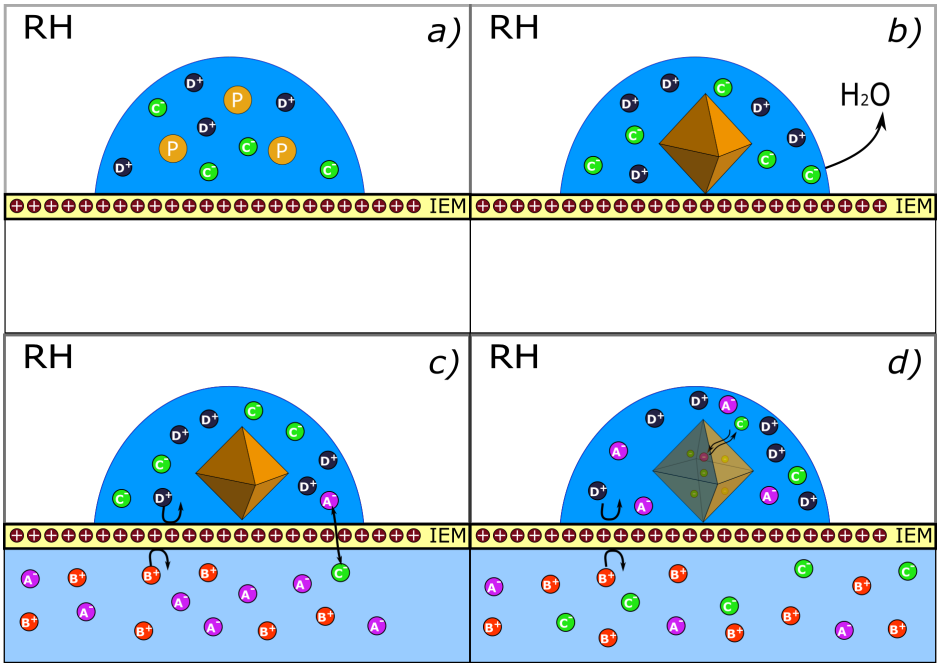

Figure 4.3: Experimental procedure for crystal growth and derivatization: (a) a drop of protein (P) solution and precipitant salt (D^+ and C^- represent the cation and anion of the salt used as precipitant, respectively) is placed onto the ion exchange membrane (IEM) in the cell in equilibrium with a hypertonic solution that controls relative humidity (RH) of the receiving compartment; (b) the solvent evaporates from the protein drop in order to reach equilibrium with the RH of the receiving compartment, supersaturation is generated, and crystals are formed; (c) heavy atom solution (A^- and B^+ represent the anion and cation of the salt used for derivatization, respectively) is brought in contact with the protein drop through the membrane; ion-exchange membranes are made of a hydrophobic backbone containing attached charged groups. The membrane selectivity for anions or cations is defined based on the charge of the groups attached to the backbone. Ions carrying opposite charge (counterions) to the membrane groups are allowed to pass through the membrane; meanwhile, ions carrying the same charge (co-ions) are rejected. In this case, the membrane with positively charged groups allows the transport of anions (A^- and C^-) and prevents the transport of cations (B^+ and D^+); (d) heavy atoms inside the protein drop diffuse inside the crystal's solvent channels.

solution (receiving solution) placed on the surface of the membrane at the receiving compartment (Figure 4.3d). The crystals were monitored everyday under the microscope to check the stability and presence of possible signs of cracking and or degradation. The experiments were conducted at 20 °C in a room with controlled temperature.

4.3.4 Conventional Soaking Experiments

To highlight the potential advantages of the membrane-assisted process, protein crystal derivatization was also carried out by conventional soaking procedures and compared to crystal derivatization using the ion-exchange membrane process. In this case, crystals were produced first in conventional hanging drop plates, and then harvested by a loop and soaked in 5 μL of solution containing 0.1 M $Na(CH_3COO)$ pH 4.6, 0.6 M NaCl, and the same heavy atom concentration expected in the protein solution at the equilibrium [11] (0.6 M NaBr, 5 mM K_2PtCl_4, 10 mM $Hg(CH_3COO)_2$. These values were estimated based on the mass transfer coefficient measurements explained below. The stability of the crystals was monitored everyday under the microscope during 1 week.

4.3.5 Experimental Mass Transfer Coefficient Measurement for Heavy AtomsIons Transport

Measurements of mass transfer coefficients of heavy atoms were performed to estimate the rate of ion-transport in the system (from the feeding solution, through the membrane, to the protein drop). The variation of pH (parameter that can affect crystal stability) was also measured during the ion-exchange process. The measurements were performed using a diffusion cell with two compartments (feeding and stripping compartments) with equal volume of solutions [32] and the same geometry and hydrodynamic conditions (flat membrane surface and no stirring of the contacting solutions) as the cell used for derivatization (Figure 4.4). In order to determine the heavy atom and halide mass transfer coefficient

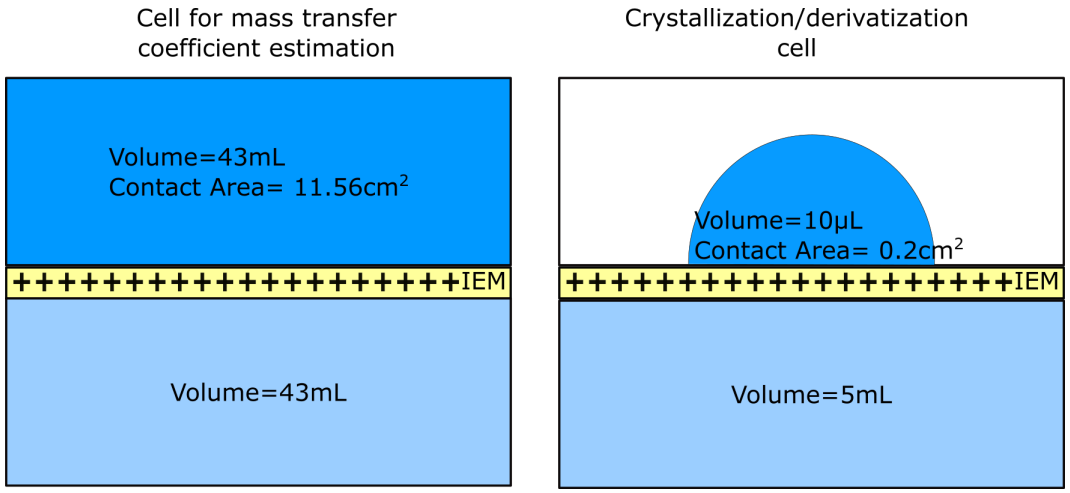

Figure 4.4: Scheme of the cells used to estimate the mass transfer coefficients and to run the crystallization and derivatization experiments. The geometry was flat in both cases, and none of the compartments was stirred. The temperature was the same in both cases.

under conditions as close as possible to the derivatization process, the compartments were filled with two solutions with equal pH and molar concentration, the feeding compartment containing the heavy atom halide to be diffused and the receiving compartment containing NaCl, both dissolved in the same buffer as the protein solution 0.1 M ($NaCH_3COO$, pH 4.6). The area of the membrane used was 11.56 cm^2, and the volume of each compartment was 43 mL (Figure 4.4). Aliquots (200 μL) were taken regularly from the solutions in the two compartments for 3 days. The values of pH and concentration of halidesmetal salts solutions were monitored using a pH-meter (CRISON BASIC 20 pH) and an Ionic Chromatograph-DIONEX, model ICS3000, for Br^-, and an ICP-AES (Inductively Coupled Plasma-Atomic Emission Spectrometer), Horiba JobinYvon, France, for Hg^{2+} and $PtCl_4^{2-}$. The molar concentration for all the species used for derivatization in both compartments was plotted against time (Figure 4.5).

4.3.6 X-ray Diffraction Analysis

HEWL crystals were equilibrated for a few seconds, first in harvesting buffer (0.1 M $NaCH_3COO$, pH 4.6, and 1 M NaCl) and then in cryo-protectant solution

(harvesting buffer and 30% (v/v) glycerol from Sigma-Aldrich). Preliminary X-ray Article set was collected from this crystal to 1.66 Å resolution at the Swiss Light Source (SLS, beamline X06DA PXIII) using radiation of 0.918 Å wavelength. Diffraction data from the mercury and platinum derivatives were collected at a fixed-wavelength beamline (0.966 Å, at which X-ray anomalous absorption effects for these heavy atoms can be measured) in the European Synchrotron Radiation Facility (ESRF, beamline ID30-A1). All synchrotron data were integrated with program MOSFLM [40] and scaled with AIMLESS [41] from the CCP4 suite. Substructure search, SAD (Single-wavelength Anomalous Dispersion) phasing, density modification, and model building were performed with program AutoSol implemented in Phenix [42]. Data collection, processing, and phasing statistics of the crystals derivatized through the ion-exchange membrane are presented in Table 5.1.

4.4 Results and Discussion

4.4.1 Contact Angle Measurement

The contact angle of the membranes used in this work was measured in order to ensure that the protein solution was stable on the membrane top over the experimental time. Contact angle is approximately 105 ± 14° for Nafion® and 66 ± 7° for Neosepta Axe, and thus, the membranes can be considered slightly hydrophobic and moderately hydrophilic, respectively. These values suggest that the protein drop is stable and that it is not absorbed by the membrane.

4.4.2 Kinetics of Ion-Transport

The mass transfer coefficients for the three ions (K_{Br}, K_{PtCl_4}, and K_{Hg}) were calculated fitting the data obtained from the transport studies (Figure 4.5) with the mass balance equations for each ion and integrating over time [32]. Since no electrical field is applied, the only driving force in the process is the concentration gradient across the membrane of the transported species; therefore, the variation

of number of moles of a species can be written as follows:

$$-\frac{dn}{dt} = KA(C - C_{eq}) \tag{4.1}$$

where K is the mass transfer coefficient, A is the area of diffusion, C is the concentration at time t, and C_{eq} is the equilibrium concentration. Since the ion-exchange membranes prevent osmosis, the concentration of the two solutions is approximately the same, and the volumes (V) of the solutions in the two compartments are assumed to be constant when the variation of the concentration of species over time can be derived.

$$-V\frac{dC}{dt} = KA(C - C_{eq}) \tag{4.2}$$

By integrating equation 4.2, equation 4.3 was obtained and used to fit the experimental data. C_0 is the initial ion concentration.

$$C = C_{eq} + (C_0 - C_{eq})e^{-\frac{KA}{V}t} \tag{4.3}$$

Table 4.1: Mass transfer coefficient of the different ions used for derivatization

Ion	**Mass Transfer Coefficient** (m/s)	$\mathbf{R^2}$
Br^-	$1.8*10^{-6}$	0.99
$PtCl_4^{2-}$	$1.9*10^{-7}$	0.99
Hg^{2+}	$1.9*10^{-9}$	0.99

The estimation of ion transport in the derivatization cell was done using equation 4.3 considering the mass transfer coefficients (shown in Table 5.1) calculated from the fitting of ion-transport curves in the receiving compartment (where the ions are diffusing to and the concentration is increasing), area of the membrane in contact with the protein solution (0.2 cm^2) and the volume of the drop, approximated to the initial drop volume (10 μL). Due to the high difference in volume between the protein drop (10 μL) and the Br^- solution (5 mL), the concentration of the exchanging solution was considered constant and used as equilibrium concentration. The ion concentrations estimated over time (Figure 4.6) allow pre-

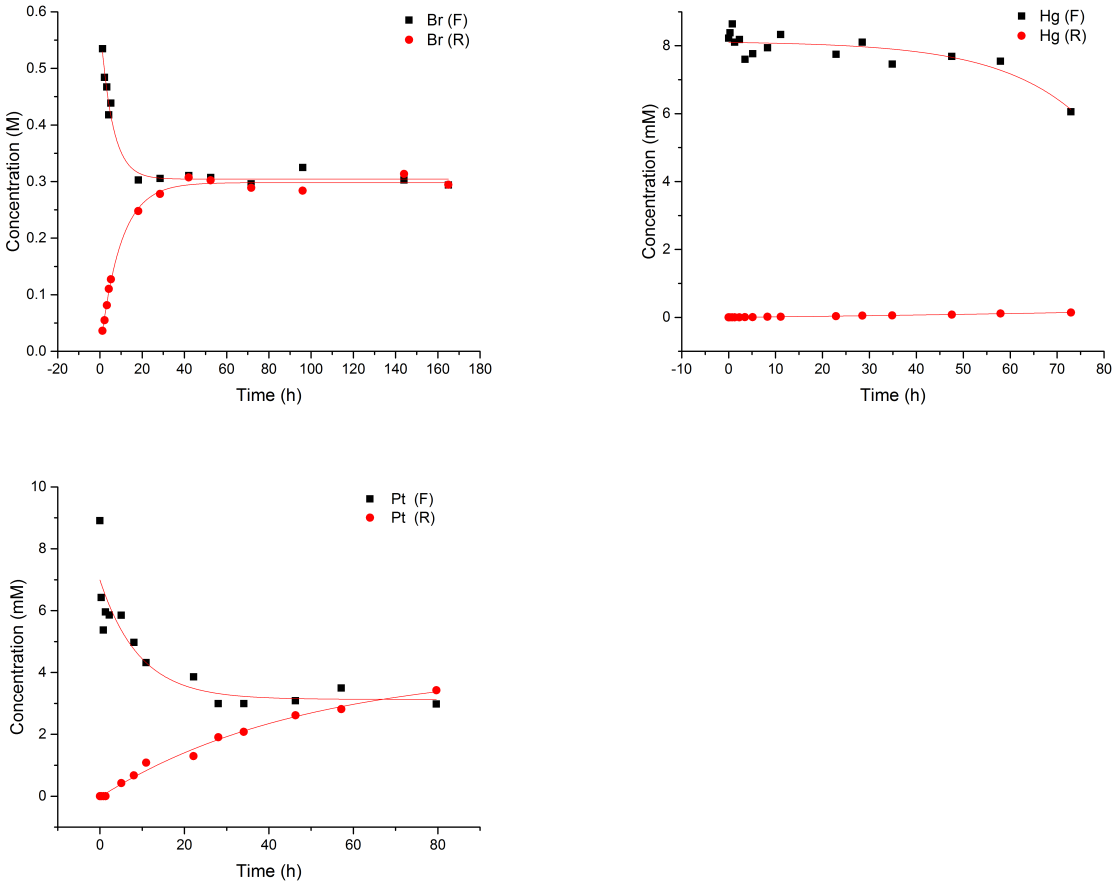

Figure 4.5: Experimental data for the calculation of the mass transfer coefficient for Br^-, $PtCl_4^{2-}$, and Hg^{2+} in the two compartments: **F** (feeding compartment) and **R** (receiving compartment)

dicting the time needed for the transport process inside the protein drop to be completed, which was found to be 1 hour for Br^-,4 hours for $PtCl_4^{2-}$, and 25 hours for Hg^{2+}.

4.4.3 Stability of the Crystals over Time

The crystals derivatized by conventional soaking and through the ion- exchange membrane process were daily checked under the microscope to monitor possible signs of cracking and degradation. In Figure 4.7, the morphology of the crystals derivatized with bromide in the cell (Figure 4.7a) was compared to that of the crystals derivatized by soaking (Figure 4.7b). The crystals derivatized in the cell

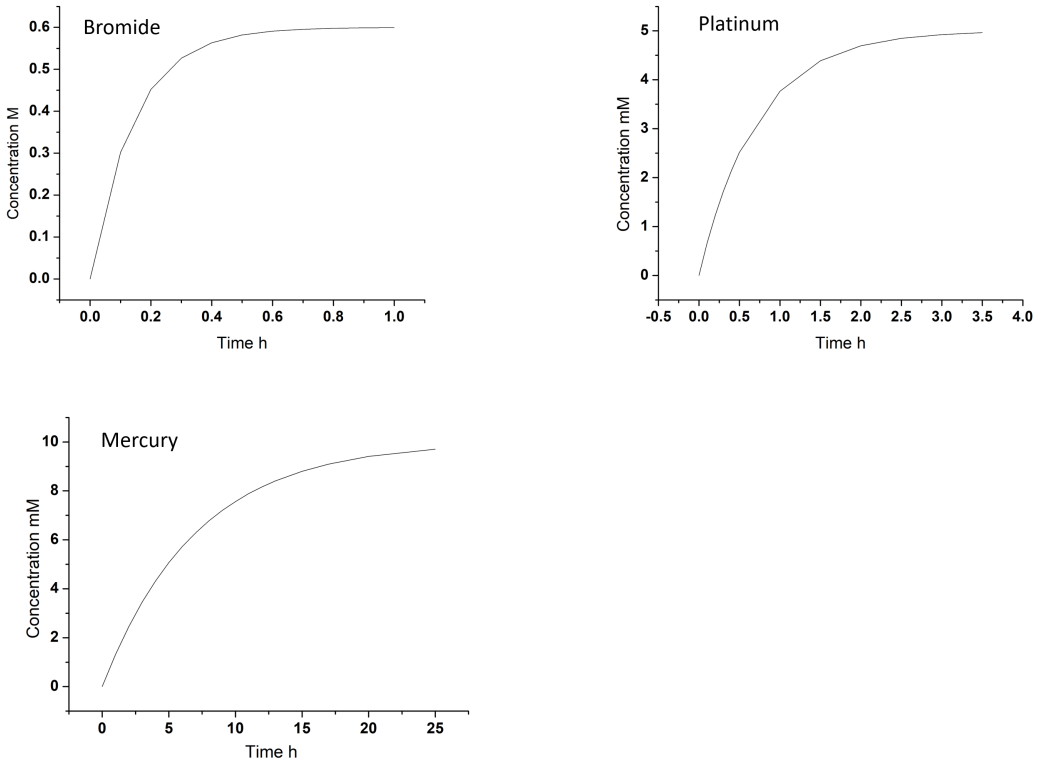

Figure 4.6: Concentration of heavy atoms to estimate time to reach equilibrium in the protein drop, based on the transport studies presented in Figure 4.5.

were checked for one month, and their appearance was stable over time. In contrast, after 12 hours,the soaked crystals started showing some defects, and after 3 days, they were clearly degraded (4.7b). In the case of the crystals derivatized with Hg^{2+}, it is clear that when conventional soaking was used, already after 4 hours (Figure 4.8) they revealed signs of degradation. These crystals diffracted to very low resolution (below 10 Å) being useless for X-ray diffraction analysis. In contrast, crystals derivatized in the cell (Figure 4.9) were regularly monitored by visual inspection and were stable over time (114 hours). According to the diffusion studies (Figure 4.6), the concentration of Hg^{2+} in the protein drop placed at the membrane surface reached the concentration of the derivatization solution used for direct soaking after 25 hours (Figure 4.6). Nevertheless, the crystals were monitored for about 5 days, a significantly long time after concentration equilibrium was reached inside the drop. The same occurred with the crystals derivatized with platinum (Figures 4.10 and 4.11). Furthermore, in this case,

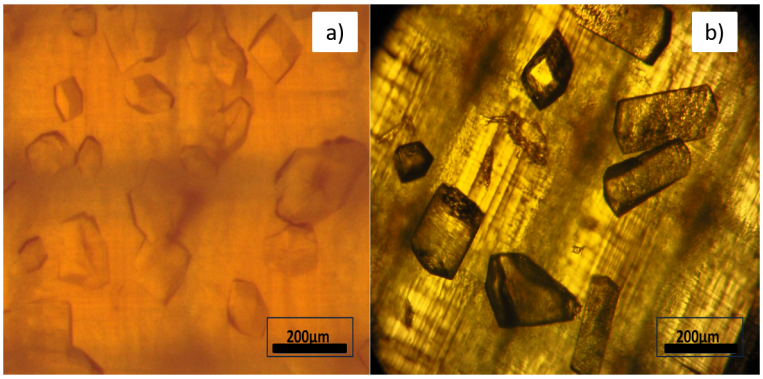

Figure 4.7: HEWL crystals derivatized with Br^- (a) in the cell and (b) by conventional soaking in drops placed on the membrane Neosepta AXE01 (solution of 0.6 M NaBr)

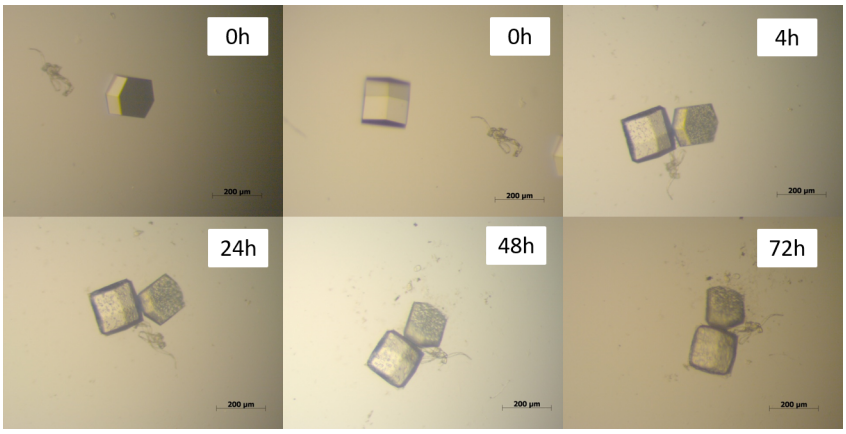

Figure 4.8: Stability of crystals derivatized with 10 mM $Hg(CH_3COO)_2$ by conventional soaking (drop placed on conventional crystallization plates) over time

crystals (Figure 4.10) started degrading at the exact moment they were brought in contact with the soaking solution. The edges were degraded, and they did not diffract, as expected. This proves that the damages on the crystals during soaking are due to the abrupt change in the crystal environment [11], and this can be avoided by the gentle and controlled transport of ions by diffusion with ion-exchange membranes.

4.4.4 X-ray Diffraction and Structure Solution

Complete X-ray diffraction data were collected from a crystal derivatized with NaBr using the ion-exchange membrane. Crystals diffracted to 1.66 Å resolution using X-rays from a synchrotron source of 0.918 Å wavelength. This wavelength

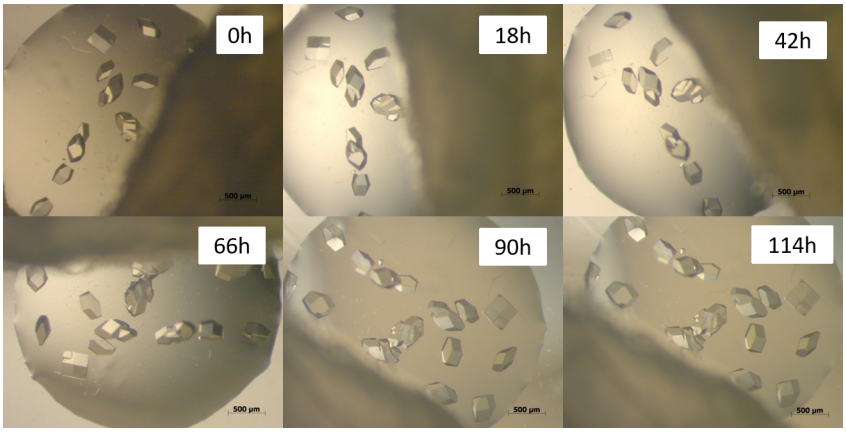

Figure 4.9: Stability of the crystals derivatized with $Hg(CH_3COO)_2$ (10 mM) in the cell (drop placed on Nafion®) over time

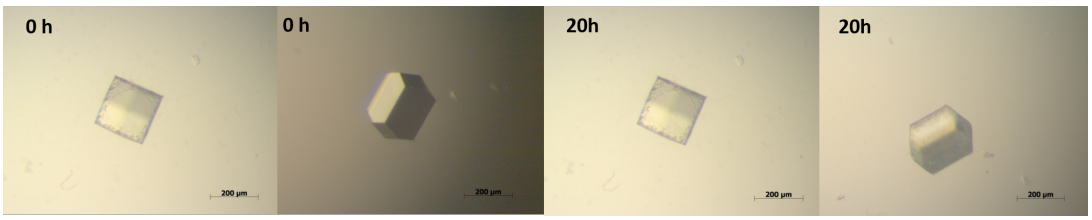

Figure 4.10: Stability of crystals derivatized with $PtCl_4^{2-}$ 5 mM by normal soaking (drop placed on conventional crystallization plate) over time

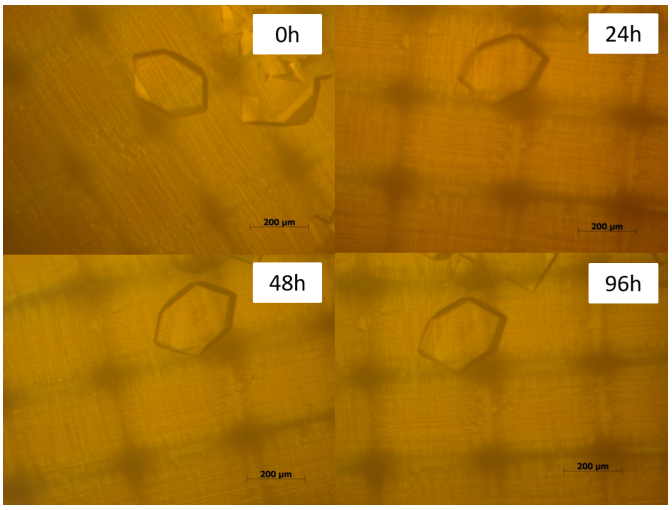

Figure 4.11: Stability of crystals derivatized with $PtCl_4^{2-}$ 5 mM in the cell (drop placed on Neosepta AXE01) over time

Table 4.2: Data Collection, SAD Phasing, and Automated Model Building Statistics of HEWL Crystals Derivatized Using the Ion- Exchange Membrane

	HEWL with NaBr	**HEWL with K_2PtCl_4**	**HEWL with $Hg(CH_3COO)_2$**
wavelenght (Å)	0.918	0.966	0.966
resolution range (Å)	56.62-1.66(1.69-1.66)	79.27-2.37 (2.46-2.37)	39.89-1.79 (1.83-1.79)
space group	80.1, 80.1, 36.2	79.3, 79.3, 37.7	79.8, 79.8, 37.4
unit cell parameters *a*,*b*,*c* (Å)	282531 (13685)	78896 (8270)	136662 (11073)
total reflections	14539 (695)	5239 (520)	11832 (677)
multiplicity	19.4 (19.7)	15.1 (15.9)	11.6 (16.4)
anomalous multiplicity	10.4 (10.2)	8.3 (8.4)	6.1 (8.3)
completeness (%)	100 (100)	100 (100)	100 (100)
anomalous completeness(%)	100 (100)	100 (100)	100 (100)
mean I/σ(I)	13.8 (3.2)	30.1 (18.9)	43.2 (9.0)
Wilson B-factor	13.7	31.1	24.8
R-merge	0.210 (2.110)	0.070(0.134)	0.162 (0.603)
R-pim	0.049 (0.479)	0.019 (0.034)	0.06 (0.153)
$CC_{1/2}$	0.997 (0.861)	0.998 (0.996)	0.987 (0.920)
SAD phasing			
No. of sites found	20	5	2
figure of merit (before/after density modification)	0.41/0.88	0.26/-	0.29/-
Automated model building and refinement from Br-SAD phase			
reflections used in refinement			13471 (1311)
reflections used for R-free			676 (63)
R-work/R-free			0.264/0.312
No. of non-hydrogn atoms			1035
macromolecule			927
heavy atoms			20
No. of protein residues			124
RMS (bonds) (Å)			0.007
RMS (angles) (deg)			0.99
Famachandran favored (%)			96
Ramachandran allowed (%)			4.3
Ramachandran outliers (%)			0
rotamer outliers (%)			2.3
average isotropic thermal parameters ($Å^2$)			17.89
macromolecule			17.60
heavy atoms			15.82
solvent			21.46

corresponded to the bromide absorption peak in the crystal, as indicated by the measured X-ray fluorescence scan (not shown). The experimental values measured for f and f were -5.07 e and 3.8 e, respectively. A different strategy was adopted to perform SAD phasing from the mercury and platinum derivatives, which were collected at a wavelength of 0.966 Å, at which anomalous signal for these heavy atoms can be experimentally obtained from highly redundant diffraction data sets. A complete SAD data set was collected from the $K2PtCl_4$-derivatized crystal to 2.37 Å resolution, while the $Hg(CH_3COO)_2$ derivatized crystal produced complete data to 1.79 Å resolution. All crystals belonged to space group $P4_32_12$, with unit-cell parameters (reported in Table 4.2) comparable to the parameters known for HEW lysozyme. The asymmetric unit comprises one monomer of HEWL with an approximate solvent content of 35%. A full pipeline of substructure search, SAD phasing, density modification, and model building was performed for the bromide-containing HEWL crystal. Data collection, processing, and phasing statistics are presented in Table 4.2. AutoSol, implemented in Phenix, output 20 possible sites for bromide ions, with occupancies ranging from 0.72 to 0.11, a figure-of-merit of 0.41, and an overall score of 48.9 ± 8.9. After density modification, a figure-of-merit of 0.88 was achieved, followed by successful automated model building from the obtained Br^- SAD phases. AutoSol could build 124 (out of 145) residues, producing a model with an R_{work} = 0.26 and an R_{free} = 0.31 and a map-model correlation coefficient of 0.81. Figure 4.12 shows the location of selected bromide atoms at the protein surface. For the research purposes, complete structure refinement was not required. For the platinum derivative, the automated search indicated five potential Pt sites, with a figure-of-merit of 0.26 and an overall score of 18.4 ± 14.3, clearly a weak phasing power for this derivative. A similar result was obtained for the mercury derivative, where AutoSol could detect two sites with respective occupancies of 0.29 and 0.34, a figure-of-merit of 0.18, and an overall score of 11.5 ± 12.6. Not surprisingly, *ab initio* model building was not successful for both Pt and Hg derivatives. The significantly low occupancies for the Hg and Pt atoms in both crystals impaired the

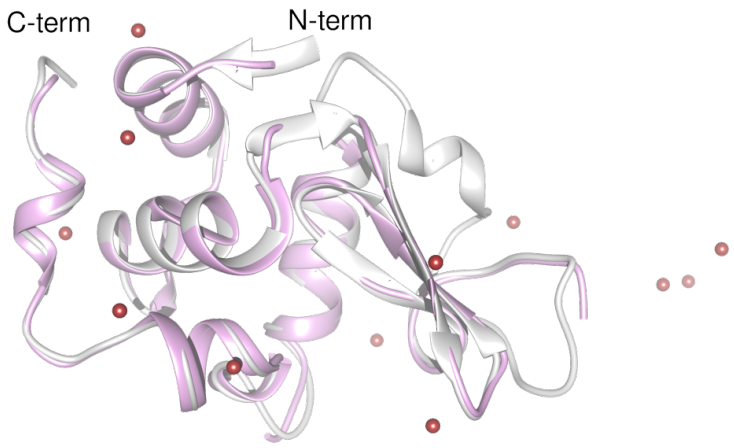

Figure 4.12: Ribbon representation of HEWL showing the surface location of several identified bromide atoms, as revealed by the measured anomalous signal. Bromide atoms are depicted as red spheres. The known structure of HEWL from Gallus gallus (PDB accession code 2LYS) is represented as a gray ribbon, overlaid on the *ab initio* model (in purple ribbon) built by AutoSol from the independent bromide phases. The superposition of both structures generates an rmsd of 0.334 Å for 109 α carbon atoms. Picture was produced with program Chimera [43, 44].

automated SAD phasing and subsequent model building. However, in combination with phases from a molecular replacement solution (obtained using a known structure of HEWL), 10 sites for Hg^{2+} could be identified (with very low occupancies ranging from 0.19 to 0.07) originating a figure-of-merit of 0.74 and an overall score of 75.6 ± 3.3. Similarly, for the phase combination of the platinum derivative with the molecular replacement solution, seven sites could be identified (with very low occupancies ranging from 0.2 to 0.05) originating a figure-of-merit of 0.79 and an overall score of 75.6 ± 3. All structures were analyzed for any differences compared to nonderivatized crystal structures. Calculation of rmsd values confirms that the structures obtained by derivatization were essentially isomorphous without significant differences from the native structures. For some heavy atom sites, clear additional electron density could be observed for the atoms (Br, Pt, and Hg) of which the nature was confirmed by the calculation of anomalous

difference maps. The failure to achieve *ab initio* model building from the weak SAD phases obtained for the mercury and platinum derivatives could be overcome with increasing concentrations of the heavy atoms and or longer incubation times. These results prove that, in the designed ion-exchange membrane cell, heavy atoms could be transported through the membrane and diffuse into the crystals. Therefore, this method could be applied to other proteins when heavy atom derivatives are required, since it provides a more gentle way of introducing metal ions or halides in the crystal lattice.

4.5 Conclusions

Protein crystal derivatization is a widely recognized technique used to introduce heavy atoms inside crystals to solve the threedimensional structure of proteins using the Multiple Isomorphous Replacement method. Soaking is a laborious and uncertain procedure, working on a trial-and-error basis, currently used to derivatize protein crystals. This technique requires the removal of the crystals from their growth environment and their slow immersion in a different solution containing the heavy atom salt for derivatization. In this work, an alternative crystal derivatization method is proposed, consisting of the smooth increase of the target ionic species concentration (derivatizing agents) in the protein environment (protein drop) achieved by controlling the diffusion of these species using an ion-exchange membrane. The ion-exchange membrane system designed in this work allowed not only a controlled transport of the ionic species from the feeding to the receiving solution (protein drop located at the membrane surface) but also the control of other factors that influence the growth and stability of protein crystals, such as pH, temperature, and osmotic pressure. The rate of ion transport through the membrane was estimated in order to know the concentration of heavy atom in the protein solution along the derivatization time, allowing to define the concentration of the derivatizing agent in the feeding compartment, needed to reach the desirable concentration of this ionic species in the protein drop (receiving compartment). This allowed a fair comparison of the derivatization process

with the conventional direct soaking, showing how a controlled diffusion leads to a better stability of the crystals during the derivatization process, with the three ions tested. X-ray diffraction analysis of the derivatives showed that the heavy atom incorporation was successful and that isomorphism was maintained in all cases. Bromide derivatives also allowed determining the protein structure using the SAD phasing technique. Although it was not possible to complete the solution process for the mercury and platinum derivatives due to the lower occupancies of the diffused atoms in the crystal lattice, this could probably be overcome by using higher concentrations of the heavy atoms. Besides the increased control on the process, the ion-exchange membrane allowed to overcome problems due to the disturbance of the vapour diffusion equilibrium and handling of the crystals, performing the process in a gentle and continuous way, avoiding several steps normally required in conventional soaking. This method, which does not intend to completely replace the traditional procedures, should be considered in difficult cases: e.g., extreme frailty of crystals, presence of volatile compounds in mother liquor, or low availability of protein. Furthermore, the system is easy to be used and highly versatile: no particular manual skills are required for preparing and conducting experiments, and it allows to play with solution composition and concentration to regulate the ion transport rate. Further studies involving the tailoring of the membrane features such as thickness, ion-exchange capacity, and area of exchange may lead to a greater level of control on the process. These results pave the way to the development of designer membranes capable of transporting other ligands of interest and, in a non-invasive procedure, diffuse these ligands in the crystals of protein of interest.

References

[1] G. L. Taylor. "Introduction to phasing." In: *Acta Crystallographica Section D: Biological Crystallography* 66.4 (2010), pp. 325–338. DOI: 10.1107/S0907444910006694.

[2] I Usón and G. M. Sheldrick. "Advances in direct methods for protein crystallography." In: *Current opinion in structural biology* 9.5 (1999), pp. 643–648. DOI: 10.1016/S0959-440X(99)00020-2.

[3] J. P. Rose and B. C. Wang. "SAD phasing: History, current impact and future opportunities." In: *Archives of Biochemistry and Biophysics* 602 (2016), pp. 80–94. DOI: 10.1016/j.abb.2016.03.018.

[4] T. J. Boggon and L. Shapiro. "Screening for phasing atoms in protein crystallography." In: *Structure* 8.7 (2000), pp. 143–149. DOI: 10.1016/S0969-2126(00)00168-4.

[5] J. Agniswamy, M. G. Joyce, C. H. Hammer, and P. D. Sun. "Towards a rational approach for heavy-atom derivative screening in protein crystallography." In: *Acta Crystallographica Section D: Biological Crystallography* 64.4 (2008), pp. 354–367. DOI: 10.1107/S0907444907068849.

[6] S. Panjikar and P. A. Tucker. "Xenon derivatization of halide-soaked protein crystals." In: *Acta Crystallographica Section D: Biological Crystallography* 58.9 (2002), pp. 1413–1420. DOI: 10.1107/S0907444902011010.

[7] M. Dauter and Z. Dauter. "Phase determination using halide ions." In: *Methods in molecular biology (Clifton, N.J.)* 364.9 (2007), pp. 149–158. DOI: 10.1385/1-59745-266-1:149.

[8] Z. Dauter, M. Dauter, and K. R. Rajashankar. "Novel approach to phasing proteins: Derivatization by short cryo-soaking with halides." In: *Acta Crystallographica Section D: Biological Crystallography* 56.2 (2000), pp. 232–237. DOI: 10.1107/S0907444999016352.

[9] B. Heras and J. L. Martin. "Post-crystallization treatments for improving diffraction quality of protein crystals." In: *Acta Crystallographica Section D: Biological Crystallography* 61.9 (2005), pp. 1173–1180. DOI: 10.1107/S0907444905019451.

[10] J. Newman. "A review of techniques for maximizing diffraction from a protein crystal in stilla." In: *Acta Crystallographica Section D: Biological Crystallography* 62.1 (2006), pp. 27–31. DOI: 10.1107/S0907444905032130.

[11] A. C. W. Pike, E. F. Garman, T. Krojer, F. von Delft, and E. P. Carpenter. "An overview of heavy-atom derivatization of protein crystals." In: *Acta crystallographica. Section D, Structural biology* 72.Pt 3 (2016), pp. 303–318. DOI: 10.1107/S2059798316000401.

[12] A. M. Hassell, G. An, R. K. Bledsoe, J. M. Bynum, H. L. Carter, S. J. J. Deng, R. T. Gampe, T. E. Grisard, K. P. Madauss, R. T. Nolte, W. J. Rocque, L. Wang, K. L. Weaver, S. P. Williams, G. B. Wisely, R. Xu, and L. M. Shewchuk. "Crystallization of protein-ligand complexes." In: *Acta Crystallographica Section D: Biological Crystallography* 63.1 (2006), pp. 72–79. DOI: 10.1107/S0907444906047020.

[13] G. Di Profio, A. Caridi, R. Caliandro, A. Guagliardi, E. Curcio, and E. Drioli. "Fine dosage of antisolvent in the crystallization of L-histidine: Effect on polymorphism." In: *Crystal Growth and Design* 10.1 (2010), pp. 449–455. DOI: 10.1021/cg901038g.

[14] E. Curcio, E. Fontananova, G. D. Profio, and E. Drioli. "Influence of the Structural Properties of Poly(vinylidene fluoride) Membranes on the Heterogeneous Nucleation Rate of Protein Crystals." In: *Journal of Physical Chemistry B* 4.1 (2006), pp. 12438–12445. DOI: 10.1021/jp061531y.

[15] F. Kertis, S. Khurshid, O. Okman, J. W. Kysar, L. Govada, N. Chayen, and J. Erlebacher. "Heterogeneous nucleation of protein crystals using nanoporous gold nucleants." In: *Journal of Materials Chemistry* 22.41 (2012), pp. 21928–21934. DOI: 10.1039/c2jm34527g.

[16] K Ino, I Udagawa, K Iwabata, Y Takakusagi, and M Kubota. "Heterogeneous Nucleation of Protein Crystals on Fluorinated Layered Silicate." In: *PLoS ONE* 6.7 (2011), p. 22582. DOI: 10.1371/journal.pone.0022582.

[17] Y. X. Liu, X. J. Wang, J. Lu, and C. B. Ching. "Influence of the roughness, topography, and physicochemical properties of chemically modified surfaces on the heterogeneous nucleation of protein crystals." In: *Journal of Physical Chemistry B* 111.50 (2007), pp. 13971–13978. DOI: 10.1021/jp0741612.

[18] G. D. Profio, M. Polino, F. P. Nicoletta, B. D. Belviso, R. Caliandro, E. Fontananova, G. De Filpo, E. Curcio, and E. Drioli. "Tailored hydrogel membranes for efficient protein crystallization." In: *Advanced Functional Materials* 24.11 (2014), pp. 1582–1590. DOI: 10.1002/adfm.201302240.

[19] G. Di Profio, S. Tucci, E. Curcio, and E. Drioli. "Selective glycine polymorph crystallization by using microporous membranes." In: *Crystal Growth and Design* 7.3 (2007), pp. 526–530. DOI: 10.1021/cg0605990.

[20] G. Di Profio, E. Fontananova, E. Curcio, and E. Drioli. "From tailored supports to controlled nucleation: Exploring material chemistry, surface nanostructure, and wetting regime effects in heterogeneous nucleation of organic molecules." In: *Crystal Growth and Design* 12.7 (2012), pp. 3749–3757. DOI: 10.1021/cg3005568.

[21] H. Hsu, O. O. Adigun, L. S. Taylor, S. Murad, and M. T. Harris. "Crystallization of acetaminophen on chitosan films blended with different acids." In: *Chemical Engineering Science* 126 (2015), pp. 1–9. DOI: 10.1016/j.ces.2014.10.046.

[22] N. P. Berezina, N. A. Kononenko, O. A. Dyomina, and N. P. Gnusin. "Characterization of ion-exchange membrane materials: Properties vs structure." In: *Advances in Colloid and Interface Science* 139.1-2 (2008), pp. 3–28. DOI: 10.1016/j.cis.2008.01.002.

[23] T. Xu. "Ion exchange membranes: State of their development and perspective." In: *Journal of Membrane Science* 263.1-2 (2005), pp. 1–29. DOI: 10.1016/j.memsci.2005.05.002.

[24] R. K. Nagarale, G. S. Gohil, and V. K. Shahi. "Recent developments on ion-exchange membranes and electro-membrane processes." In: *Advances in Colloid and Interface Science* 119.2-3 (2006), pp. 97–130. DOI: 10.1016/j.cis.2005.09.005.

[25] C. Klaysom, S. H. Moon, B. P. Ladewig, G. Q. M. Lu, and L. Wang. "Preparation of porous ion-exchange membranes (IEMs) and their characterizations." In: 371.1-2 (2011), pp. 37–44. DOI: 10.1016/j.memsci.2011.01.008.

[26] T. Mohammadi, S. Chieng, and M. Skyllas Kazacos. "Water transport study across commercial ion exchange membranes in the vanadium redox flow battery." In: *Journal of Membrane Science* 133.2 (1997), pp. 151–159. DOI: 10.1016/S0376-7388(97)00092-6.

[27] D. E. Otzen. "Protein unfolding in detergents: effect of micelle structure, ionic strength, pH, and temperature." In: *Biophysical journal* 83.4 (2002), pp. 2219–30. DOI: 10.1016/S0006-3495(02)73982-9.

[28] N. E. Chayen. "Turning protein crystallisation from an art into a science." In: *Current Opinion in Structural Biology* 14.5 (2004), pp. 577–583. DOI: 10.1016/j.sbi.2004.08.002.

[29] S. Sugiyama, M. Maruyama, G. Sazaki, M. Hirose, H. Adachi, K. Takano, S. Murakami, T. Inoue, Y. Mori, and H. Matsumura. "Growth of protein crystals in hydrogels prevents osmotic shock." In: *Journal of the American Chemical Society* 134.13 (2012), pp. 5786–5789. DOI: 10.1021/ja301584y.

[30] A. McPherson and J. A. Gavira. "Introduction to protein crystallization." In: *Acta Crystallographica Section F:Structural Biology Communications* 70.1 (2014), pp. 2–20. DOI: 10.1107/S2053230X13033141.

[31] N. Asherie. "Protein crystallization and phase diagrams." In: *Methods* 34.3 (2004), pp. 266–272. DOI: 10.1016/j.ymeth.2004.03.028.

[32] J. Luo, C. Wu, T. Xu, and Y. Wu. "Diffusion dialysis-concept, principle and applications." In: *Journal of Membrane Science* 366.1-2 (2011), pp. 1–16. DOI: 10.1016/j.memsci.2010.10.028.

[33] J. Luo, C. Wu, Y. Wu, and T. Xu. "Diffusion dialysis of hydrochloride acid at different temperatures using PPO-SiO2 hybrid anion exchange membranes." In: *Journal of Membrane Science* 347.1-2 (2010), pp. 240–249. DOI: 10.1016/j.memsci.2009.10.029.

[34] J. Luo, C. Wu, Y. Wu, and T. Xu. "Diffusion dialysis processes of inorganic acids and their salts: The permeability of different acidic anions." In: *Separation and Purification Technology* 78.1 (2011), pp. 97–102. DOI: 10.1016/j.seppur.2011.01.028.

[35] C. Y. Zhang, D. C. Yin, Q. Q. Lu, Y. Z. Guo, W. H. Guo, X. K. Wang, H. S. Li, H. M. Lu, and Y. J. Ye. "Cycling temperature strategy: A method to improve the efficiency of crystallization condition screening of proteins." In: *Crystal Growth and Design* 8.12 (2008), pp. 4227–4232. DOI: 10.1021/cg800689j.

[36] "Lysozyme User Guide, Hampton Research." In: (2014), pp. 1–2.

[37] Y. Liu, X. Wang, and C. B. Ching. "Toward further understanding of lysozyme crystallization: Phase diagram, protein-protein interaction, nucleation kinetics, and growth kinetics." In: *Crystal Growth and Design* 10.2 (2010), pp. 548–558. DOI: 10.1021/cg900919w.

[38] a. Kimble, W.L.; Paxton, T. E.; Rousseau, R. W.; Sambanis. "The effect of mineral substrates on the crystallization of lysozyme." In: *Journal of Crystal Growth* 187 (1998), pp. 268–276. DOI: 10.1016/S0022-0248(97)00838-5.

[39] G. Tosi, S. Fermani, G. Falini, J. A. Gavira Gallardo, and J. M. Garcia Ruiz. "Crystallization of proteins on functionalized surfaces." In: *Acta Crystallographica Section D: Biological Crystallography* 64.10 (2008), pp. 1054–1061. DOI: 10.1107/S0907444908025079.

[40] T. G. G. Battye, L. Kontogiannis, O. Johnson, H. R. Powell, and A. G. W. Leslie. "iMOSFLM: A new graphical interface for diffraction-image processing with MOSFLM." In: *Acta Crystallographica Section D: Biological Crystallography* 67.4 (2011), pp. 271–281. DOI: 10.1107/S0907444910048675.

[41] P. R. Evans and G. N. Murshudov. "How good are my data and what is the resolution?" In: *Acta Crystallographica Section D: Biological Crystallography* 69.7 (2013), pp. 1204–1214. DOI: 10.1107/S0907444913000061.

[42] P. D. Adams, P. V. Afonine, G. Bunkóczi, V. B. Chen, I. W. Davis, N. Echols, J. J. Headd, L. W. Hung, G. J. Kapral, R. W. Grosse-Kunstleve, A. J. McCoy, N. W. Moriarty, R. Oeffner, R. J. Read, D. C. Richardson, J. S. Richardson,

T. C. Terwilliger, and P. H. Zwart. "PHENIX: A comprehensive Python-based system for macromolecular structure solution." In: *Acta Crystallographica Section D: Biological Crystallography* 66.2 (2010), pp. 213–221. DOI: 10.1107/S0907444909052925.

[43] E. F. Pettersen, T. D. Goddard, C. C. Huang, G. S. Couch, D. M. Greenblatt, E. C. Meng, and T. E. Ferrin. "UCSF Chimera visualization system for exploratory research and analysis." In: *Journal of Computational Chemistry* 25.13 (2004), pp. 1605–1612. DOI: 10.1002/jcc.20084.

[44] T. D. Goddard, C. C. Huang, and T. E. Ferrin. "Visualizing density maps with UCSF Chimera." In: *Journal of Structural Biology* 157.1 (2007), pp. 281–287. DOI: 10.1016/j.jsb.2006.06.010.

CHAPTER 5

NAFION® INTEGRATED MICRODEVICE FOR PROTEIN CRYSTALLIZATION AND PROTEIN CRYSTALS DERIVATIZATION

5.1 Summary

Protein crystallization and protein crystals derivatization are rather empirical sciences; several conditions have to be tested to obtain highly diffractive crystals. In this work, the advantages of microfluidics technology for protein crystallization (high throughput, low budget) were combined with the fine control that membranes can provide to the crystallization and derivatization process. Hence, a Nafion® membrane was sandwiched between a channels layer and a wells layer of PDMS in order to build a microdevice with 75 micro-contactors in which nano to micro volumes of solution can be used to control protein crystallization. Crystallization experiments with Hen Egg White Lysozyme (HEWL) were performed in order to test reproducibility and the functionality of the device. Number and size of crystals were modulated by changing the volume of solution in the microdevice wells for the same area of transport through the membrane. Crystals obtained in the microdevice were stable over time and demonstrated a high diffraction

quality during X-ray diffraction analysis.

5.2 Introduction

The attainment of high quality diffracting crystals is still the main limitation in protein crystallography applied for the resolution of the three-dimensional molecular structure of proteins. The diffraction quality of protein crystals may depend on several crystallization parameters: pH, temperature, solvent removal rate, additives, among others. Therefore, when the structure of a new protein has to be unraveled, an enormous number of conditions have to be tested, before an adequate recipe is found that leads to a well-diffracting crystal suitable for accurate crystallography analysis [1]. Microfluidic technology has been revolutionary for protein crystallization: The creativity of scientists has led to the development of several intricate chip designs (valve-based [2], droplet-based[3], slip chips [4], or centrifugal designs [5]) that allowed for the fast screening of hundreds of process conditions, using only very low amounts of protein [6]. On the other hand, advances in membrane technology has contributed to excellent control of the solvent removal rate, required for regulation of the crystallization process, by modulating the porosity of hydrophobic microporous membranes, such as polypropylene, and by controlling the difference in water activity between the protein solution and the stripping solution [7]. This allowed to control the crystal growth rate [8], shape [9], polymorphism [10] and, consequently, the diffraction quality [11]. In some cases, the obtained crystals diffract poorly, despite all the effort, while in other cases, such as for completely unknown structures, routine diffraction analysis (Molecular Replacement Techniques) is not able to resolve the structure. In these cases it becomes essential to introduce heavy atoms into the crystal (derivatization), in order to facilitate the resolution process using Isomorphous Replacement Techniques [12–16]. Similar to crystallization, derivatization is also a challenging procedure. Finding the right heavy atom and concentration for a specific protein requires persistence. Crystals may easily crack and get damaged due to the use of a wrong heavy atom or due to abrupt changes in the local

growth environment and the handling of crystals. Attempts were made to predict the interaction between the protein and the heavy atoms [17, 18], but for most protein cases, a screening of different heavy atoms and concentrations becomes essential. Recently, ion-exchange membranes were successfully used to facilitate the derivatization of protein crystals with heavy atoms [19]. Ion-exchange membranes are tipically made of a hydrophobic backbone with attached charged groups [20]. Such membranes are able to mediate the selective diffusion of ions (cations or anions depending on the type of fixed charged groups attached to the membrane) inside the protein crystal solution determining a smooth and controlled increase of the target ion-concentration, reducing the risks of cracking due to abrupt changes of the crystals environment and handling [19]. Besides the selective ion transport, ion-exchange membranes promote water transport when a difference in water activity occurs between the two sides of the membrane: water spontaneously moves from the least to the most concentrated compartment [21]. Hence, controlled diffusion of water by osmosis could be exploited to generate supersaturation and promote nucleation. In this work, an ion-exchange membrane (Nafion®) was integrated into a PDMS microdevice to form 75 microcontactors where ion-exchange membrane-driven crystallization and derivatization conditions can be explored. The device is made of three parts: a channel layer that can be filled with a stripping or a derivatization solution, a wells layer where each well can accommodate nano or microliter volumes of protein solution, defining the area of water diffusion or ion-exchange for crystallization or derivatization, and a sandwiched ion-exchange membrane to control the diffusion process.

The tasks performed in this work were:

i. Evaluation of water, NaCl and Hg^{2+} (typical ion used in the derivatization of protein crystals[12, 17]) mass transfer coefficients through the membrane;

ii. Modelling of the transport of water, NaCl and Hg^{2+} in the microdevice;

iii. Evaluate the performance of protein crystallization in the microdevice;

iv. Determine the crystal derivatization efficiency in the microdevice by X-ray Diffraction analysis.

5.3 Materials and Methods

5.3.1 Crystallization solutions

Hen Egg White Lysozyme (HEWL) from Sigma Aldrich was used as a model protein. HEWL was dissolved in 0.1 M CH_3COONa (pH 4.6, Scharlab S.L., Barcelona, Spain). 3.5 % NaCl (Applichem Panreac, Barcelona, Spain) dissolved in 0.1 M CH_3COONa (pH 4.6) was used as a precipitant and stripping solution.

5.3.2 Design and fabrication of the microdevice

The microdevice was fabricated by soft lithography [22–24]. Two photomasks, one for a microwell layer and another one for a channel layer, were designed using CleWin software (WieWeb software, Hengelo, the Netherlands). Master molds were fabricated by photolithography (Figure 5.1 A)[25]. A negative photoresist resin (SU-8 2150, MicroChemicals GmbH, Ulm, Germany), was spun onto 100mm diameter silicon wafers, baked and exposed to UV light in order to transfer the pattern from the mask to the photoresist layers on the wafers. The subsequent use of an SU-8 developer allowed to remove the soluble (non-exposed) parts of the resin. The final thickness of photoresist structures was measured with a micrometer, and it was found to be 300 ± 50 µm for both moulds. PDMS mixture (Sylgard 184, Dow Corning, prepolymer:curing agent = 10:1) was casted onto the master moulds and baked at 80 °C for 1 hour (Figure 5.1 B). For the channel layer, an amount of PDMS was casted to cover the mold completely (Figure 5.1 B). Instead, in the case of the wells layer, the volume of PDMS casted was calculated in order to give a thickness lower than the height of the pillars, determining the formation of holes, instead of cavities (Figure 5.1 B). In order to flow the solutions inside the channels, an inlet and an outlet were created by punching. Each device has 5 lines of 15 wells for a total of 75 wells. The wells have a circular shape with 1 mm diameter (this diameter was chosen to allow the harvesting of crystals with conventional crystallography loops) and 250 µm depth. The channel part comprises 5 channels, matching with the 5 lines of wells; therefore, 5 different solutions can be used simultaneously as stripping solutions (1 per

channel) for crystallization. The driving force in each channel will be dependent on the solution inside the wells. The same channels may be used later to circulate the solutions selected for crystal derivatization.

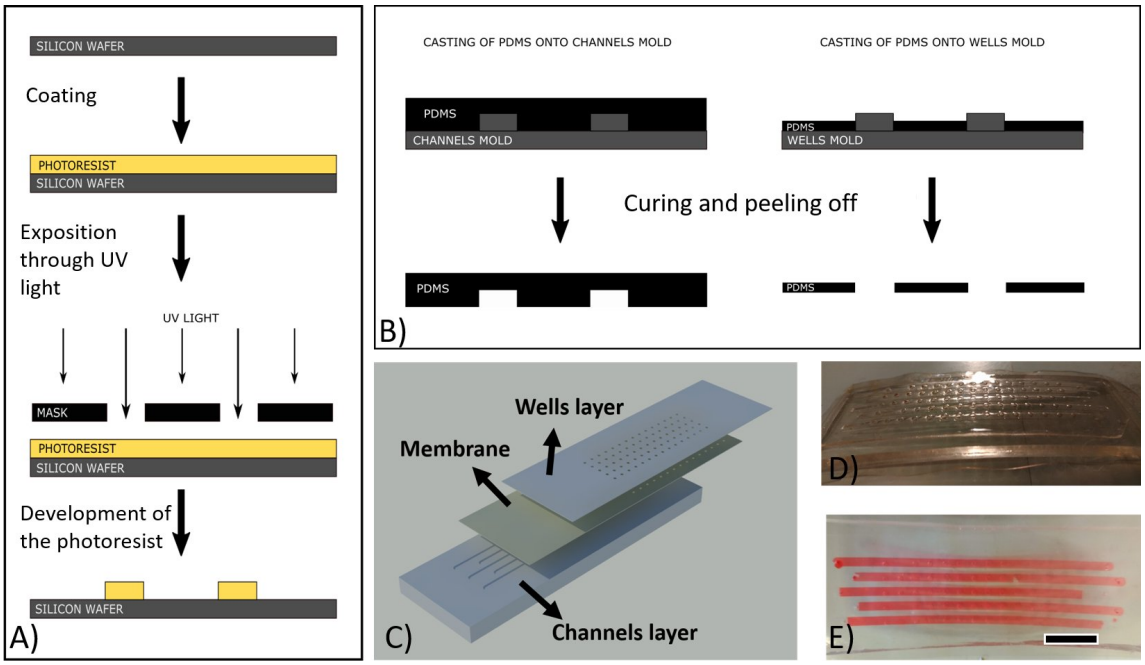

Figure 5.1: A) Photolithography process: Coating of the SIlicon Wafer with the photoresist; exposition to UV light through the designed mask; development of the photoresist and attainment of the final mold. The molds produced by photolithography were used for PDMS Casting: B). C) AutoCAD rendering of the microdevice; D) and E) pictures of the fabricated device. The scale bar in figure E) corresponds to 1 cm.

An AutoCAD (Autodesk, San Rafael, USA) rendering of the three layers of the device is shown in Figure 5.1 C; photos of the fabricated device are shown in Figure 5.1 D and 5.1 E. A Nafion® membrane was sandwiched between the channel and the well layers. Nafion® is a material with a high degree of swelling. Therefore the bonding with PDMS was quite challenging. Several attempts are described in the literature [26–29] but, eventually, the only protocol available for a commercial membrane, developed by Pham et al., was optimized and used in this work [30]. Briefly, the Nafion® membrane was cleaned in 3 % H_2O_2 at 80 °C for 1 hour, H2O at 80 °C for 1 hour, 1 M H_2SO_4 at 80 °C for 1 hour and H_2O at 80 °C for 1 hour. The membrane was dried at 80 °C for 24 hours and then treated for 15 minutes at 150 °C in order to reduce the swelling behavior; indeed, according

to the literature [31], the thermal treatment determines a change of the internal structure of the polymer from amorphous to crystalline, leading to a lower water uptake. The PDMS was treated with oxygen plasma for 60 seconds, in order to form hydroxide groups, then immersed in 4 % triethoxyvinylsilane (VTES), purchased from Sigma-Aldrich, in 90 % Ethanol for 2 minutes and baked at 100 °C for 15 minutes to allow the grafting to occur. The washed and thermally treated Nafion® was modified with a corona discharge (BD-20AC Laboratory Corona Treater) for 10 minutes in order to generate hydroperoxide groups (attempts were made with plasma oxygen equipment; however the strong vacuum determined a severe shrinkage of the membrane that turned to be too wavy to create a good contact with the PDMS). After the surface modification, Nafion® was contacted with the grafted PDMS and baked at 100 °C for 2 hours to let the heat promote the formation of radical groups on the membrane which would attach to the vinyl group in PDMS-VTES and form the bonding.

5.3.3 Crystallization experiments

Crystallization experiments were performed in order to confirm the ability of the device to produce the crystals. A Hen Egg White Lysozyme (HEWL) solution at a concentration of 50 mg/ml in 0.1 M CH_3COONa at pH 4.6 was mixed with 3.5 % NaCl dissolved in 0.1 M CH_3COONa at pH 4.6 in order to have a starting crystallization solution composed of 25 mg/mL HEWL, 1.75 % NaCl and 0.1 M CH_3COONa at pH 4.6. For the crystallization experiments, firstly, the channels of the device were filled with the stripping solution (3.5 % NaCl dissolved in 0.1 M CH_3COONa at pH 4.6) using a syringe pump and later, the wells were filled with the protein solution using a micropipette. Three different volumes of solution were used (500 μL, 1 μL, and 2 μL) for the same membrane area, in order to impose different water removal rates. Each condition was repeated at least 9 times for reproducibility testing. Finally, the chip was placed in a sealed box to prevent evaporation, in a room with controlled temperature (20 °C).

5.3.4 Modelling of water, sodium chloride and mercury acetate transport through the Nafion® membrane.

In this device, the role of the Nafion® membrane is first to generate super-saturation inside the protein solution leading to nucleation, and later for derivatization. Nafion® is a cation-exchange membrane with a polytetrafluoroethylene (PTFE) backbone with negatively fixed charged groups attached. Two types of transport characterize this type of membrane:

1. Water transport: when a difference in water activity is generated across the membrane, water diffuses by osmosis, towards the compartment with the highest solute concentration, until equilibrium is reached;

2. Selective transport of cations due to the negatively charged groups: when different cationic species are present on the two sides of the membrane, over time they will tend to equilibrate.

The water transport has been exploited in this work to remove water from the protein solution and achieve supersaturation to facilitate nucleation. The transport of water in the microdevice has been generated by filling the channels with a stripping solution with a lower water activity compared to the protein solution placed in the wells (more details are reported in the 'Crystallization experiments' section). In order to understand the transport of water and NaCl that promotes the crystallization process, a diffusion cell was set-up to mimic the conditions of the crystallization environment in the micro-device and measurements were performed in order to calculate the water and NaCl mass transfer coefficients across the membrane. The diffusion cell, a sandwiched Nafion® membrane between two compartments, is shown in Figure 5.2a. Compartment A was filled with distilled water, and compartment B was filled with 0.55 M NaCl in order to create a driving force. Two graduated pipettes were connected to the extremities of the cell to record changes in volume as a function of time. In this case, even though the membrane is selective for cations, due to the high difference in osmotic pressure a small amount of NaCl can cross the membrane. Therefore, the permeability

of the NaCl was measured by detecting changes in conductivity from the two sides of the membrane represented in Figure 5.2a. The selective transport of

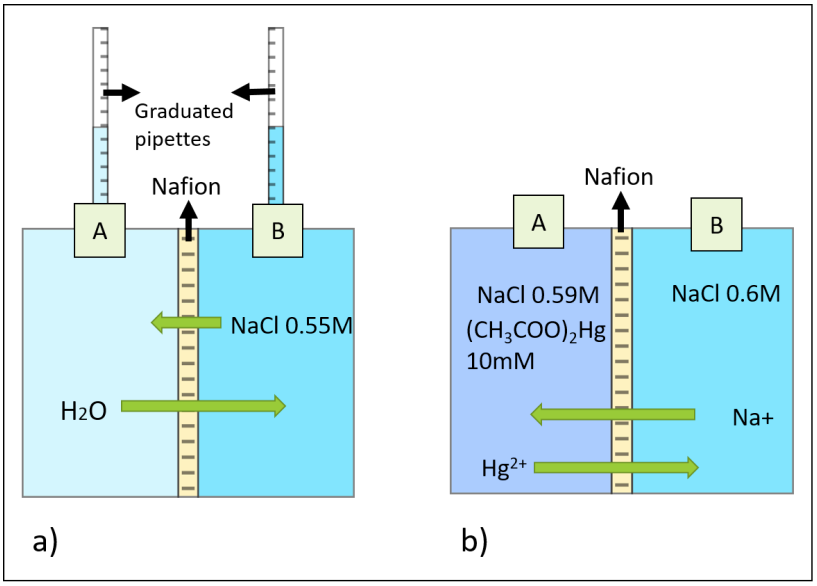

Figure 5.2: Diffusion cell used to measure water and NaCl mass transfer coefficients in Nafion®; b) Diffusion cell used to measure Hg^2+ mass transfer coefficient in Nafion®

cations promoted by the membrane might instead be exploited for promoting a controlled diffusion of ions to/from the protein crystals solution and perform gentle derivatization. Protein crystals derivatization is normally performed after the crystals are formed in order to maintain the isomorphism [12]. Hence, when derivatization is performed, the protein crystal solution composition is already equilibrated with the stripping solution because they have the same osmotic pressure. Therefore, in order to investigate the transport of cations for derivatization in the microdevice a second diffusion cell (shown in Figure 5.2b) was set-up in which conditions for derivatization were simulated. The diffusion cell was used to calculate the mass transfer coefficient of Hg^{2+} (a cation commonly used for the derivatization of protein crystals) across the membrane. Two solutions with the same osmotic pressure were used. Compartment A was filled with a solution containing 0.59 M NaCl and 0.01 M $(CH_3COO)_2Hg$. Compartment B was filled with a solution of 0.6 M NaCl. In this case, Na^+ and Hg^{2+} will exchange until they reach equilibrium. Samples were taken over time, and the concentration of Hg^{2+} was measured by ICPAES (Inductively Coupled PlasmaAtomic Emission

Spectrometer, Horiba Jobin-Yvon, France).

5.3.5 X-ray diffraction analysis

HEWL crystals were equilibrated for a few seconds, first in harvesting buffer (0.1 M CH_3COONa, pH 4.6, and 1 M NaCl) and then in cryo-protectant solution (harvesting buffer with 30 % (v/v) glycerol from Sigma-Aldrich). X-ray diffraction analysis, to evaluate diffraction quality was performed using an in-house X-ray diffractometer (IμS 3.0 microfocus D8 Venture from Bruker, with CuKα radiation), coupled to a CMOS Photon 100 detector, at 110 K. Indexing, integration and scaling were done using PROTEUM3 software pipeline (Bruker AXS 2015). Scaled and merged intensities were converted to amplitudes using program COMBAT from the CCP4i suite [32]. Phases were calculated using Expert MR-PHASER from CCP4ii suite. The pdb model from the pdb database used for phase calculation was the 3a8z. Model building and refinement were done, iteratively, using COOT [33] and REFMAC5 [34]. A final model was built using BUCCANEER [35] and viewed in CCP4mg [36] . Program MOLPROBITY [37] was used for the validation of the final model.

5.4 Results and Discussion

5.4.1 Estimation of water and sodium permeation across Nafion® membrane

Water mass transfer coefficient was used to estimate the variation of concentration of salt and protein in the protein solution due to osmosis. The mass transfer coefficient of Hg^{2+} was used to estimate the Hg^{2+} concentration profile over time in the protein crystals solution during the derivatization process. When a cation-exchange membrane (as Nafion®) contacts a pure water solution in one side and a salt solution on the other side, water will move from the water compartment to the salt solution compartment and a small amount of salt (salt leakage) may move to the water compartment, until the osmotic pressure is equilibrated. Therefore,

in the water compartment, it is possible to detect an increasing concentration of NaCl as a function of time, due to both the increase of NaCl transport and a reduction of the amount of water. The reduction of water content was measured as a decrease of volume over time (Figure 5.3) in compartment A of the diffusion cell (represented in Figure 5.2a); meanwhile, the intake of NaCl was detected measuring the solution's conductivity. At the beginning of the osmosis process, the volume decreases linearly with time, and the amount of salt crossing the membrane is negligible. Therefore, the volumetric flow rate of water across the membrane (Q_w) corresponds to the slope of the line in Figure 5.3.

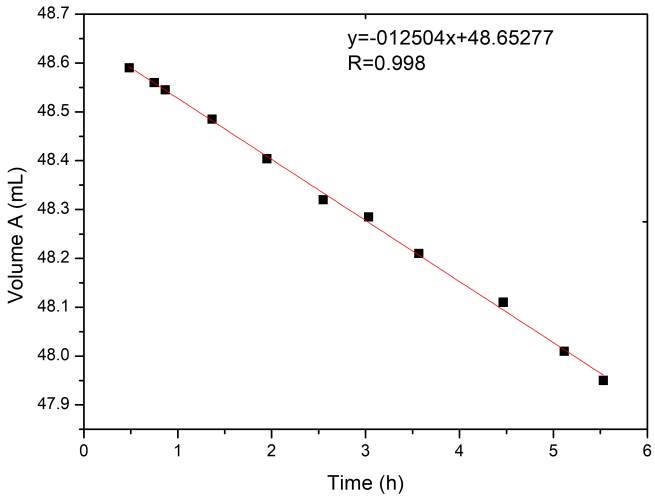

Figure 5.3: Volume of water over time in compartment A of the diffusion cell in Figure 5.2a).

From Q_w, considering the values of density (d), molecular weight (M_w) of water and the membrane area (A) (7.54 cm^2), it is possible to calculate the molar flux of water J_w as follows:

$$J_w = \frac{Q_w d}{A M_w} \tag{5.1}$$

From J_w the mass transfer coefficient K_w was calculated as follows:

$$J_w = \frac{K_w(\Delta p - \Delta \pi)}{l} \tag{5.2}$$

$$K_w = \frac{J_w l}{\Delta p - \Delta \pi} \tag{5.3}$$

Where Δp is the hydrostatic pressure difference, $\Delta\pi$ is the osmotic pressure difference, l is the membrane thickness. In Figure 5.4 the change of NaCl concentration over time is displayed.

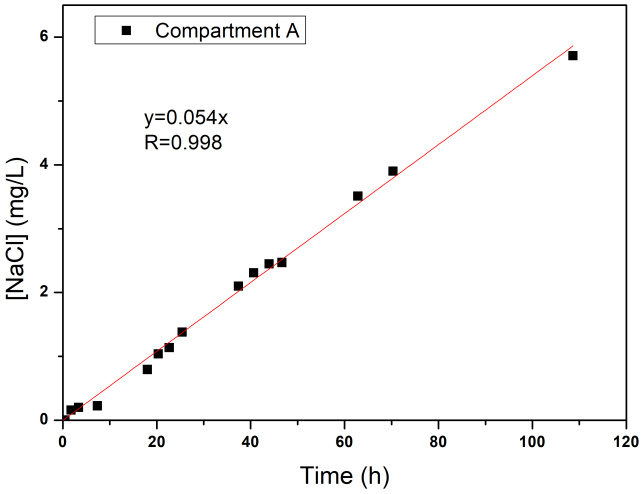

Figure 5.4: Apparent concentration of NaCl in Compartment A of the cell in figure 5.2a)

The change of concentration is due to both, increased concentration of NaCl in compartment A and decreased water volume due to its transport to compartment B. Therefore, the transport rate calculated by fitting this curve can be considered as an apparent transport of NaCl. In order to know the real amount of NaCl in compartment A, the concentration of NaCl over time was multiplied by the volume in compartment A at that time and divided by the molecular weight of NaCl. Results from this calculation are reported in Figure 5.5.

From Figure 5.5, by dividing the slope of the curve by the area of the membrane (A), the molar flux of NaCl (J_{NaCl}) was calculated (eq. 5.4).

$$J_{NaCl} = \frac{mol_{NaCl}}{tA} \tag{5.4}$$

The J_{NaCl} can be also defined as:

$$J_{NaCl} = K_{NaCl}\Delta C \tag{5.5}$$

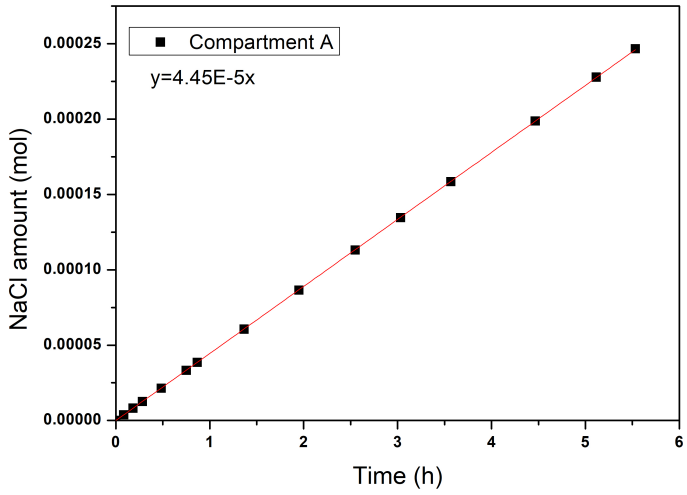

Figure 5.5: Real amount of NaCl in compartment A of the cell over time

Where K_{NaCl} is the mass transfer coefficient and ΔC is the NaCl concentration difference between the two sides of the membrane (0.55 M). Hence, K_{NaCl} was calculated as:

$$K_{NaCl} = \frac{J_{NaCl}}{\Delta C} \tag{5.6}$$

The mass transfer coefficients calculated for water and NaCl are represented in Table 1. In order to calculate the mass transfer coefficient for Hg^2+, the concentration of Hg^2+ over time was measured in the cell shown in Figure 5.2b. In this case, the osmotic pressure on the two sides at the beginning of the experiment is the same. However, the charge difference between Hg^2+ and Na^+ leads to the exchange of $2Na^+$ for each Hg^2+, changing the osmotic equilibrium between the two solutions. In order to reinstate the osmotic equilibrium, some water might cross the membrane. However, since the amount of Hg^2+ used here is very low (10 mM) compared to the concentration that is responsible for the total osmotic pressure (0.7 M) on both sides of the membrane the water transport has been considered negligible, and the volume of the solutions on the two sides of the membrane was considered constant (confirmed experimentally). Keeping this into account, the molar flux (J_{Hg}) was calculated by dividing the slope of the curve in Figure 5.6 by

the area of the membrane (A) and multiplying by the Volume (V) (eq.5.7):

$$J_{Hg} = \frac{mol_{Hg}}{tA} \tag{5.7}$$

J_{Hg} can be also defined as:

$$J_{Hg} = K_{Hg}\Delta C \tag{5.8}$$

Where K_{Hg} is the mass transfer coefficient and ΔC is the Hg^{2+} concentration difference between the two sides of the membrane (10 mM). Hence, K_{Hg} was calculated as:

$$K_{Hg} = \frac{J_{Hg}}{\Delta C} \tag{5.9}$$

The mass transfer coefficients of water, NaCl and Hg^{2+} through the Nafion® membrane are compared in Table 1. According to this data, the mass transfer coefficient of water is 2 orders of magnitude higher than the one for Na^{+}. This implies that water transport is the event that is controlling the attaining of supersaturation in the protein solution. Instead, the low mass transfer coefficient of Hg^{2+} indicates a slow diffusion of this cation through the membrane, which is an excellent characteristic regarding the need to promote a gentle derivatization process.

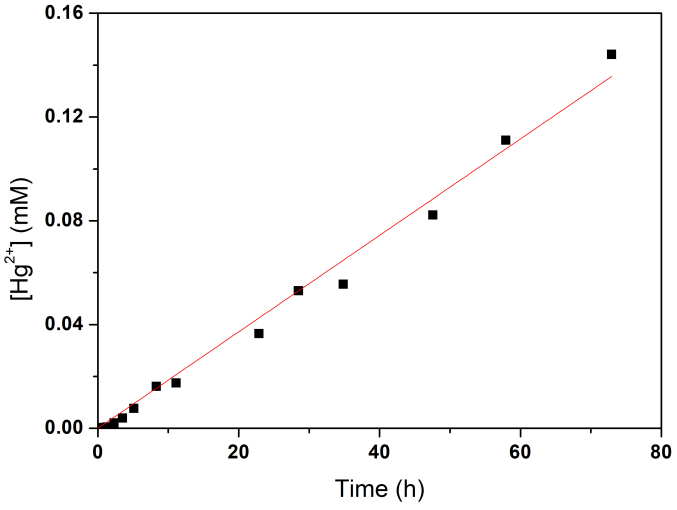

Figure 5.6: Hg^{2+} concentration over time in compartment A of the diffusion cell

Table 5.1: Mass transfer coefficient for water, NaCl, and Hg^2+

Substance	**Mass Transfer Coefficient** (m/s)
water	$4.1*10^{-6}$
NaCl	$2.7*10^{-8}$
Hg^{2+}	$1.9*10^{-9}$

5.4.2 Experimental simulation of transport in the microdevice

Crystallization experiments in the microdevice were performed using a widely investigated protein: Hen Egg White Lysozyme (HEWL). Crystallization conditions for HEWL are well known using the phase diagram of the protein [35]. The phase diagram of HEWL combined with simulations of the evolution of the salt concentration in the micro-device were used to predict when conditions for nucleation were reached. The evolution of the initial protein solution composition (25 mg/mL protein concentration and 1.75% NaCl concentration) to the final concentration equilibrated with the stripping solution (50mg/mL protein concentration and 3.5% NaCl) was overlaid to the phase diagram in Figure 5.7. It is possible to notice that when the salt concentration is about 2.9%, the solution is supersaturated at a level where nucleation is likely to occur. From the information of the measured water mass transfer coefficient and by knowing the geometry of the device it was possible to simulate the NaCl concentration in the protein well over time, when a stripping solution of 3.5% NaCl was used in the channels to promote osmosis. Results of the simulation are reported in Figure 5.8 .

The experimental simulation was run for three different volumes (V_1=0.5μL, V_2=1μL, V_3=2μL) of solution for the same area (A_{wells} = 7.85cm^2) of transport, hence, obtaining different kinetics. The time at which nucleation may start was highlighted and for the 3 different volumes the nucleation condition is reached in a short fraction of an hour, meaning that the kinetics is very fast.

In order to investigate the impact of Hg^{2+} on the crystals, a simulation was run for calculating the increase of Hg^{2+} in the wells (Figure 5.9). The protein solution deposited in the wells in the beginning of the experiments has a NaCl

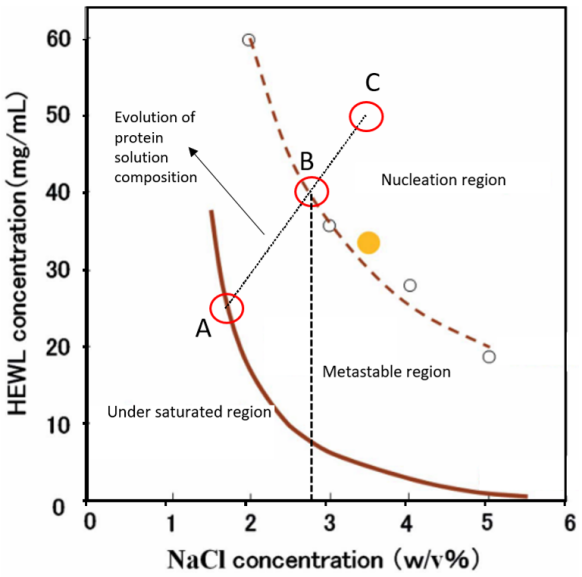

Figure 5.7: Solubility diagram of Lysozyme extracted from [35]. A) corresponds to the composition of the crystallizing solution in the beginning of the experiment (25mg/mL HEWL and 1.75% NaCl); B) corresponds to the composition of the crystallizing solution when crossing the boundary for nucleation to occur (41 mg/mL HEWL , 2.9% NaCl); C) corresponds to the equilibrium point with the stripping solution (50 mg/mL HEWL, %3.5 NaCl).

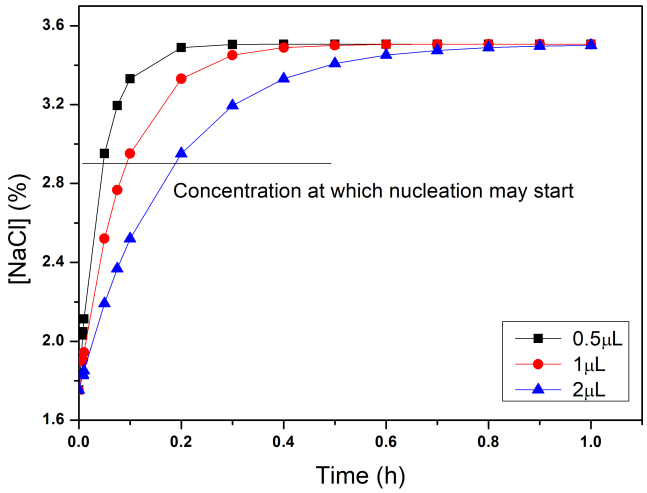

Figure 5.8: NaCl concentration in the wells of the micro-device over time for different volumes of protein solution

concentration of 1.75%. Instead, the solution used as stripping in the channels has a NaCl concentration of 3.5%.

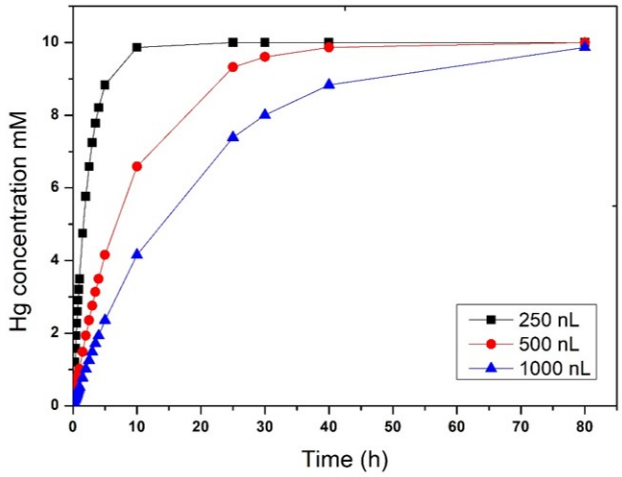

Figure 5.9: Evolution of Hg^{2+} concentration in the protein solution

Taking into consideration that the buffer type, concentration and pH (0.1M $NaCH_3COO$ at pH 4.6) are the same for both solutions and that the contribution of the protein molecules to the osmotic pressure is negligible, the protein solution presents an osmotic pressure that is half of the stripping solution. The channels volume (33 μL) is significantly higher than the volume of solution placed in the wells (0.5-2 μL). Therefore, during the osmosis process, the change of concentration in the channels will be minimal and the solution in the well will tend to equal the concentration in the channel. Since equilibrium will be reached mainly by water transport, the volume at equilibrium in the wells will be half of the initial volume. The derivatization with Hg^{2+} would be performed only when crystallization is completed (in order to keep isomorphism [17]). For this reason, the volumes used for the calculation of the increase of Hg^{2+} concentration in the wells are the half of initial volumes placed. In this case the maximum cation concentration is reached in about 20 hours for 250 nL, 40 hours for 500 nL and about 80 hours for 1μL of solution. These long diffusion times will allow a gentle transport of the derivatization ions reducing the risk of crystal cracking and damage during the process. Furthermore, the different kinetics between different volumes might be useful for controlling the stability of the crystals and the efficiency of derivatization.

5.4.3 Crystallization results

The first crystallization experiments performed in the microdevice were used to test the stability of the crystals. When crystallization experiments are performed directly after the bonding of the PDMS parts with Nafion®, crystals form after short time (2 hours), in accordance with the simulations in Figure 5.8, however they quickly degrade until they completely disappear (Figure 5.10). The osmotic pressure difference across the membrane determined water removal and consequently nucleation. However, since the membrane is used in its acidic form, it

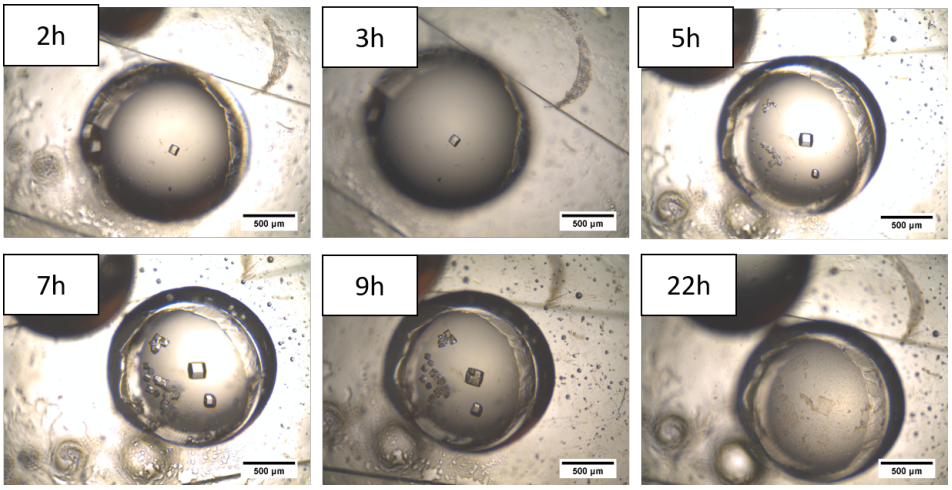

Figure 5.10: Crystals degradation in the microdevice due to acidic pH of the membrane

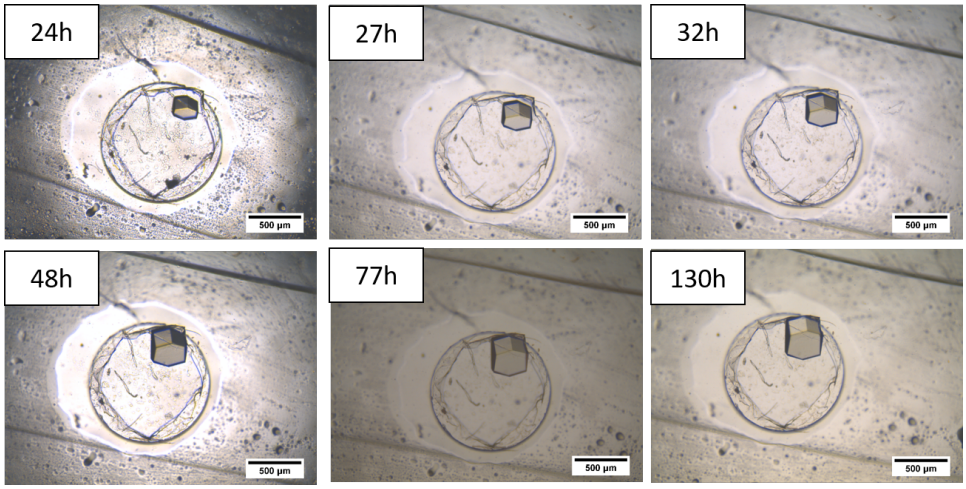

Figure 5.11: Crystallization experiments after the microdevice was soaked in 2M NaCl

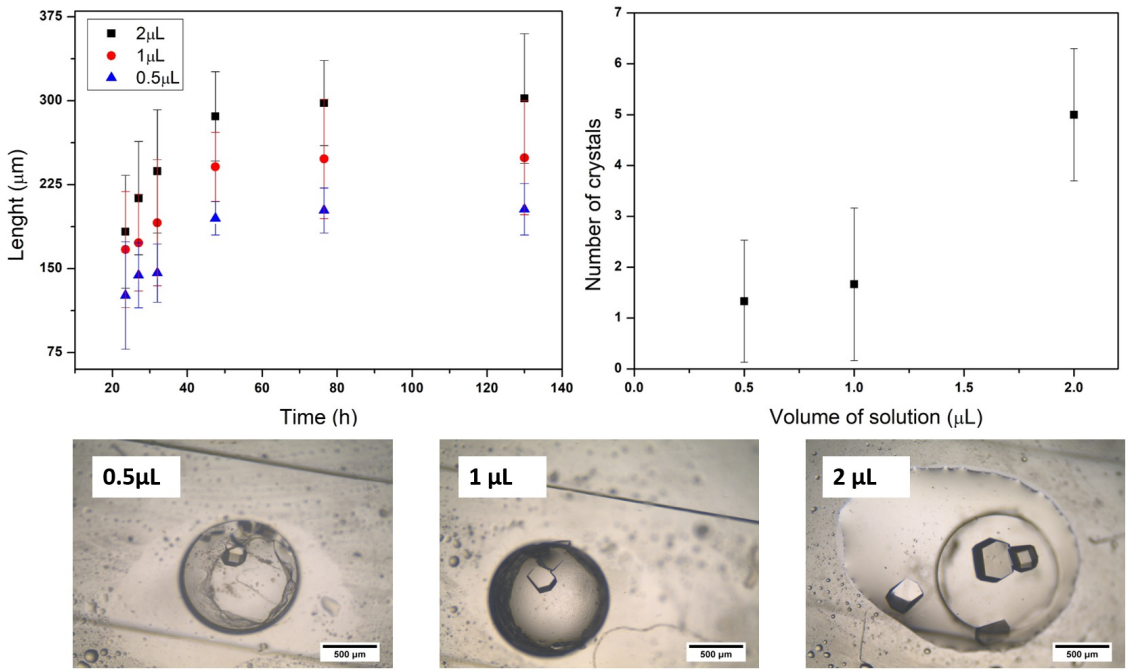

Figure 5.12: Crystal growth kinetics (top left), and number of crystals per volume of solution (top right). On the bottom: crystals grown in different volumes of solution, observed after 130 hours

exchanges protons with the cations in the protein solution, gradually lowering the pH to an extreme condition unbearable for the crystals, which consequently will degrade. In order to avoid this inconvenience, after PDMS-Nafion® bonding (the bonding was not successful if a Na-membrane was used) the microdevice was soaked in a solution of 2M NaCl in order to exchange the H^+ ions previously taken up and convert the membrane to the Na-Nafion® form. The pH of the solution was monitored over time and the NaCl solution replaced until the pH stayed neutral and constant. Crystallization experiments were repeated in the micro-device after soaking in NaCl. Pictures of the crystals are shown in Figure 5.11. In this case it is possible to notice that crystals continue growing for several days and do not show any sign of degradation. This makes clear that, in order to use a Nafion® membrane as a support for protein crystallization, it is essential to exchange the proton of Nafion® with a cation, in order to avoid pH-driven degradation. Reproducibility tests were performed for different volumes of solution. Each condition was repeated 9 times. Figure 5.12 displays the results related to the lenght and the number of crystals obtained, using different volumes for the

same membrane contact area. Even though the final equilibrium condition is supposedly the same, the number and size of crystals increases with the volume of solution used. This may be attributed to the higher amount of protein available for nucleation and crystal growth. Instead, no differences were found in the time required for the first crystals to appear. This behaviour is probably due to the low time shift for reaching nucleation conditions between the different volumes. In general, it is possible to conclude that the designed micro-device allows to control crystal number and size, by changing the volume of solution used. The crystals obtained show to be extremely stable over a long time.

5.4.4 X-ray diffraction analysis

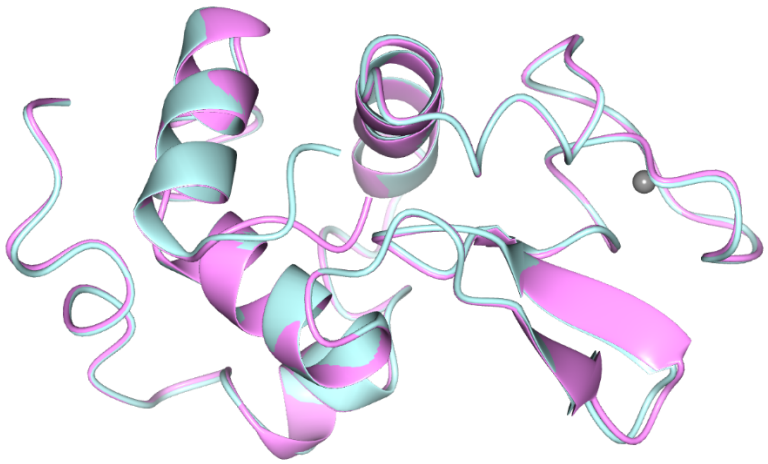

Figure 5.13: Ribbon representation of HEWL. The model obtained by molecular replacement using the in-house collected data (pink) is superposed on the known structure of HEWL (light blue) (PDB code: 3a8z). The superposition of the pdb model and the calculated structure generate and rmsd of 0.22 Å for 126 α carbon atoms. The picture was produced by using the program CCP4mg.

In order to assess the diffraction quality of the crystals grown on the Nafion® membrane in the micro-device, a diffraction analysis was performed using a in-house diffractometer at a wavelength of 1.5418 Å. Data collection, processing and phasing are reported in Table 5.2. The crystals diffracted to a maximum resolution of 1.6 Å. The collected, indexed and integrated data were scaled and

Table 5.2: Statistics of X-ray diffraction data collection and automated model building and refinement (values for the last resolution shell are in parenthesis)

X-ray diffraction	
space group	P $4_3 2_1 2$
wavelength (Å)	1.5418
resolution range (Å)	21.50-1.60 (1.63-1.60)
unit cell parameters (Å) a, b, c	77.5, 77.5, 37.2
total reflections	26912 (1142)
unique reflections	15197 (706)
multiplicity	1.8 (1.6)
completeness (%)	98.0 (93.5)
mean I / σ (I)	8.7 (4.4)
Wilson B factor	1.77
R_{merge}	0.068 (0.337)
R_{meas}	0.097 (0.447)
R_{pim}	0.068 (0.337)
CC1/2	0.988 (0.78)
Refinement	
R_{work}/R_{free}	0.238/0.266
N of non-hydrogen atoms	1121
macromolecules atoms	1007
N of protein residues	129
ligands atoms	23
water molecules	91
RMSD (bonds) (Å)	0.0092
RMSD (angles) (deg)	1.629
Ramachandran favoured (%)	98.43
Ramachandran allowed (%)	1.56
Ramachandran outliers (%)	0.00
rotamers outliers (%)	0.01
all-atom clashscore	9
Molprobity score	1.48
Average B-factor molecules	9.4
Average B-factor macromolecules	8.7
Average B-factor ligands	23.3
Average B-factor waters	12.9

merged using the software pipeline in PROTEUM3 (Bruker AXS 2015). The analysed crystals belongs to space group $P4_32_12$. The diffraction data of the crystals are characterized by a low R_{merge} value, high signal-to-noise ratio. Multiplicity is 98%. The electron density map was generated after structure solution by molecular replacement (MR) using 3a8z as a reference structure. The R_{work}/R_{free} ratio after refinement was lowered to 0.238/0.266. According to Ramachandran statistics analysis the 98.4% of the residues were found in favoured regions, 1.6% were found in allowed regions, no outlier residues were found. A ribbon representation of the HEWL molecule is displayed in Figure 5.13. Summarizing, all the parameters evaluated in Table 5.2 and described in this section are indicators of high diffraction quality. Additionally, for situations where the crystals obtained diffract poorly or for completely unknown structures, derivatization of the crystals might be performed using the same microdevice. In these cases, the derivatization process can be controlled by the selective diffusion of ions across the membrane, avoiding abrupt changes of the local environment and handling of the crystals [19].

5.5 Conclusions

Trial and error is still the leading strategy for finding conditions for protein crystallization and for crystals derivatization. Microfluidics technology provides advantages to the crystallization field with several designs that allow a lower consumption of reagents for a higher number of trials. Also, membrane technology concurred to the control of supersaturation and ligand diffusion helps to obtain a high diffraction quality of the crystals. In this work, a Nafion® membrane was integrated with a PDMS microdevice for protein crystallization. Functionality of the device was tested for the crystallization of HEWL. Stability tests showed that Nafion® should be used in the salt form in order to avoid exchange of H^+ with the protein solution that lowers the pH to extreme conditions with consequent degradation of the crystals. Furthermore, size and number of crystals were tuned by changing the volume of solution in the microdevice wells. Finally, the crystals

grown in the micro-device were picked up and analyzed by X-rays showing a high diffraction quality. The presence of the 75 wells might allow a parallel screening of 75 different conditions were it is possible to play with concentration and volume of solution, furthermore the presence of the ion-exchange transport mediated by Nafion® membrane may be exploited for performing an in-situ gentle derivatization, avoiding abrupt changes of the local environment and handling of the crystals [19].

References

[1] J. A. Gavira. "Current trends in protein crystallization." In: *Archives of Biochemistry and Biophysics* 602 (2016), pp. 3–11. DOI: 10.1016/j.abb.2015.12.010.

[2] L. Li and R. F. Ismagilov. "Protein Crystallization Using Microfluidic Technologies Based on Valves, Droplets, and SlipChip." In: *Annu. Rev. Biophys* 39 (2010), pp. 139–58. DOI: 10.1146/annurev.biophys.050708.133630.

[3] B. G. Abdallah, S. Roy-Chowdhury, R. Fromme, P. Fromme, and A. Ros. "Protein Crystallization in an Actuated Microfluidic Nanowell Device." In: *Crystal Growth and Design* 16.4 (2016), pp. 2074–2082. DOI: 10.1021/acs.cgd.5b01748.

[4] W. Du, L. Li, K. P. Nichols, and R. F. Ismagilov. "SlipChip." In: *Lab on a Chip* 9.16 (2009), p. 2286. DOI: 10.1039/b908978k.

[5] L. Wang, K. Sun, X. Hu, G. Li, Q. Jin, and J. Zhao. "A centrifugal microfluidic device for screening protein crystallization conditions by vapor diffusion." In: *Sensors and Actuators B: Chemical* 219 (2015), pp. 105–111. DOI: 10.1016/J.SNB.2015.04.105.

[6] Y. Yu, X. Wang, D. Oberthür, A. Meyer, M. Perbandt, L. Duan, and Q. Kang. "Design and application of a microfluidic device for protein crystallization using an evaporation-based crystallization technique." In: *Journal of Applied Crystallography* 45.1 (2012), pp. 53–60. DOI: 10.1107/S0021889811048047.

[7] E. Curcio, A. Criscuoli, and E. Drioli. "Membrane crystallizers." In: *Industrial and Engineering Chemistry Research* 40.12 (2001), pp. 2679–2684. DOI: 10.1021/ie000906d.

[8] G. D. Di Profio, E. Curcio, A. Cassetta, D. Lamba, and E. Drioli. "Membrane crystallization of lysozyme: Kinetic aspects." In: *Journal of Crystal Growth* 257.3-4 (2003), pp. 359–369. DOI: 10.1016/S0022-0248(03)01462-3.

[9] G. Di Profio, E. Curcio, and E. Drioli. "Trypsin crystallization by membrane-based techniques." In: *Journal of Structural Biology* 150.1 (2005), pp. 41–49. DOI: 10.1016/j.jsb.2004.12.006.

[10] S. Simone, E. Curcio, G. Di, M. Ferraroni, and E. Drioli. "Polymeric hydrophobic membranes as a tool to control polymorphism and protein – ligand interactions." In: *Jornal of Membrane Science* 283 (2006), pp. 123–132. DOI: 10.1016/j.memsci.2006.06.028.

[11] G. D. Profio, M. Polino, F. P. Nicoletta, B. D. Belviso, R. Caliandro, E. Fontananova, G. De Filpo, E. Curcio, and E. Drioli. "Tailored hydrogel membranes for efficient protein crystallization." In: *Advanced Functional Materials* 24.11 (2014), pp. 1582–1590. DOI: 10.1002/adfm.201302240.

[12] A. C. W. Pike, E. F. Garman, T. Krojer, F. von Delft, and E. P. Carpenter. "An overview of heavy-atom derivatization of protein crystals." In: *Acta crystallographica. Section D, Structural biology* 72.Pt 3 (2016), pp. 303–318. DOI: 10.1107/S2059798316000401.

[13] G. L. Taylor. "Introduction to phasing." In: *Acta Crystallographica Section D: Biological Crystallography* 66.4 (2010), pp. 325–338. DOI: 10.1107/S0907444910006694.

[14] M. Dauter and Z. Dauter. "Phase determination using halide ions." In: *Methods in molecular biology (Clifton, N.J.)* 364.9 (2007), pp. 149–158. DOI: 10.1385/1-59745-266-1:149.

[15] J. P. Morth, T. L. M. Sørensen, and P. Nissen. "Membrane's eleven: Heavy-atom derivatives of membrane-protein crystals." In: *Acta Crystallographica*

Section D: Biological Crystallography 62.8 (2006), pp. 877–882. DOI: 10.1107/S0907444906023547.

[16] C. Giacovazzo, M. Ladisa, and D. Siliqi. "The approach of the joint probability distribution functions: the SIR-MIR, SAD-MAD and SIRAS-MIRAS, cases." In: *Zeitschrift für Kristallographie - Crystalline Materials* 217.12 (2002), pp. 703–709. DOI: 10.1524/zkri.217.12.703.20660.

[17] M. G. Joyce, S. Radaev, and P. D. Sun. "A rational approach to heavy-atom derivative screening." In: *Acta Crystallographica Section D: Biological Crystallography* 66.4 (2010), pp. 358–365. DOI: 10.1107/S0907444909053074.

[18] J. Agniswamy, M. G. Joyce, C. H. Hammer, and P. D. Sun. "Towards a rational approach for heavy-atom derivative screening in protein crystallography." In: *Acta Crystallographica Section D: Biological Crystallography* 64.4 (2008), pp. 354–367. DOI: 10.1107/S0907444907068849.

[19] M. Polino, A. Luísa Carvalho, L. Juknaite, C. A. M Portugal, I. M. Coelhoso, M. J. Romao, and J. G. Crespo. "Ion-Exchange Membranes for Stable Derivatization of Protein Crystals." In: *Crystal Growth & Design* 17 (2017), pp. 4563–4572. DOI: 10.1021/acs.cgd.7b00315.

[20] T. Xu. "Ion exchange membranes: State of their development and perspective." In: *Journal of Membrane Science* 263.1-2 (2005), pp. 1–29. DOI: 10.1016/j.memsci.2005.05.002.

[21] "Multivariate statistically-based modelling of a membrane bioreactor for wastewater treatment using 2D fluorescence monitoring data." In: *Water Research* 46.11 (2012), pp. 3623–3636. DOI: 10.1016/j.watres.2012.04.010.

[22] D. Qin, Y. Xia, and G. M. Whitesides. "Soft lithography for micro- and nanoscale patterning." In: *Nature Protocols* 5.3 (2010), pp. 491–502. DOI: 10.1038/nprot.2009.234.

[23] F. Yan, A. Ding, M. Gironès, R. G. Lammertink, M. Wessling, L. Börger, K. Vilsmeier, and W. A. Goedel. "Hierarchically structured assembly of polymer microsieves, made by a combination of phase separation micromolding

and float-casting." In: *Advanced Materials* 24.12 (2012), pp. 1551–1557. DOI: 10.1002/adma.201104642.

[24] Y. Xia and G. M. Whitesides. "Soft-lithography." In: *Angewandte Chemie International Edition* 37.0 (1998), pp. 550–575. DOI: 10.1039/c1lc20189a.

[25] A. Pimpin and W. Srituravanich. "Review on Micro- and Nanolithography Techniques and their Applications." In: *Engineering Journal* 16.1 (2012), pp. 37–55. DOI: 10.4186/ej.2012.16.1.37.

[26] D.-T. Phan, C. Yang, and N.-T. Nguyen. "A sugar-template manufacturing method for microsystem ion-exchange membranes Characterization of C-PDMS electrodes for electrokinetic applications in microfluidic systems A-L Deman, M Brun, M Quatresous et al. - Fabrication of nanoporous junctions using o." In: *Journal of Micromechanics and Microengineering* 27 (2017), pp. 1–9.

[27] P. K. Yuen, H. Su, V. N. Goral, and K. A. Fink. "Three-dimensional interconnected microporous poly(dimethylsiloxane) microfluidic devices." In: 11 (2011), pp. 1541–1544. DOI: 10.1039/c01c00660b.

[28] D.-T. Phan, C. Yang, and N.-T. Nguyen. "Fabrication of nanoporous junctions using off-the- shelf Nafion membrane." In: *Journal of Micromechanics and Microengineering* 25 (2015), pp. 1–7. DOI: 10.1088/0960-1317/25/11/115019.

[29] Z. Slouka, S. Senapati, and H.-C. Chang. "Microfluidic Systems with Ion-Selective Membranes." In: 7 (2014), pp. 317–355. DOI: 10.1146/annurev-anchem-071213-020155.

[30] M. H. Pham and D. P. Barz. "Bonding Nafion® with polydimethysiloxane: A versatile approach towards ion-exchange membrane microfluidic devices." In: *Journal of Membrane Science* 537.May (2017), pp. 310–314. DOI: 10.1016/j.memsci.2017.05.020.

[31] H.-y. Jung and J. Won. "Role of the glass transition temperature of Nafion 117 membrane in the preparation of the membrane electrode assembly in a direct methanol fuel cell (DMFC)." In: *International Journal of Hydrogen*

Energy 37.17 (2012), pp. 12580–12585. DOI: 10.1016/j.ijhydene.2012.05.121.

[32] P. R. Evans, H. T. Jenkins, R. Keegan, E. Krissinel, K. Stevenson, A. Lebedev, S. J. Mcnicholas, R. A. Nicholls, M. Noble, N. S. Pannu, C. Roth, G. Sheldrick, and P. Skubak. "CCP 4 i 2 : the new graphical user interface to the CCP 4 program suite research papers." In: *acta crystallographica section D: Structural biology* (2018), pp. 68–84. DOI: 10.1107/S2059798317016035.

[33] P. Emsley and K. Cowtan. "Coot : model-building tools for molecular graphics research papers." In: *Acta Crystallographica Section D: Biological Crystallography* D60 (2004), pp. 2126–2132. DOI: 10.1107/S0907444904019158.

[34] G. N. Murshudov, P. Skubák, A. A. Lebedev, N. S. Pannu, R. A. Steiner, R. A. Nicholls, M. D. Winn, F. Long, and A. A. Vagin. "REFMAC5 for the refinement of macromolecular crystal structures." In: *Acta Crystallographica Section D: Biological Crystallography* 67.4 (2011), pp. 355–367. DOI: 10.1107/S0907444911001314.

[35] K. Cowtan. "The Buccaneer software for automated model building. 1. Tracing protein chains." In: *Acta Crystallographica Section D: Biological Crystallography* 62.9 (2006), pp. 1002–1011. DOI: 10.1107/S0907444906022116.

[36] S. McNicholas, E. Potterton, K. S. Wilson, and M. E. Noble. "Presenting your structures: The CCP4mg molecular-graphics software." In: *Acta Crystallographica Section D: Biological Crystallography* 67.4 (2011), pp. 386–394. DOI: 10.1107/S0907444911007281.

[37] V. B. Chen, W. B. Arendall, J. J. Headd, D. A. Keedy, R. M. Immormino, G. J. Kapral, L. W. Murray, J. S. Richardson, and D. C. Richardson. "MolProbity: All-atom structure validation for macromolecular crystallography." In: *Acta Crystallographica Section D: Biological Crystallography* 66.1 (2010), pp. 12–21. DOI: 10.1107/S0907444909042073.

CHAPTER 6

OUTLOOK AND FUTURE WORK

6.1 Outlook

In this PhD thesis the use of ion-exchange membranes has been investigated for the production and derivatization of protein crystals in order to determine their structure by X-ray crystallography. The work was divided in three parts, hence, the general outlook for each part of the work will be here drawn. The aim of the first part of the work was to investigate the topographical effect on nucleation avoiding membrane's surface chemistry changes. In order to achieve this objective, 117 Nafion® and NR50 Nafion® membranes' topography was modified by soft lithographic techniques. Three surface topographic patterns with different scales were designed with CleWin software: cylindrical wells with nano sized diameter, triangular prism wells with micro sized dimensions and a hierarchical surface patterning composed by micro sized triangular prism wells with nano sized cylindrical wells inside. Moulds with the designed topographies were produced by photolithography and soft lithography and used for patterning the commercial membranes by thermal nanoimprint lithography or casting of the polymer solution. The effect of the membrane surface pattern on its roughness was investigated by Atomic Force Microscopy (AFM). The analysis of AFM images showed that the nanostructure affected the roughness at nanoscopic level,

but no significant change in the roughness value compared to the plain membrane was observed for the microstructure since the size of the imprinted topographical features was larger than the size range of analysis. Instead, microscopical topographical features (with a high actual/projected area ratio) had a stronger impact on the apparent contact angle compared to nano structures (with actual/projected area ratio closer to 1). Calculations of the theoretical Wenzel and Cassie-Baxter contact angles were also performed in order to establish the predominant wetting regime on the membranes. According to the results of these calculations the Wenzel model is predominant in the case of the 117-Nafion® based membranes, meanwhile Cassie-Baxter state may or may not occur in the case of NR50-Nafion® based membranes. A theoretical model for calculating the ratio between Gibbs free energy variation of heterogeneous to homogeneous nucleation that takes into account the impact of surface topography has been already presented in the literature. This model was adapted to the specific geometry and dimensions of the designed membranes (evaluated by Scanning Electron Microscopy (SEM) and optical microscopy) and used to calculate the effect of the patterned membranes on nucleation. Theoretical calculations were compared with experimental results of nucleation and crystal growth rate of Trypsin from Bovine Pancreas on the patterned membranes. An enhancement of crystals number in all the patterned membranes compared to the same membrane without patterning was observed. Different mechanisms of nucleation were proposed, according to the scale of the topographical features: large surface features that determine a significant decrease of contact angle may induce an enhancement in nucleation rate due to the higher contact area between protein solution and membrane surface; instead, small topographical features may promote local accumulation of protein molecules. Finally, this first part of the work provides a methodology for designing surfaces with specific characteristics and topographies for protein crystallization, which helps for a better control of protein nucleation and crystallization, through the understanding of local supersaturation phenomena due to the specific features created at the membrane surface. The second part of this PhD thesis was focused on the development of a membrane-based method

for a controlled and stable derivatization of protein crystals. Post-crystallization treatments for resolution purposes imply the handling and removal of the crystals from their native environment with consequent shock and high risk of crystals damage. In this part of the work, two ion-exchange membranes, Nafion® (anion-exchange membrane) and Neosepta01 (cation-exchange membrane) were used to gently and selectively diffuse heavy atoms in ionic form into the crystals solution avoiding handling, breaking of vapour diffusion equilibrium and any other abrupt change of environmental conditions, guaranteeing the stability of the crystals over time. The transport kinetics of ions commonly used for derivatization (Br^-, $PtCl_4^{2-}$, Hg^{2+}) was studied by monitoring the variation of concentration of the ions over time and used for modelling the transport in the experimental crystallization set-up. The crystallization and derivatization experiments were performed in a membrane contactor where two compartments were separated by the ion-exchange membrane. In the first compartment an unsaturated protein solution was crystallized by controlling the relative humidity with a hypertonic solution. The second compartment was filled (after crystallization) with a solution containing the ion for derivatization. Stability of the crystals derivatized by ion-exchange membranes was monitored over time by optical microscopy analysis and compared with the stability of crystals derivatized with conventional soaking. Crystals derivatized with conventional soaking started degrading after few hours, while crystals derivatized by the ion-exchange membrane were stable for over 1 month after the end of the diffusion process (hence after reaching the same ion concentration used during conventional soaking). Synchrotron analysis of the derivatized crystals allowed to confirm the presence of the three heavy atoms tested in the crystal lattice and resolve the structure of the protein by Isomorphous Replacement. Hence, in the second part of the work a new concept for performing in-situ derivatization of protein crystals has been developed avoiding the main drawbacks of the conventional technique. In the third part of this PhD thesis, the concept of derivatization by ion-exchange membrane was integrated in a polydimethylsiloxane (PDMS) microfluidic device in order to improve the throughput. A microdevice was designed by CleWin software and fabricated

by soft lithography. An ion-exchange membrane was sandwiched in between two layers of PDMS by grafting. In this case, crystallization experiments were carried out by controlling the removal of water from the protein solution by osmosis through the membrane. Hence, experiments to measure the water and salt diffusion kinetics through Nafion® were performed in order to model their transport inside the microdevice. Crystallization experiments were performed for testing reproducibility, functionality of the device and crystals stability. Increasing the volume of solution for the same area of transport it was possible to obtain larger size and higher number of crystals due to a higher availability of protein molecules. The crystals grown in the microdevice showed a high diffraction quality after processing of the x-ray diffraction collected data. Finally, in this last part of this work a micro-device was developed where, with a low consumption of protein solution, it was possible to perform protein crystallization controlled by ion-exchange membranes. The same device may be exploited for screening ions for the derivatization of protein crystals.

6.2 Future work

This PhD thesis investigated the application of ion-exchange membranes for enhanced protein crystallization and protein crystals derivatization. This work made a step towards the possibility of understanding better the topographical effect of the membrane on protein crystallization and suggested guidelines for broader experimental studies that can help the development of a more accurate model for predicting the topographical effect. Hence, a more extensive work can be done for experimenting a wider number of conditions in terms of shapes and size for different types of proteins, also comparing the effect of the same topography on different types of materials and to attempt the development of a model that can comprehend a wider number of occurring phenomena. This work also allowed the development of an *in-situ* method for the derivatization of protein crystals. The *in-situ* transport concept might be extended to other types of ligands (also using different types of membranes) such as drugs or carbohydrates in order

to facilitate the study of protein-ligand interactions. Furthermore, , the use of other types of membranes also for the transport of glycerol in order to membrane-regulate the cryoprotection process and further reduce the handling of crystals by operators, is recommended. The microdevice developed in this thesis is made of PDMS in order to simplify the sealing process with the membrane. However, some efforts should be devoted to the investigation of X-ray transparent and not gas permeable materials and in finding a method for an easier bonding of these materials with the membrane. When a new method is developed, in order to test it, the first step cannot be different than using it for the crystallization of a model protein. This gives insights on where this method stands in terms of advantages and disadvantages compared to what already exists in the literature. For this reason, all the experiments reported in this PhD thesis were performed with model proteins. However, once advancements of this work are performed, it would be useful to finally test the developed concept and micro-device for the crystallization of proteins that are usually difficult to crystallize such as membrane proteins.

Conclusões e trabalho futuro

Conclusões

Nesta tese de doutoramento, foi investigada a utilização de membranas de permuta iónica para produção e derivatização de cristais de proteínas, a fim de determinar a sua estrutura por cristalografia de raios-X. O trabalho foi dividido em três partes, encontrando-se aqui as conclusões gerais para cada parte do trabalho. O objetivo da primeira parte do trabalho foi investigar o efeito topográfico na nucleação, evitando alterações químicas na superfície da membrana. Para alcançar este objetivo, a topografia das membranas Nafion® 117 e Nafion® NR50 foi modificada por *soft*- litografia. Foram desenhados três padrões topográficos de superfície diferentes com diferentes escalas, utilizando o software CleWin: poços cilíndricos com nano diâmetros, poços de prisma triangulares com dimensões micro e um padrão de superfície hierarquizado composto por micro-poços de prisma triangulares e nano-poços cilíndricos. Foram produzidos moldes, por fotolitografia e *soft*-litografia com as topografias descritas e utilizados para padronizar as membranas comerciais por litografia térmica de nano-impressão ou por casting da solução polimérica. O efeito do padrão da superfície na rugosidade da membrana foi investigado por Microscopia de Força Atómica (AFM). A análise das imagens por AFM revelou que a nanoestrutura afectou a rugosidade ao nível nanoscópico, mas não foram observadas alterações significativas no valor da rugosidade da microestrutura, comparativamente com a membrana simples, uma vez que o tamanho das características topográficas impressas é superior ao intervalo da análise. Por outro lado, o ângulo de contato das superfícies com padrões foi afetado pela relação entre a área real e a área projetada, mais do que a rugosidade

no nível nanoscópico. Assim, as características topográficas microscópicas (com uma elevada rázão entre área real/área projetada) tiveram um impacto superior no ângulo de contato, em comparação com as nanoestruturas (com uma razão de área real/área projetada próximo de 1). Foram efectuados cálculos dos ângulos de contato teóricos através das equações de Wenzel e de Cassie-Baxter para estabelecer o regime de humedecimento predominante nas membranas. De acordo com os resultados destes cálculos, o modelo de Wenzel é predominante no caso das membranas derivadas do 117-Nafion®; por outro lado o estado de Cassie-Baxter pode ocorrer ou não nas membranas derivadas do NR50-Nafion®. Encontra-se descrito na literatura um modelo teórico que considera o impacto da topografia da superfície, através do cálculo da razão da variação da energia livre de Gibbs entre a nucleação heterogénea e homogénea. Este modelo foi adaptado à geometria e dimensões específicas (obtidas por Microscopia Eletrónica de Varrimento (SEM) e microscopia óptica) das membranas desenhadas e utilizado para calcular o efeito dos padrões das membranas na nucleação. Os resultados experimentais obtidos, para as membranas com padrões, na nucleação e na velocidade do crescimento dos cristais da tripsina do pâncreas de bovinos, foram comparados com os cálculos teóricos. Observou-se um aumento do número de cristais em todas as membranas com padrões em comparação com a mesma membrana sem padronização. Foram propostos diferentes mecanismos de nucleação, de acordo com a escala dos detalhes topográficos: grandes detalhes na superfície que determinam uma diminuição significativa do ângulo de contato podem induzir um aumento na velocidade de nucleação devido à maior área de contato entre a solução proteica e a superfície da membrana; por outro lado, pequenos detalhes topográficos podem promover uma acumulação local de moléculas de proteína. Finalmente, esta primeira parte do trabalho fornece uma metodologia para desenhar superfícies com características e topografias específicas para a cristalização de proteínas, o que ajuda a um melhor controlo da nucleação e cristalização das proteínas, através da compreensão dos fenómenos de supersaturação locais devido aos detalhes específicos criados na superfície das membranas. A segunda parte desta tese de doutoramento teve como

foco o desenvolvimento de um método baseado em membranas para a derivatização controlada e estável de cristais de proteína. Tratamentos de pós-cristalização para fins de resolução implicam o manuseio e remoção dos cristais do seu ambiente nativo com consequente choque e alto risco de danos nos cristais. Nesta parte do trabalho, duas membranas de permuta iónica, Nafion® (membrana de permuta catiónica) e Neosepta01 (membrana de permuta aniónica) foram usadas para difundir suavemente e seletivamente átomos pesados na forma iónica para a solução de cristais, evitando o manuseio, quebra do equilíbrio de difusão de vapor e qualquer outra alteração abrupta das condições ambientais, garantindo a estabilidade dos cristais ao longo do tempo. A cinética do transporte de iões habitualmente utilizados para derivatização (Br^-, $PtCl_4^{2-}$, Hg^{2+}) foi estudada através da monitorização da variação de concentração dos iões ao longo do tempo e utilizada para modelar o transporte na configuração experimental de cristalização. Os ensaios de cristalização e derivatização foram realizados num contactor de membranas, onde dois compartimentos foram separados pela membrana de permuta iónica. No primeiro compartimento, uma solução proteica insaturada foi cristalizada controlando a humidade relativa com uma solução hipertónica. O segundo compartimento foi preenchido (após a cristalização) com uma solução contendo o ião para a derivatização. A estabilidade dos cristais derivatizados das membranas de permuta iónica foi monitorizada ao longo do tempo, por análise de microscopia óptica e comparada com a estabilidade dos cristais derivatizados por imersão. Os cristais derivatizados por imerção começaram a degradar após algumas horas, enquanto que os cristais derivatizados com a membrana de permuta iónica permaneceram estáveis por mais de 1 mês após o término do processo de difusão (portanto, após alcançar a mesma concentração de iões utilizada na imersão convencional). A análise por Synchrotron dos cristais derivatizados permitiu confirmar a presença dos três átomos pesados testados na rede cristalina e resolver a estrutura da proteína por substituição isomórfica. Assim, na segunda parte do trabalho, foi desenvolvido um novo conceito para a derivatização *in-situ* de cristais de proteínas, evitando-se as principais desvantagens da técnica convencional. Na terceira parte desta tese de doutoramento, foi integrado o conceito

de derivatização por membrana de permuta iónica num dispositivo microfluídico de polidimetilsiloxano (PDMS) para melhorar o rendimento. Foi desenhado um microdispositivo através do software CleWin e fabricado por *soft*-litografia. Uma membrana de permuta iónica foi prensada entre duas camadas de PDMS por grafting. Neste caso, as experiências de cristalização foram realizadas controlando a remoção de água da solução de proteína por osmose através da membrana. Assim, foram realizados ensaios para medir a cinética de difusão de água e do sal através de membrana de Nafion®,para modelar o transporte dentro do microdispositivo. Foram realizados ensaios de cristalização para testar a reprodutibilidade, funcionalidade do dispositivo e estabilidade dos cristais. Foi possível obter maior número e tamanho de cristais aumentando o volume de solução para a mesma área de transporte, devido à maior disponibilidade de moléculas de proteína. Os cristais formados no microdispositivo, apresentaram elevada qualidade de difração após o processamento dos dados recolhidos por difração de raios-X. Finalmente, nesta última parte do trabalho, foi desenvolvido um micro-dispositivo onde, com um baixo consumo de solução proteica, foi possível realizar a cristalização de proteínas controlada por membranas de permuta iónica. O mesmo dispositivo pode ser explorado para a derivatização de cristais de proteína.

Trabalho futuro

Nesta tese de doutoramento foi investigada a utilização de membranas de permuta iónica, para cristalização de proteínas e derivatização dos cristais de proteínas. Este trabalho deu um passo na direção de um melhor entendimento do efeito topográfico da membrana, na cristalização de proteínas e sugeriu diretrizes para estudos experimentais mais amplos, que possam auxiliar no desenvolvimento de um modelo mais preciso para a previsão do efeito topográfico. Assim, pode ser realizado um trabalho mais extenso considerando um maior número de condições, em termos de forma e tamanho para diferentes tipos de proteínas, comparando também o efeito da mesma topografia em diferentes tipos de materiais e tentar o desenvolvimento de um modelo, que pode compreender um número maior de

fenómenos que ocorrem. Esta tese também possibilitou o desenvolvimento de um método para a derivatização *in-situ* de cristais de proteínas. O conceito de transporte in situ pode ser estendido a outros tipos de ligantes (utilizando também diferentes tipos de membranas), tais como drogas ou carboidratos, a fim de facilitar o estudo das interações proteína-ligante. Além disso, é recomendada a utilização de outros tipos de membranas, também para o transporte de glicerol, a fim de regular o processo de crioproteção com uma membrana e reduzir ainda mais o manuseio de cristais pelos operadores. O microdispositivo desenvolvido nesta tese é feito de PDMS, a fim de simplificar o processo de vedação com a membrana. No entanto, devem ser direccionados alguns esforços para a investigação de materiais transparentes e impermeáveis a gases e encontrar um método para uma ligação mais fácil destes materiais com a membrana. Quando um novo método é desenvolvido, para testá-lo, o primeiro passo deve ser a sua implementação na cristalização de uma proteína modelo. Assim, alcançamos a compreensão sobre as o vantagens e desvantagens do método, em comparação com o que se encontra na literatura. Por esta razão, todos os ensaios descritos nesta tese de doutoramento foram realizados com proteínas modelo. No entanto, uma vez que sejam realizados avanços sobre este trabalho, seria útil testar finalmente o conceito desenvolvido e o microdispositivo para a cristalização de proteínas que são geralmente difíceis de cristalizar, tais como proteínas de membrana.

Conclusiones y trabajo futuro

Conclusiones

En esta tesis doctoral, se ha investigado el uso de membranas de intercambio iónico para la producción y derivación de cristales de proteínas con el fin de determinar su estructura mediante cristalografía de rayos X. El trabajo se dividió en tres partes, por lo tanto, aquí se dibujarán las perspectivas generales para cada parte del trabajo. El objetivo de la primera parte del trabajo fue investigar el efecto topográfico en la nucleación evitando cambios en la química de la superficie. Para lograr este objetivo, se modificó la topografía de las membranas 117 Nafion® y NR50 Nafion® mediante técnicas de *soft*-litografía. Se diseñaron tres patrones topográficos de superficie diferentes con diferentes escalas con el software CleWin: pozos cilíndricos con diámetros de tamaño nanométrico, pozos de prisma triangular con dimensiones de tamaño micro y un patrón de superficie jerárquico compuesto por pozos de prisma triangular de tamaño micro con pocillos cilíndricos de tamaño nanométrico en el interior. Los moldes con las topografías diseñadas se produjeron mediante fotolitografía y *soft*-litografía y se utilizaron para modelar las membranas comerciales mediante litografía por nanoimpresión térmica o colada de la solución de polímero. El efecto del patrón de la superficie de la membrana sobre su rugosidad se investigó mediante un microscopio de fuerza atómica (AFM). El análisis de las imágenes de AFM mostró que la nanoestructura afectó la rugosidad a nivel nanoscópico, pero no se observó ningún cambio significativo en el valor de la rugosidad en comparación con la membrana plana para la microestructura, ya que el tamaño de las características

topográficas impresas fue mayor que el rango de tamaño del análisis. En cambio, el ángulo de contacto de las superficies modeladas resultó afectado por la relación entre el área de superficie real y proyectada más que la rugosidad a nivel nanoscópico. Por lo tanto, las características topográficas microscópicas (con una alta relación de área real / proyectada) tuvieron un mayor impacto en el ángulo de contacto final en comparación con las nano estructuras (con una relación de área real / proyectada más cercana a 1). También se realizaron cálculos del ángulo de contacto teórico de Wenzel y Cassie-Baxter para establecer el régimen de humectación predominante en las membranas. De acuerdo con los resultados de estos cálculos, el modelo de Wenzel es predominante en el caso de las membranas basadas en 117-Nafion®, mientras que el estado de Cassie-Baxter puede ocurrir en el caso de las membranas basadas en NR50-Nafion®. En la literatura ya se ha presentado un modelo teórico para calcular la relación entre la energía libre de Gibbs de nucleación heterogénea a homogénea que tiene en cuenta el impacto de la topografía de superficie. Este modelo se adaptó a la geometría y dimensiones específicas de las membranas diseñadas (evaluadas mediante microscopía electrónica de barrido (SEM) y microscopía óptica) y se utilizó para calcular el efecto de las membranas modeladas en la nucleación. Los cálculos teóricos se compararon con los resultados experimentales de la nucleación y la tasa de crecimiento cristalino de la tripsina del páncreas bovino en las membranas con dibujos. Se observó un aumento del número de cristales en todas las membranas con patrón en comparación con la misma membrana sin patrón. Se propusieron diferentes mecanismos de nucleación, según la escala de las características topográficas: las grandes características de la superficie que determinan una disminución significativa del ángulo de contacto pueden inducir un aumento en la velocidad de nucleación debido a la mayor área de contacto entre la solución de proteínas y la superficie de la membrana; en cambio, las pequeñas características topográficas pueden promover la acumulación local de moléculas de proteína. Finalmente, esta primera parte del trabajo proporciona una metodología para diseñar superficies con características específicas y topografías para la cristalización de proteínas, que ayuda a un mejor control de la nucleación y la cristalización de proteínas, a

través de la comprensión de los fenómenos de sobresaturación locales debido a las características específicas creadas en el superficie de la membrana. La segunda parte de esta tesis doctoral se centró en el desarrollo de un método basado en membrana para una derivatización controlada y estable de cristales de proteínas. Los tratamientos posteriores a la cristalización con fines de resolución implican el manejo y la eliminación de los cristales de su entorno nativo con el consiguiente shock y el alto riesgo de daño de los cristales. En este trabajo, se utilizaron dos membranas de intercambio iónico, Nafion® (membrana de intercambio de aniones) y Neosepta01 (membrana de intercambio de cationes) para difundir de forma suave y selectiva átomos pesados en forma iónica en la solución de cristales, evitando el manejo y la ruptura del equilibrio de difusión de vapor. y cualquier otro cambio brusco de las condiciones ambientales, que garantice la estabilidad de los cristales a lo largo del tiempo. La cinética de transporte de los iones comúnmente utilizados para la derivación (Br-, PtCl42-, Hg2 +) se estudió al monitorear la variación de la concentración de los iones a lo largo del tiempo y se utilizó para modelar el transporte en la configuración de cristalización experimental. Los experimentos de cristalización y derivatización se realizaron en un contactor de membrana en el que dos compartimentos estaban separados por la membrana de intercambio iónico. En el primer compartimento se cristalizó una solución de proteína insaturada controlando la humedad relativa con una solución hipertónica. El segundo compartimento se llenó (después de la cristalización) con una solución que contenía el ion para la derivatización. La estabilidad de los cristales derivatizados por membranas de intercambio iónico se monitorizó a lo largo del tiempo mediante análisis de microscopía óptica y se comparó con la estabilidad de los cristales derivatizados con remojo convencional. Los cristales derivados con remojo convencional comenzaron a degradarse después de unas pocas horas, mientras que los cristales derivados por la membrana de intercambio iónico se mantuvieron estables durante más de 1 mes después del final del proceso de difusión (por lo tanto, después de alcanzar la misma concentración de iones utilizada durante el remojo convencional). El análisis sincrotrón de los cristales derivados permitió confirmar la presencia de los tres átomos pesados probados

en la red cristalina y resolver la estructura de la proteína por *Isomorphous Replacement*. Por lo tanto, en la segunda parte del trabajo, se ha desarrollado un nuevo concepto para realizar la derivación in situ de cristales de proteínas, evitando los principales inconvenientes de la técnica convencional. En la tercera parte de esta tesis doctoral, el concepto de derivatización por membrana de intercambio iónico se integró en un dispositivo microfluídico de polidimetilsiloxano (PDMS) para mejorar el rendimiento. El software CleWin diseñó un microdispositivo y se fabricó mediante *soft*-litografía. Una membrana de intercambio iónico se emparedó entre dos capas de PDMS mediante injerto. En este caso, los experimentos de cristalización se llevaron a cabo controlando la eliminación del agua de la solución proteica mediante ósmosis a través de la membrana. Por lo tanto, se realizaron experimentos para medir la cinética de difusión del agua y la cinética de la sal a través de Nafion® para modelar su transporte dentro del microdispositivo. Se realizaron experimentos de cristalización para probar la reproducibilidad, la funcionalidad del dispositivo y la estabilidad de los cristales. Al aumentar el volumen de solución para la misma área de transporte, fue posible obtener un tamaño más grande y un mayor número de cristales debido a una mayor disponibilidad de moléculas de proteína. Los cristales crecidos en el microdispositivo mostraron una alta calidad de difracción después del procesamiento de los datos recolectados por difracción de rayos X. Finalmente, en la última parte de este trabajo se desarrolló un microdispositivo en el que, con un bajo consumo de solución proteica, fue posible realizar una cristalización de proteínas controlada por membranas de intercambio iónico. El mismo dispositivo puede ser explotado para seleccionar iones para la derivatización de cristales de proteínas.

Trabajo Futuro

Esta tesis doctoral investigó la aplicación de membranas de intercambio iónico para la cristalización de proteínas y la derivatización de cristales de proteínas. Este trabajo dio un paso hacia la posibilidad de comprender mejor el efecto topográfico de la membrana en la cristalización de proteínas y sugirió pautas para

estudios experimentales más amplios que pueden ayudar al desarrollo de un modelo más preciso para predecir el efecto topográfico. Por lo tanto, se puede realizar un trabajo más extenso para experimentar un número más amplio de condiciones en términos de formas y tamaños para diferentes tipos de proteínas, comparando también el efecto de la misma topografía en diferentes tipos de materiales y para intentar el desarrollo de un modelo que Puede comprender un número más amplio de fenómenos que ocurren. Esta tesis también trabajó en el desarrollo de un método para la derivación in-situ de cristales de proteínas. El concepto de transporte insitu podría extenderse a otros tipos de ligandos (también utilizando diferentes tipos de membranas) como medicamentos o carbohidratos para facilitar el estudio de las interacciones proteína-ligando. Además, sugeriría explorar la posibilidad de usar otros tipos de membranas también para el transporte de glicerol con el fin de regular también el proceso de crioprotección por membrana y reducir aún más el manejo de los cristales por parte de los operadores. El microdispositivo desarrollado en esta tesis está hecho de PDMS para simplificar el proceso de sellado con la membrana. Sin embargo, se deben dedicar algunos esfuerzos a la investigación de materiales transparentes a los rayos X y no permeables a los gases, y a encontrar un método para unir más fácilmente estos materiales con la membrana. Cuando se desarrolla un nuevo método, para probarlo, el primer paso no puede ser diferente a usarlo para la cristalización de una proteína modelo. Esto da una idea de dónde se encuentra este método en términos de ventajas y desventajas en comparación con lo que ya existe en la literatura. Por este motivo, todos los experimentos en esta tesis doctoral se realizaron con proteínas modelo. Sin embargo, una vez que se realicen avances en este trabajo, sería útil probar finalmente el concepto desarrollado y el microdispositivo para la cristalización de proteínas que generalmente son difíciles de cristalizar, como las proteínas de membrana.

Vooruitblik en toekomstig werk

Vooruitblik

In dit PhD proefschrift is het gebruik van ionuitwisselingsmembranen voor de productie en derivatie van proteïnekristallen onderzocht, om zo hun structuur te kunnen bepalen via röntgen kristallografie. Het onderzoek was verdeeld in drie delen, voor elk deel zal hier beschreven worden. Het doel van het eerste onderzoeksdeel was het onderzoeken van het topografische effect van nucleatie, waarbij verandering van de oppervlaktechemie worden vermeden. Om dit doel te behalen, is de topografie van 117-Nafion® en NR50 Nafion® membranen gemodificeerd door middel van zachte lithografie technieken. Drie verschillende oppervlaktopografische patronen met verschillende groottes werden ontworpen met CleWin-software: cilindrische putjes met een diameter van nano-formaat, driehoekige prisma putjes met micro afmetingen en een hiërarchisch oppervlaktepatroon, van binnen samengesteld door driehoekige driehoekige prisma putjes met cilindrische putjes van nano-afmetingen aan de binnenkant. Matrijzen met de ontworpen topografieën werden geproduceerd door fotolithografie en zachte lithografie en gebruikt voor het bewerken van de commerciële membranen via thermische nano-opdruk lithografie of gieten van de polymeeroplossing. Het effect van het membraanoppervlaktepatroon op de ruwheid werd onderzocht door Atomic Force Microscope (AFM). Analyse van de AFM-afbeeldingen toonde aan dat de nanostructuur de ruwheid op nanoscopisch niveau beïnvloedde, maar er werd geen significante verandering in de ruwheidswaarde in vergelijking met het gewone membraan waargenomen voor de microstructuur, omdat de grootte van de bedrukte topografische kenmerken groter was dan de grootte van het analysegebie. In

plaats daarvan bleek de contacthoek van de patroonoppervlakken meer te worden beïnvloed door de verhouding tussen het werkelijke en het geprojecteerde oppervlak dan de ruwheid op nanoscopisch niveau. Hieruit bleek dat microscopische topografische kenmerken (met een hoge werkelijke / geprojecteerde oppervlakverhouding) een sterkere invloed hadden op de uiteindelijke contacthoek dan nanostructuren (met een werkelijke / geprojecteerde oppervlakteverhouding dichter bij 1). Berekeningen met de theoretische Wenzel en Cassie-Baxter contacthoek werden ook uitgevoerd om het overheersende bevochtigingsregime op de membranen vast te stellen. Volgens de resultaten van deze berekeningen is het Wenzel-model het predominante model in het geval van de op 117-Nafion® gebaseerde membranen, terwijl de Cassie-Baxter-toestand zich kan voordoen in het geval van op NR50-Nafion® gebaseerde membranen. Een theoretisch model voor het berekenen van de verhouding tussen Gibbs vrije energie van heterogene tot homogene nucleatie, die rekening houdt met de impact van oppervlaktetopografie, is al in de literatuur gepresenteerd. Dit model werd aangepast aan de specifieke geometrie en dimensies van de ontworpen membranen (zoals geëvalueerd door Scanning Electron Microscope (SEM) en optische microscopie) en gebruikt om het effect van de patroonmembranen op nucleatie te berekenen. De theoretische berekeningen werden vergeleken met experimentele resultaten van nucleatie en kristalgroeisnelheid van rundertrypsine op de patroonmembranen. Een verhoging van het aantal kristallen in alle patroonmembranen vergeleken met hetzelfde membraan zonder patroontoevoeging werd waargenomen. Verschillende mechanismen van nucleatie werden voorgesteld, volgens de schaal van de topografische kenmerken: grote oppervlaktekenmerken, die een significante afname van de contacthoek bepalen, kunnen een verhoging in nucleatiesnelheid creëren vanwege

het hogere contactoppervlak tussen de eiwitoplossing en het membraanoppervlak; terwijl kleine topografische kenmerken de lokale accumulatie van eiwitmoleculen bevorderen. Ten slotte biedt dit eerste deel van het werk een methodologie voor het ontwerpen van oppervlakken met specifieke kenmerken en topografieën voor eiwitkristallisatie, die helpt bij een betere controle van de nucleatie en kristallisatie van eiwitten, door het in acht nemen van lokale oververzadigingsverschijnselen door de specifieke kenmerken die zijn gecreëerd bij de membraan oppervlak. Het tweede deel van dit proefschrift was gericht op de ontwikkeling van een membraan-gebaseerde methode voor een gecontroleerde en stabiele derivatisering van eiwitkristallen. Post-kristallisatiebehandelingen voor resolutiedoeleinden impliceren de hantering en verwijdering van de kristallen uit hun natieve omgeving, wat kan relatering in shock en een hoog risico op beschadigingen aan de kristallen. In dit onderzoek werden twee ionuitwisselingsmembranen, Nafion® (anion-uitwisselingsmembraan) en Neosepta01 (kationenuitwisselingsmembraan) gebruikt om voorzichtig en selectief zware atomen in ionvorm in de kristallenoplossing te diffunderen terwijl hantering, het breken van het dampdiffusie-evenwicht en elke andere abrupte verandering van omgevingsomstandigheden die de stabiliteit van de kristallen in de loop van de tijd garandeert werd gemeden. De transportkinetiek van ionen die gewoonlijk worden gebruikt voor derivatisering (Br^-, $PtCl_4^{2-}$, Hg^{2+}) werd bestudeerd door het volgen van de variatie in concentratie van de ionen in de tijd en gebruikt voor het modelleren van het transport in de experimentele kristallisatie-opzet. De kristallisatie- en derivatisatie-experimenten werden uitgevoerd in een membraan contactor waarbij twee compartimenten werden gescheiden door het ionuitwisselingsmembraan. In het eerste compartiment werd een onverzadigde eiwitoplossing gekristalliseerd door de relatieve vochtigheid te regelen met een hypertone oplossing. Het tweede compartiment werd (na kristallisatie) gevuld met een oplossing die het ion voor derivatisering bevat. Stabiliteit van de door ionenuitwisselingsmembranen gederivatiseerde kristallen werd over tijd gevolgd via optische microscopieanalyse en vergeleken met de stabiliteit van met conventioneel onderdompelen gederivatiseerde kristallen. Kristallen die waren gederivatiseerd met conventioneel weken

begonnen na enkele uren te degraderen, terwijl kristallen gederivatiseerd door het ionuitwisselingsmembraan gedurende meer dan 1 maand na het einde van het diffusieproces (dus na het bereiken van dezelfde ionconcentratie die werd gebruikt tijdens conventioneel onderdompelen) stabiel waren. Synchrotron-analyse van de gederivatiseerde kristallen maakte het mogelijk de aanwezigheid van de drie zware atomen die in het kristalrooster waren getest te bevestigen en de structuur van het eiwit door isomorfe vervanging te analyseren. Dat wil zeggen dat in het tweede deel van het werk een nieuw concept is ontwikkeld voor het uitvoeren van in-situ derivatisering van eiwitkristallen, waarbij de belangrijkste nadelen van de conventionele techniek worden vermeden. In het derde deel van dit proefschrift werd het concept van derivatisering door ionuitwisselingsmembraan geïntegreerd in een microfluïdisch polydimethylsiloxaan (PDMS) apparaat om de doorvoer te verbeteren. Een micro-apparaat werd ontworpen door CleWin-software en gefabriceerd door zachte lithografie. Een ionuitwisselingsmembraan werd ingeklemd tussen twee lagen PDMS via enten. In dit geval werden kristallisatie-experimenten uitgevoerd door het controleren van de verwijdering van water uit de eiwitoplossing via osmose door het membraan. Hierom werden experimenten om de waterdiffusiekinetiek en zoutkinetiek door Nafion® te meten uitgevoerd, om hun transport in het micro apparaat te modelleren. Kristallisatie-experimenten werden uitgevoerd voor het testen van de reproduceerbaarheid, de functionaliteit van het apparaat en de stabiliteit van de kristallen. Door het volume van de oplossing over hetzelfde transportgebied te vergroten, was het mogelijk om een grotere afmeting en een groter aantal kristallen te verkrijgen vanwege een hogere beschikbaarheid van eiwitmoleculen. De kristallen gekweekt in het micro apparaat vertoonden een hoge diffractiekwaliteit na verwerking van de door röntgendiffractie verzamelde gegevens. Ten slotte werd in het laatste deel van dit werk een micro apparaat ontwikkeld waarbij, met een laag eiwitverbruik, het mogelijk was om eiwitkristallisatie uit te voeren die werd gecontroleerd door ionuitwisselingsmembranen. Hetzelfde apparaat kan worden gebruikt voor het screenen van ionen voor de derivatisering van eiwitkristallen.

Aanbevelingen voor toekomstig werk

Dit proefschrift onderzocht de toepassing van ionuitwisselingsmembranen voor verbeterde eiwitkristallisatie en derivaatvorming van eiwitkristallen. Dit werk maakte een stap in de richting van de mogelijkheid om het topografische effect van het membraan op eiwitkristallisatie beter te begrijpen en stelde richtlijnen voor bredere experimentele studies voor die kunnen helpen bij de ontwikkeling van een nauwkeuriger model voor het voorspellen van het topografische effect. Vandaar dat er uitgebreider werk kan worden gedaan op het gebied van experimenteren met een groter aantal variaties in vormen en afmetingen voor verschillende soorten eiwitten, ook kan het vergelijken van het effect van dezelfde topografie op verschillende soorten materialen en het ontwikkelen van een model voor groter aantal voorkomende fenomenen worden ondernomen. Dit proefschrift heeft ook gewerkt aan de ontwikkeling van een in-situ methode voor de derivatisering van eiwitkristallen. Het in-situ transportconcept kan worden uitgebreid naar andere soorten liganden (ook met behulp van verschillende soorten membranen), zoals geneesmiddelen of koolhydraten, om de studie van eiwit-ligand-interacties te vereenvoudigen. Verder zou ik willen voorstellen om de mogelijkheid te onderzoeken om andere soorten membranen ook te gebruiken voor het transport van glycerol om het cryoprotectieproces membraan-gereguleerd te maken en de hantering van kristallen door operators verder te verminderen. Het micro apparaat dat in dit proefschrift is ontwikkeld, is gemaakt van PDMS om het afdichtproces met het membraan te vereenvoudigen. Er moet echter enige moeite worden gestoken in het onderzoeken van röntgenstralingsdoorzichtige en niet gasdoorlatende materialen en om een methode te vinden voor een gemakkelijkere binding van deze materialen aan het membraan. Wanneer een nieuwe methode wordt ontwikkeld kan, om deze te testen, de eerste stap niet anders zijn dan deze te gebruiken voor de kristallisatie van een standaard eiwit. Dit geeft inzicht in waar deze methode staat in termen van voor- en nadelen in vergelijking met wat al bestaat in de literatuur. Om deze reden zijn alle experimenten die in dit proefschrift zijn beschreven, uitgevoerd met standaard eiwitten. Echter, zodra verbeteringen van dit werk worden uitgevoerd, zou het nuttig zijn om eindelijk

het ontwikkelde concept en het micro apparaat te testen voor de kristallisatie van eiwitten die gewoonlijk moeilijk te kristalliseren zijn, zoals membraaneiwitten.

Appendix

A.1 Differential Scanning Calorimetry analysis

Thermal Nanoimprint Lithography (or hot embossing) transfers a pattern from a mould to a thermoplastic substrate. The process is commonly performed by heating the material to be imprinted at a temperature 20-50 °C higher than the glass transition temperature (Tg) of the substrate and afterwards high pressure is applied to improve the contact between the mould and the substrate. Therefore, in order to assess the conditions for a successful imprinting, the Tg of Nafion® was determined by DSC analysis. The measurements were performed within a temperature interval of 35-250 °C, with a heating rate of 10 °C/min. Since, according to the literature [1, 2], the water content of the polymer might affect the Tg because of plasticization effects, and Nafion® membranes easily change the water content according to environmental humidity variations, measurements were carried out for a range (from 0% to 24%) of water content of Nafion®. In order to control the membrane water content, membranes were left equilibrating in closed vessels with different saturated salt solutions (all conditions are reported in Table A.1), and weight measured over time until no variation was recorded.

The results reported in Figure A.1 show a Tg value of 114 ± 2 °C and no significant differences were found for different water content of Nafion®. The Tg

Table A.1: Nafion® at different water contents

Membrane	Water content(%)
Nafion® dried at 80 °C	0
Untreated Nafion®	4.5
Nafion® equilibrated with K2CO3 saturated solution RH=43%	9.8
Nafion® equilibrated with KCl saturated solution RH=85%	18.4
Hydrated Nafion®	24.0

measured for this work is in agreement with the values reported in the literature (115 °C) [1, 2]. In light of this result it was decided to perform the imprinting process at 135 °C.

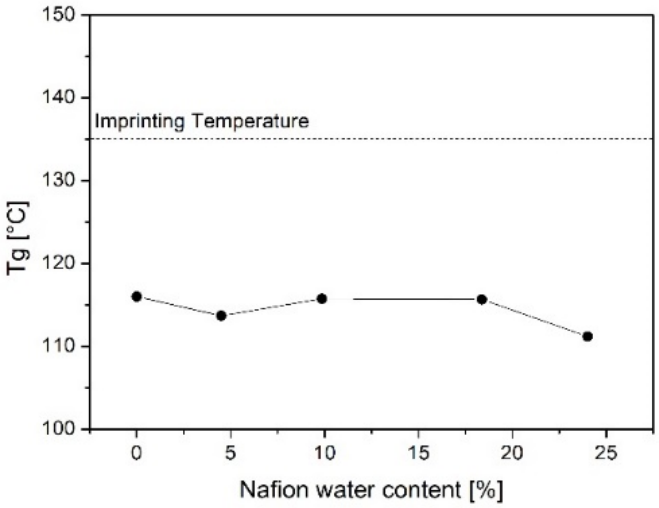

Figure A.1: DSC results for Nafion® at different water contents

A.2 Photolithography process

The design has been made using the CleWin software (WieWeb software, Hengelo, NL) and transferred to a photolithography mask. A negative photoresist (SU-8

50 DE MicroChem) was spin-coated onto a Silicon wafer and exposed to UV light through the mask design in order to transfer the pattern onto the SU-8 layer. The SU-8 wafer was baked and developed with SU-8 developer, in order to remove the non-cross-linked photoresist (Figure A.2). A Poly(dimethylsiloxane) (PDMS)

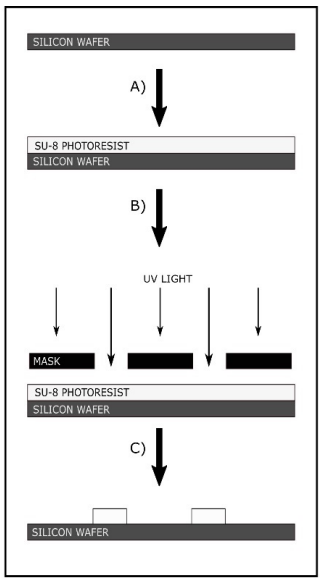

Figure A.2: Photolithography process: A) Spin-coating of the photoresist onto the silicon wafer; B) UV light exposure trough the designed mask; C) Development of the photoresist and attainment of the final mould

purchased by Sylgard 184 Dow Corning, Midland, MI, micromold made of pillars with a triangle shape with 160 μm side and 100 μm height was made by casting a mixture of PDMS pre-polymer and curing agent (10:1) onto a SU-8 master mold previously produced by photolithography. The PDMS solution casted onto the mold was baked at 80 °C for 50 minutes in order to cure the PDMS and obtain the final mould by release [3].

A.3 Calculation of the percentage area of Nafion® NR50 and Nafion® 117 in the hierarchical membrane

The hierarchical membrane is made of the 117-Nano overlapped with a NR50 membrane with triangle shaped holes. The repeating unit area (A_{rep}) of the holes

containing 1 triangle is 355µmx187µm. The triangles are equilateral with the side of 164 μm. Hence the triangle area (A_{tri}) was calculated as:

$$A_{tri} = \frac{\sqrt{3}}{4} L^2 \tag{A.1}$$

The fraction of 117 membrane (f_{117}) was calculated as:

$$f_{117} = \frac{A_{tri}}{A_{rep}} \tag{A.2}$$

The fraction of NR50 membrane (f_{NR50}) was calculated as:

$$f_{NR50} = 1 - \frac{A_{tri}}{A_{rep}} \tag{A.3}$$

The total roughness (Ra) for the Hierarchical membrane was calculated as:

$$Ra = f_{117} Ra_{117} + f_{NR50} Ra_{NR50} \tag{A.4}$$

A.4 Calculation of Gibbs free energy variation ratio of heterogeneous to homogeneous nucleation

According to the Classical Nucleation Theory (CNT) ΔG_{Het} is defined as:

$$\Delta G_{Het} = -\frac{\Delta\mu}{\Omega} V_N + A_{NL}\gamma_{NL} - A_{NS}(\gamma_{SL} - \gamma_{NS}) \tag{A.5}$$

where μ is the chemical potential, Ω is the molar Volume, V_N is the Volume of the nucleus, A_{NL} is the area of the interface between liquid and nucleus, γ_{NL} is the interfacial energy between the nucleus and the liquid, A_{NS} is the interfacial area between the nucleus and the surface, γ_{SL} and γ_{NS} are the interfacial energy between the substrate and the liquid and between the nucleus and the substrate, respectively. We can define geometrical relations:

$$\alpha = \frac{r}{R} \tag{A.6}$$

$$\beta = \frac{h}{R} \tag{A.7}$$

If the topography is applied to a Wenzel's surface [4], where the protein solution is able to follow the geometry filling the cavities, V_N will be given by the

sum of the volume of the spherical cap and the volume of the wells on the surface covered by the cap.

$$V_N = \frac{1}{3}\pi R^3[(1-cos\theta)^2(2+cos\theta) + \pi R^3 n\alpha^2\beta] \tag{A.8}$$

A_{NS} (the surface between the nucleus and the surface) will be given by the surface of contact between the nucleus and the surface, including the walls of the wells.

$$A_{NS} = \pi R^2(sin^2\theta + sn\alpha\beta) \tag{A.9}$$

A_{NL} (the surface between the liquid and the nucleus) will be given by the surface of the spherical cap

$$A_{NL} = 2\pi R^2(1-cos\theta) \tag{A.10}$$

The Young Equation states:

$$\gamma_{SL} - \gamma_{NS} = \gamma_{NL} cos\theta_Y \tag{A.11}$$

where θ_Y is the Young's contact angle (contact angle for an ideally flat surface) of the solution on the substrate. When the solution is following the geometry of the surface, θ_Y can be related to the apparent contact angle θ by the Wenzel's equation[5] :

$$cos\theta_Y = \frac{cos\theta}{\Gamma} = \frac{cos^2\theta}{sin^2\theta + 2n\alpha\beta} \tag{A.12}$$

Replacing equations A.12 in equation A.11 and later equations A.8, A.9, A.10, A.11 in equation A.5, we obtain:

$$\Delta G_{Het} = -\frac{\Delta\mu}{\Omega}\frac{1}{3}\pi R^3[(1-cos^2\theta)(2+cos\theta)+3n\alpha^2\beta]+\pi\gamma_{SL}R^2[2(1-cos\theta)-cos\theta sin^2\theta] \tag{A.13}$$

As it is evident from equation A.13 , ΔG_{Het} is given by a combination of the free energy variation of two events:

- the formation of a new phase (a spontaneous process that gives a negative contribution to the total variation of free energy, increasing as the volume of the nucleus increases);

- the formation of a new interface between nucleus and surface and nucleus and liquid (an energetically disfavoured process that has a positive contribution to the total variation of free energy, increasing as the surface of the nucleus increases).

The nucleus size (the radius) determines which of the two energy contributions is prevailing on the total value of Gibbs free energy variation of nucleation. Indeed, small nuclei exhibit high surface to volume ratio, therefore, the interface free energy component has predominance on the new-phase free energy component causing stabilization of the nuclei by their dissolution. Instead, for nuclei of larger size, the surface of the nuclei is associated with a much larger volume, hence, the new-phase free energy dominates the total free energy determining the stabilization of the nuclei by growth. Therefore, the critical nucleus radius (R^*) can be calculated as follows [6]:

$$\frac{\delta \Delta G_{Het}}{\delta R} = 0 \tag{A.14}$$

$$R^* = \frac{2\gamma_L[2(1-cos\theta)-cos\theta sin^2\theta]}{\left(\frac{\Delta\mu}{\Omega}\right)^2[(1-cos\theta)^2(2+cos\theta)+3n\alpha^2\beta]} \tag{A.15}$$

Replacing R^* in Equation A.13 we obtain ΔG^*_{Het}:

$$\Delta G^*_{Het} = \frac{16}{3}\pi\left(\frac{\Delta\mu}{\Omega}\right)^2 \gamma_{L^3}\frac{[2(1-cos\theta)-cos^2\theta]^3}{[(1-cos\theta)^2(2+cos\theta)+3n\alpha^2\beta]^2} \tag{A.16}$$

From CNT we can define the variation of free energy for homogeneous nucleation for the formation of a nucleus of critical size ΔG_{Hom} as:

$$\Delta G^*_{Hom} = \frac{16}{3}\pi\gamma_L^3\left(\frac{\Delta\mu}{\Omega}\right)^2 \tag{A.17}$$

Therefore, finally we can obtain $\phi_{117Nano}$:

$$\Phi_{117Nano} = \frac{\Delta G^*_{Het}}{\Delta G^*_{Hom}} = \frac{1}{4}\frac{[2(1-cos\theta)-cos\theta sin\theta^2]^3}{[(1-cos\theta)^2(2+cos\theta)+3n\alpha^2\beta]^2} \tag{A.18}$$

In the case of 117-Micro and NR50-Micro the same model (replacing the geometric parameters of a cylinder with the ones of a triangular prism) was applied,

for a Wenzel surface. Therefore, the following geometrical relationships were defined:

$$\alpha_1 = \frac{l}{R} \tag{A.19}$$

$$\beta_1 = \frac{h_1}{R} \tag{A.20}$$

Where l is the side of the triangle base of the prisma well and h_1 is the depth.

$$\Phi_{Micro} = \frac{\Delta G^*_{Het}}{\Delta G^*_{Hom}} = \frac{1}{4} \frac{[\pi^2 2(1 - cos\theta) - cos\theta sin\theta^2]^3}{[\pi(1 - cos\theta)^2(2 + cos\theta) + \frac{3}{2}\sqrt{3}3n_1\alpha_1^2\beta_1]^2} \tag{A.21}$$

Where n_1 is the number of wells on the contact area between the nucleus and the surface. For the Hierarchical membrane (Triangular prism wells with cylindrical wells inside), both geometries of the cylinder and prisma were included in the model, resulting:

$$\Phi_{Hierarchical} = \frac{\Delta G^*_{Het}}{\Delta G^*_{Hom}} = \frac{1}{4} \frac{[\pi^2 2(1 - cos\theta) - cos\theta sin\theta^2]^3}{[\pi(1 - cos\theta)^2(2 + cos\theta) + \frac{3}{2}\sqrt{3}3n_1\alpha_1^2\beta_1^2 + 3n\alpha^2\beta]2} \tag{A.22}$$

References

[1] S. H. de Almeida and Y. Kawano. "Thermal Behavior of Nafion Membrane." In: *Journal of Thermal Analysis and Calorimetry* 58 (1999), pp. 569–577. DOI: 10.1023/A:1010196226309.

[2] H.-y. Jung and J. Won. "Role of the glass transition temperature of Nafion 117 membrane in the preparation of the membrane electrode assembly in a direct methanol fuel cell (DMFC)." In: *International Journal of Hydrogen Energy* 37.17 (2012), pp. 12580–12585. DOI: 10.1016/j.ijhydene.2012.05.121.

[3] D. Qin, Y. Xia, and G. M. Whitesides. "Soft lithography for micro- and nanoscale patterning." In: *Nature Protocols* 5.3 (2010), pp. 491–502. DOI: 10.1038/nprot.2009.234.

[4] T. S. Meiron, A. Marmur, and I. S. Saguy. "Contact angle measurement on rough surfaces." In: *Image (Rochester, N.Y.)* 274 (2004), pp. 637–644. DOI: 10.1016/j.jcis.2004.02.036.

[5] E. Celia, T. Darmanin, E. T. D. Givenchy, S. Amigoni, and F. Guittard. "Recent advances in designing superhydrophobic surfaces." In: *Journal of Colloid and Interface Science* 402 (2013), pp. 1–18. DOI: 10.1016/j.jcis.2013.03.041.

[6] Y. X. Liu, X. J. Wang, J. Lu, and C. B. Ching. "Influence of the roughness, topography, and physicochemical properties of chemically modified surfaces on the heterogeneous nucleation of protein crystals." In: *Journal of Physical Chemistry B* 111.50 (2007), pp. 13971–13978. DOI: 10.1021/jp0741612.